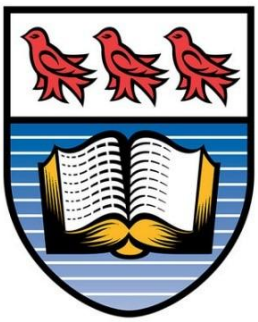

University of Victoria

MECH 360

Fall 2022

Stage 3

Gearbox Design

17 December 2022

Group 8

Josh Jacoby	V00942978
Colm Molder	V00937879
Aidan Sarkozy	V00937139
Scott Pederson	V00941511
Blaine Tubungbanua	V00918128

1 - Abstract

This report presents the design of a gearbox for a hybrid-electric tubgoat, developed for Robert Allan Naval Architects & Marine Engineers (RAL). The goal of the project was to design a gearbox that could be housed on a tugboat, considering factors such as lifespan, efficiency, overall size, weight, and ease of assembly/maintenance. The gearbox was designed to combine an input power of 2500kW from a diesel prime mover, and 1500kW from an electric engine, reducing the shaft speeds from 1000 rpm and 3000 rpm respectively, to 400 rpm. The gearbox used two compound gear trains to achieve a gear reduction of 4:30 and 2:5 for the diesel and electric drivetrains respectively, transmitting power into a single output shaft. The loads faced by the gears, shafts, and bearings were calculated based on the tugboat's operational load profile, provided by RAL. Fatigue calculations were conducted on the gears, bearings, and shafts, ensuring a lifetime of 20 years, with a safety factor of 1.2. Overall, the gearbox was designed to have a lifespan of 20 years, operate with an efficiency of 97%, occupy a volume of 14.4m^2, and weigh 44,700kg.

Table of Contents

List of Figures

1 Preface

This section contains an introduction, providing the motivation behind this report, followed by a brief overview, which provides the important background information. This is followed by a review of literature, including a review of similar technologies, and a market survey. Finally, objectives and constraints for the design project are tabulated.

1.2 Introduction

Robert Allan Naval Architects & Marine Engineers (RAL) have contracted us to design a gearbox for their new high-efficiency hybrid-electric tugboat. Considering high fuel costs, and the adverse effects of burning fossil fuels it is important for industries to transition to greener transportation alternatives such as electric and hybrid drivetrains. Tugboats are a particularly good candidate for hybrid drivetrains as full power is only required for 5% of their daily operation. This allows the electric motor to be used for the majority of the time, which can be charged from a renewable power source. Our task is to complete a full detailed design of the gearbox that would be implemented in the tugboat given the performance specifications provided by RAL. This includes looking at assemblability, cost, and maintainability of the gearbox in order to design a feasible gearbox that could realistically be housed on board the tugboat while minimizing the impact on the tugboat's performance.

1.3 Background

Many combustion engines have an optimal operating speed that facilitates sustained combustion, depending on the engine piston and cylinder design. These operating speeds tend to be much higher than the output mechanism. To translate these high speeds to lower reasonable speeds to drive tires or a propeller, a gear train or power transmission system is used. Gears are an application of mechanical advantage, trading speed for force. Throughout the power train, multiple gears are used to step-down the speed rotation, while increasing the torque. It must be noted that power is conserved, and the tradeoff in speed is manifested in torque. Power losses are a major consideration in a power transfer system such as a drivetrain. To allow smooth rotation of shafts, bearings are used to allow smooth rotation of drive shafts.

The gearbox will consist of two input shafts, a system of gears, and one output shaft. One of the input shafts is coupled to the electric motor while the other is coupled to the diesel prime mover. The system of gears will take the input power of the electric and diesel engines and convert it through gear ratios to the required full-power propeller speed of 400 rpm. The propeller speed and torque will then be transferred along the output shaft. In order to support and maintain this power transfer through the gear box, bearings and couplings must also be included in the design. The amount of bearings and couples used in the design is dependent on the loads the gearbox shafts face which can be calculated based on the operational load profile. The operational load profile is a distribution of the power output over a period of time. In the case of the tugboat, it will require different power outputs over the course of a work day as it undergoes its tasks. The load profile is expressed as a percent of a day that the power system experiences a certain power output. RAL has provided its expected operation load profile of the tugboat which will be used to determine load and fatigue values which in turn will affect the gearbox design choices in order to create a reliable product.

1.4 Review of Literature

This section explores a review of similar technologies, to inform the design of the gearbox, along with a market survey, assessing the market value of hybrid-electric marine gearboxes.

1.4.1 Review of Similar Technologies

Since a gearbox is a proprietary mechanical system, there are few full designs available to the public. Often only cutaway pictures of a basic gearbox are provided by the gearbox manufacturers with the output power range. One company that provides this is Novagear. Novagear is a Swiss gearbox specialist that designs a variety of gearboxes including ones for marine applications. In **Figure 1** below, a two input, one output gearbox can be observed.

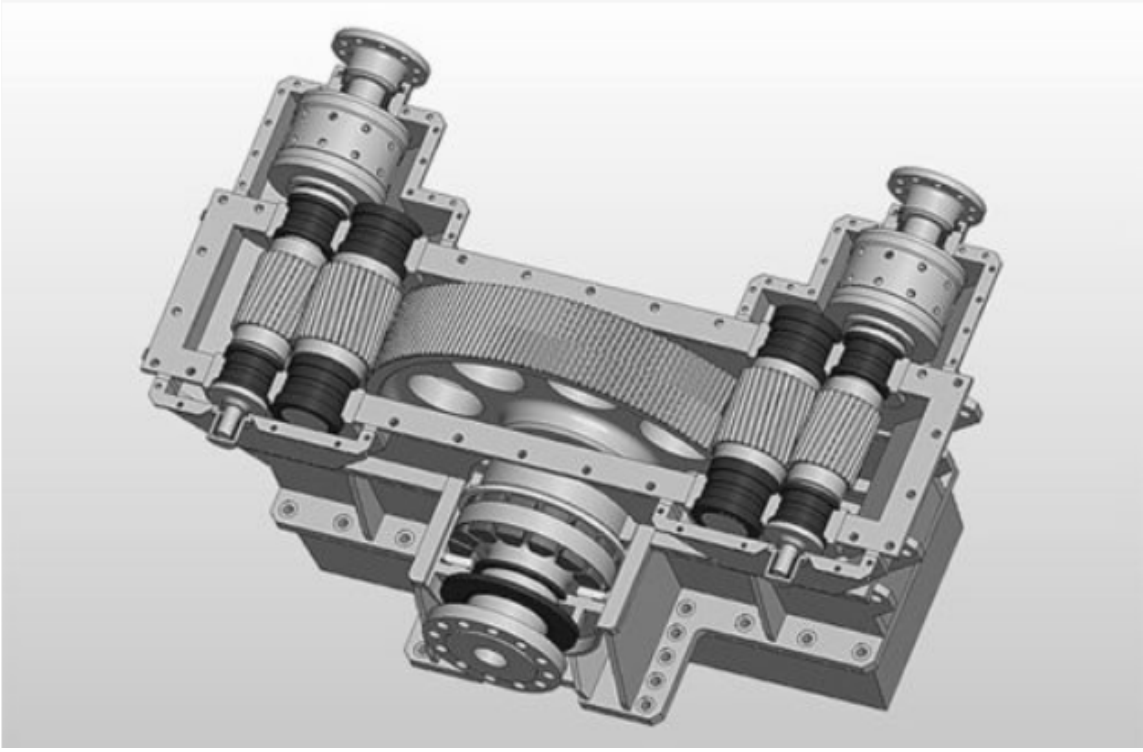

***Figure 1**: Novagear two input, one output gearbox [1]*

This is a very useful diagram as it demonstrates how two inputs can be combined into a single output, just like what is required for this project. In this particular case, both inputs

originate from equivalent diesel engines. It can also be assumed from the diagram that the two inputs are equal based on the similar size and geometry of the gears on both sides of the output gear. The diesel engines can be connected and disconnected from the input shaft by disc friction clutches. The input shafts are then connected to helical gears and supported by white metal journal bearings. The intermediate gears transfer the power horizontally through these helical gears until the power from each input combines at the large output gear and is then transferred to the output shaft. Looking at the overall design, it can be noticed that helical gears are a common and useful gear type to use in this application. The diagram also demonstrates how housing and bearings are laid out for gearboxes, providing practical knowledge for the housing design.

Flender is another world renowned transmission manufacturer that has also committed to designing hybrid gearboxes. In **Figure 2** below, a schematic of their NAVILUS 2-speed gearbox can be analyzed.

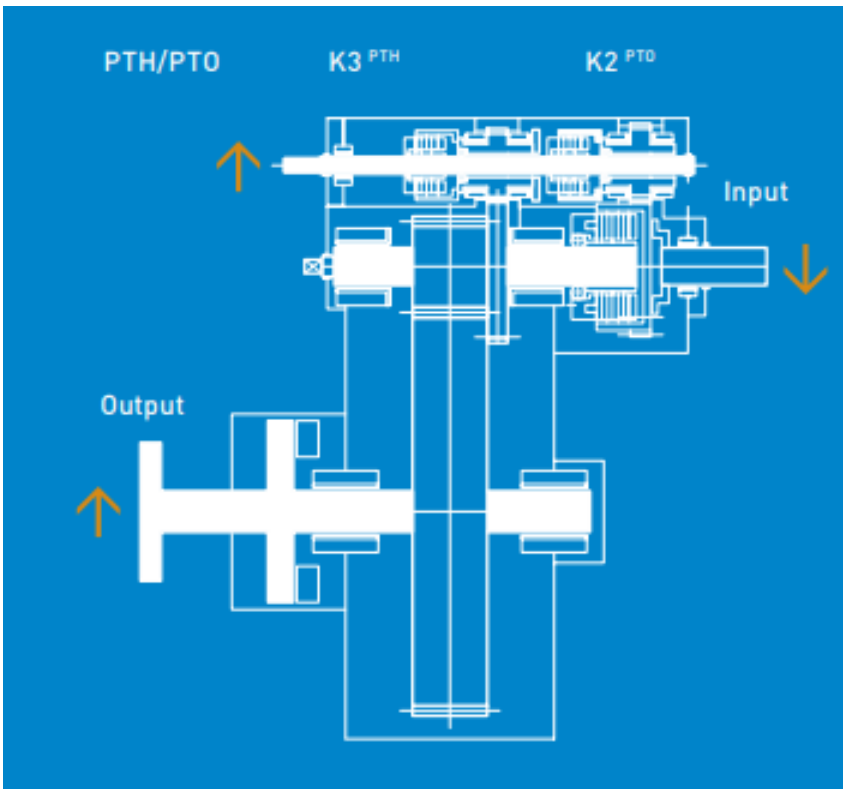

***Figure 2**: Schematic of Flender's NAVILUS gearbox [2].*

The NAVILUS gearbox can be configured for many applications and power ratings including hybrid drive. In the schematic it can be noticed that there is an input, output, and a PTH/PTO shaft. The PTH/ PTO works as the electrical power section of the system. PTH stands for Power Take Home and PTO stands for Power Take Off. They are similar in that they can both provide electrical power to the gearbox as an additional source of power. A PTO system works by taking off excess power from the prime mover if the required work is lower than the prime mover output. That power can then be stored in a battery and then reapplied as an input to the gearbox system. A PTH system is then just an electric motor that can be used in unison with the prime mover such as in a hybrid propulsion system. This design is relevant for this project's scope as it showcases a different internal gear box design that still has two inputs and one output. Looking closely at the schematic allows the bearing locations to be observed similarly to the Novagear diagram.

These two gearbox designs were fundamental in providing an initial understanding of real life gearbox layouts and applications. This information was then implemented into the design of the gearbox detailed in this report. While the math behind the gearbox design was calculated from lecture material and gear equations, the intuitive understanding of gearboxes were derived from these diagrams.

1.4.2 Market Survey

Hybrid-electric powertrain designs have become more commonplace in the naval industry recently. Gearboxes that combine input power from both internal combustion and electric motors into one output are a frequently growing requirement for tugboats and larger ships alike. The main customer of this hybrid electric gearbox is the contractor Robert Allen, but there may be more customers in the future if the design performs as intended. Other customers in Canada that could be targeted include Kotug Canada and Seaspan [3,4]. Understanding that the scope of this project is to solely produce a detailed design of a gearbox and not manufacture it,will require a cost analysis that exemplifies this. The cost of designing anything relies mainly on the working time of the experts contracted to generate the calculations and schematics of the design. A design engineer in Vancouver makes an annual average salary of $66,583 based on the

website Payscale.com [5]. Estimating that an engineer will be needed to specialize in each component of the gearbox means that the project will require 5 design engineers. One for each of shafts, bearings, couples, gears, and housing. This also happens to be the same sized team as the one actually undertaking this project. The engineers will of course be allowed to share each other's workload but this seems like a reasonably sized team for designing one mechanical system. Based on the fact that this project is created to be finished in a term, a timeline of 1 month will be given to the full time professional engineers to complete the gearbox design.

The software and resources used by the engineers should also be accounted for in this budget analysis. A typical mechanical design software used by mechanical engineers is Solidworks, which costs $4,195 per license per year [6]. This leads to a total of $1,748 in Solidworks licenses for all engineers over the 1 month of working on this project. Summing all the costs gives a grand total of approximately $30,000.

1.5 Objectives and Constraints

The major objectives and constraints set by both the client and the design team are outlined in **Table 1** and **Table 2** below. Justification of the importance of each objective and constraint are also provided, along with a target value or range where applicable.

***Table 1**: Project constraints*

Constraint	Justification	Target Value/Range	Status
Design Lifespan	The final design should exhibit strong reliability in order to reduce operating costs and cost of replacement. 20 years was selected as an appropriate lifespan as most other components of the tug would need replacement before that time period.	> 20 years	A lifespan of 20 years was achieved. (Section 4)
Gearbox Efficiency	The gearbox design should be highly efficient in transferring power from the input shafts to the output in order to maximize overall system efficiency. This efficiency range was chosen as a realistic, yet ambitious goal to maximize efficiency.	95-97% efficiency	The gearbox has a calculated efficiency of 97.03% (Section 2.6.4)

Table 2: Project objectives

Objective	Justification	Target Value/Range	Status
Overall size	The gearbox assembly should be as small in size as is possible and functional without negatively impacting any other objectives or constraints. Having a small volume allows for placement of the assembly in the most optimal position within the hull of the tug.	Volume < $2m^3$	Volume = $14.4m^3$ Stresses on gearbox elements were underestimated, and the gearbox had to be scaled up to increase safety factor. (Section 4.4)
Overall weight	The assembly and housing should have a weight that is negligible in the application of a tugboat to avoid negatively impacting performance. The weight range was chosen in order to account for the necessary rigidity of the gearbox components, while not negatively impacting the performance of the tug.	< 450 kg	44,726.38kg Because of the underestimates stresses, sizing of components was greatly mis-judged
Ease of maintenance	The gearbox assembly should be contained in a housing such that maintenance can be conducted quickly and without damaging the assembly. The gearbox should also have a minimal amount of components with limited life spans (Gears, bearings)	<15 Bearings <10 Gears	8 bearings are implemented, 6 gears are implemented. (Section 4.3, Section 2.6.2)

2 Design Stage One: Initial Design of Drive Train

The following section will outline the initial design work completed for the gearbox. This includes the proposed gear layout, gear parameters, required gear ratios, conceptual gearbox housing and some initial load calculations.

2.6 Concept Design and Load Sets

The implementation of a hybrid-electric gearbox can be reduced to the following simple representation. There are two shafts providing input torque, one from the prime mover (internal combustion engine), and the other from the electric motor. These two shafts must interface in a gear reduction in order to power the output shaft to drive the propeller.

2.6.1 Initial Calculations and Overall Concept

Our group chose to tackle the posed design problem with a simple gearbox using two compound gear trains for the diesel and electric sources transmitting power into a single output shaft. This decision was made to increase speed reduction while ensuring the gearbox was small in size. The initial concept sketch and gear names are seen below in **Figure 3**.

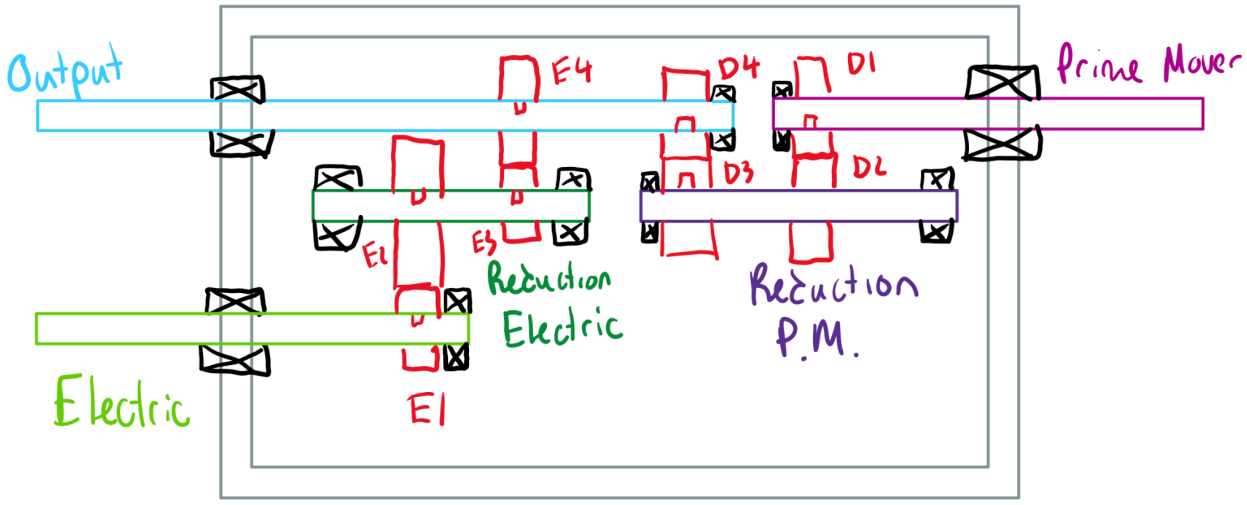

***Figure 3**: Initial Concept Layout*

The first step in the design of this gearbox was determining the required speed ratios. This was determined from the full power scenario with the input and output data tabulated in **Table 3** below.

***Table 3**: Input and Output at Full Power*

Input Source	Quantity	Value
Diesel (2)	Power [PD]	2500 kW
	Shaft Speed [nD]	1000 RPM
Electric (1)	Power [PE]	1500 kW
	Shaft Speed [nE]	3000 RPM
Output Source	**Quantity**	**Values**
Full Power	Power [PO]	3800 kW
	Shaft Speed [nO]	400 RPM

From this data, the desired input and output speeds in rad/s and torques were determined using the following relationships:

$$\omega = n\frac{2\pi}{60} \quad , \quad T = \frac{P}{\omega}$$

This data is tabulated below in **Tables 4** and **5**.

***Table 4**: Desired Speed Input and Output in Rad/s*

Input and Output in Rad/s	
Diesel Input Speed [wD]	104.7197551 rad/s
Electric Input Speed [wE]	314.1592654 rad/s
Desired Output Speed [wO]	41.88790205 rad/s

***Table 5**: Desired Torque Input and Outputs*

Input and Output Torques	
Diesel Input Torque [TD]	23873.24146 Nm
Electric Input Torque [TE]	47746.48293 Nm
Desired Output Torque [TO]	90718.31756 Nm
Output Torque [TO] (No Losses)	95492.96586 Nm

From these values the required speed ratios for the electric and diesel gear trains were determined as follows:

$$\text{Electric: } e_{E4/E1} = wO/wE = 41.888/314.159 = 4/30$$

$$\text{Diesel: } e_{D4/D1} = wO/wD = 41.888/104.719 = 2/5$$

Next, the gear ratios were related to teeth numbers for the two gear trains. This was completed as follows:

$$\text{Electric Train: } e_{E4/E1} = \frac{\omega_{E4}}{\omega_{E1}} = \frac{\omega_{E4}}{\omega_{E3}}\frac{\omega_{E2}}{\omega_{E1}} = \frac{N_{E3}}{N_{E4}}\frac{N_{E1}}{N_{E2}}$$

$$\text{Diesel Train: } e_{D4/D1} = \frac{\omega_{D4}}{\omega_{D1}} = \frac{\omega_{D4}}{\omega_{D3}}\frac{\omega_{D2}}{\omega_{D1}} = \frac{N_{D3}}{N_{D4}}\frac{N_{D1}}{N_{D2}}$$

To enforce these ratios, they were used to determine the number of teeth in the first gear of each train by using the following constraint equations:

Electric: $$N_{E1} = \frac{e_{E4/E1} N_{E2} N_{E4}}{N_{E3}}$$

Diesel: $$N_{D1} = \frac{e_{D4/D1} N_{D2} N_{D4}}{N_{D3}}$$

Next, other constraint equations were determined based on the scenario and assembly of our chosen gearbox. These constraints are:

1. Input gear torques must be equal to full power input torques
2. Input gear speeds must be equal to full power input speeds
3. Speeds of gears on the same shaft must be the same
4. Modules of meshing gears must be the same
5. The final gear torques on the output shaft must add up to the desired output torque

The constraints on each gear are tabulated below in **Table 6**.

***Table 6**: Constraint Equations on Gears*

Gear Name	Constraints		
	Speed w	Torque T	Module m
E1	E1w=wE	TE1=TE	mE1=mE2
E2	n/a	n/a	mE1=mE2
E3	E2w=E3w	n/a	mE3=mE4
E4	E4w=wO	TE4+TD4=TO	mE3=mE4
D1	D1w=WD	DE1=DE	mD1=mD2
D2	n/a	n/a	mD1=mD2
D3	E3w=E2w	n/a	mD3=mD4
D4	D4w=wO	TE4+TD4=TO	mD3=mD4

With the constraints all set, the next step in determining gears was making design decisions. The first decision was to pick a module of 0.01m for all gears. This module was used to determine gear radius based on chosen teeth numbers by the following equation:

$$r = \frac{mN}{2}$$

Once radii were found, torques for each gear were determined by the following equation:

$$T_2 = \frac{r_2}{r_1} T_1$$

Speed values were found based off selected teeth numbers by the following equation:

$$\omega_2 = \frac{N_1}{N_2} \omega_1$$

With these constraints and equations set, the only design decisions left were to determine teeth numbers for gears. Because the input gears' teeth counts are determined by the speed ratios, teeth count numbers that produced integer values for the input gears were required. Teeth counts were determined by ensuring the final gears were not excessively large or small. **Table 7** below outlines the data for each gear. Green cells indicate values determined by constraint equations, pink values were determined by desired inputs, and blue cells were design decisions.

***Table 7**: Gear Data*

Gear Name	Teeth Number N	Radius r [m]	Module m	Speed w	Torque T
E1	16	0.08	0.01	314.1592654	4774.648293
E2	60	0.3	0.01	83.7758041	17904.9311
E3	40	0.2	0.01	83.7758041	17904.9311
E4	80	0.4	0.01	41.88790205	35809.8622
D1	32	0.16	0.01	104.7197551	23873.24146
D2	40	0.2	0.01	83.7758041	29841.55183
D3	40	0.2	0.01	83.7758041	29841.55183
D4	80	0.4	0.01	41.88790205	59683.10366

From this table, it can be observed that the output speed for both gear E4 and D4 is 41.89 rad/s as required. It can also be seen that the summation of torques provided by the electric and diesel train is the required 0.0955 Nm:

$$T_{out} = T_{D4} + T_{E4} = 35809.8622 + 59683.10366 = 95500\,Nm$$

2.6.2 GearBox Elements

As shown in Figure 1, the design indicates the input shafts coming from the prime mover and the electric motor in purple and green, respectively. Both of these shafts then undergo a gear reduction in which their angular speed is reduced over the course of four gears. Specifically, torque is first transferred to an intermediate shaft that houses two gears. Finally, after being transferred across the intermediate shafts, torque is applied to the output shaft by one or both of the input power sources. This design decision was made in order to limit stresses on any one gear that may have arisen from attempting to achieve the required gear reduction with only one gear. It was theorized that this layout, involving more gears, would better distribute the stresses between all components, reducing the likelihood of failure. However, these facts remain to be investigated in further iterations of the design.

Due to the fact that many of the gears share characteristics, as outlined in Table 5 above, the gearbox design can be simplified to reduce the total number of shafts and gears. This could be done in a few locations, one of which being at gear D2. Specifically, since gears D2 and D3 have the same number of teeth and equal radii, their respective outer edges will be rotating at the same angular speed. Therefore, gear D2 could be removed, and gear D2 could interface directly with the output shaft. This would also cut down the length requirement for the shaft D2 and D3 are housed on, or even remove the shaft entirely if D3 were mounted in another fashion. These simplifications are shown in **Figure 4**, which shows the relative layout of the assembly's gears (not to scale) and also includes the general bearing locations within the assembly.

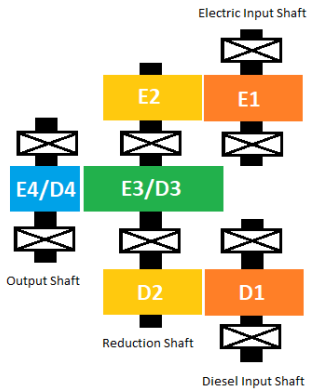

***Figure 4**: Relative layout of gears, shafts, and bearings*

Combining the relative layout from Figure 4 with the gear radii specified in Table 6, a preliminary CAD model was produced for the gearbox (see **Figures 5** and **6**). All gears are were planned to be to be axially located using clamping collars and transmit torque to their shaft via keys and keyways. All shafts are supported by two bearings (shown as white in CAD model), one locating and one non-locating.

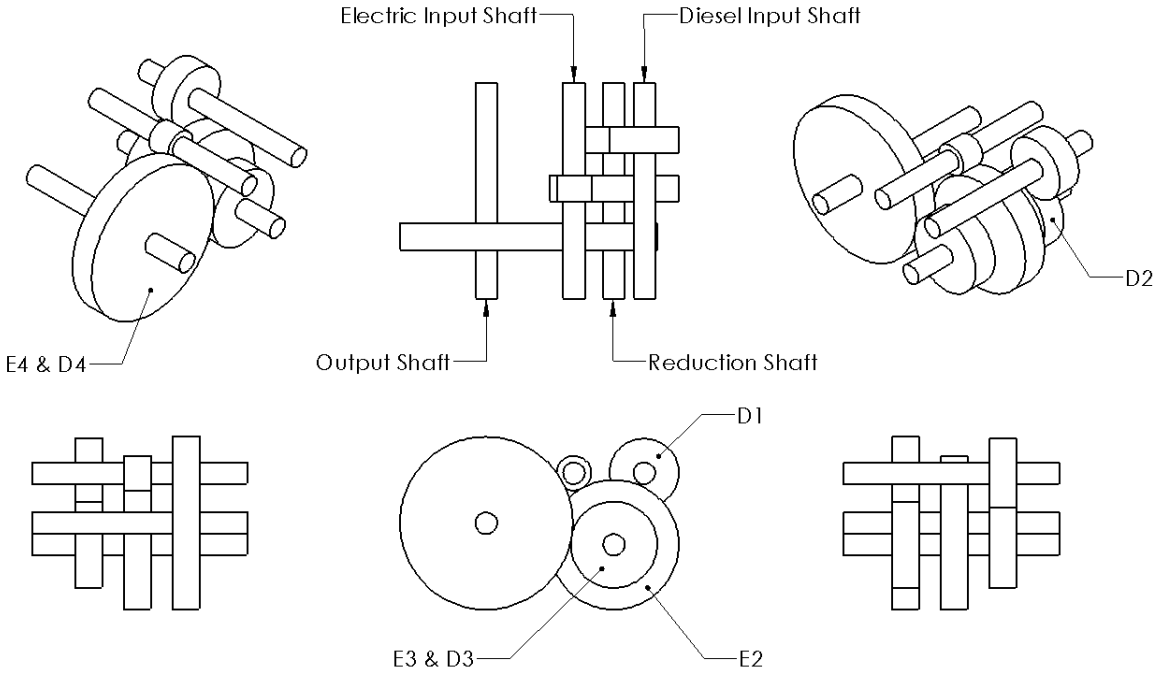

***Figure 5**: Preliminary CAD drawing of gears and shaft arrangement*

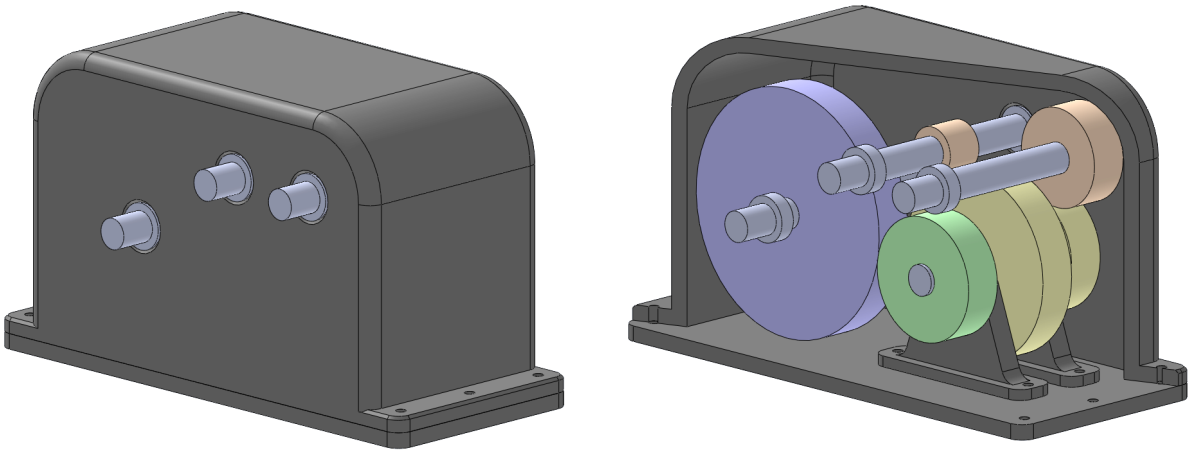

***Figure 6**: External and section view of the preliminary CAD assembly*

In this assembly, gear E1 is mounted to the electric input shaft (**Figure 7**), which is mounted to bearings supported by the walls of the gearbox housing.

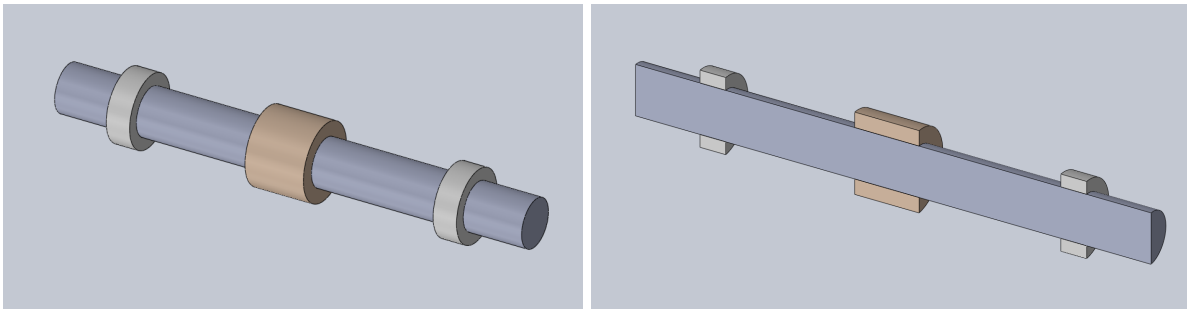

***Figure 7**: Isolated and section view of electric input shaft and gear E1*

In parallel with the electric input shaft, gear D1 is mounted to the diesel input shaft (**Figure 8**), which is also mounted to bearings supported by the walls of the gearbox housing.

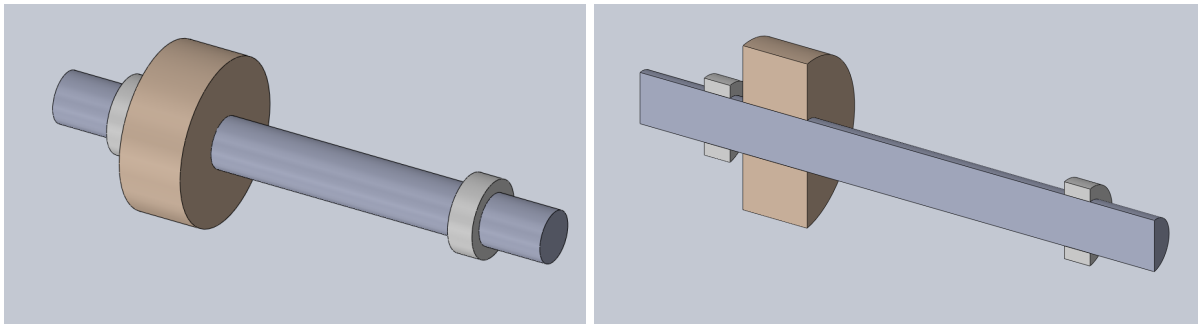

***Figure 8**: Isolated and section view of diesel input shaft and gear D1*

Gears E1 and D1 mesh with gears E2 and D2, which are both mounted to the reduction shaft (**Figure 9**). The reduction shaft is supported by bearings in mounting brackets connected to the base of the gearbox. Gear E3/D3 is also mounted to the reduction shaft, combining the torque applied by the electric motor and diesel engine.

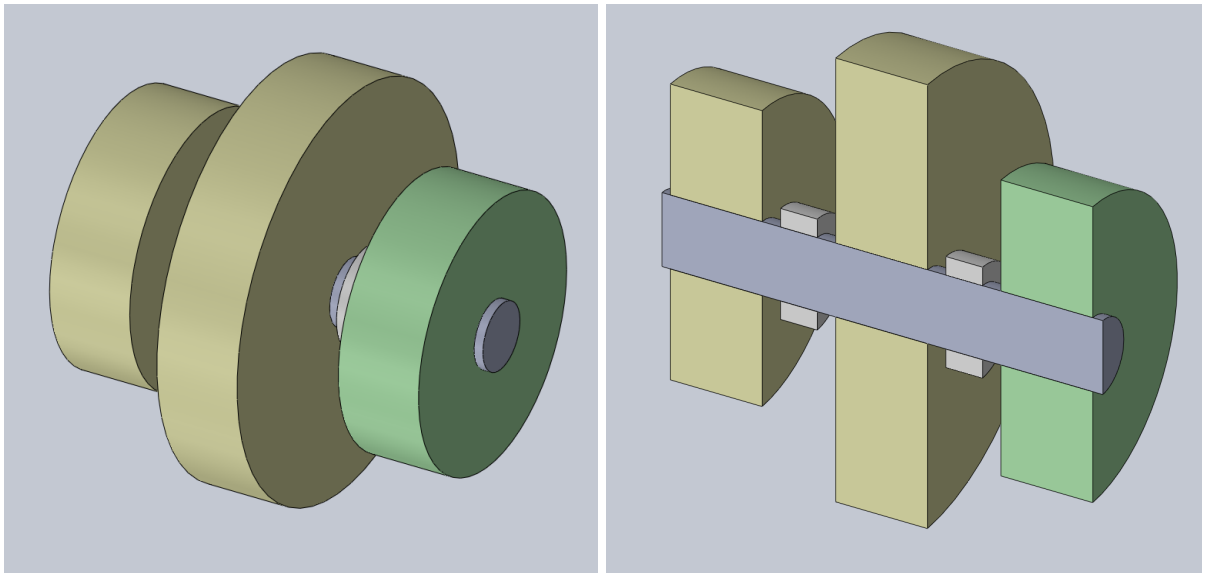

***Figure 9**: Isolated and section view of reduction shaft and gears D2, E2, and E3/D3*

Gear E3/D3 is the only gear to mesh with the output gear (E4/D4), which is mounted on the output shaft (see **Figure 10**). Like the two input shafts, the output shaft is mounted to bearings supported by the walls of the gearbox housing.

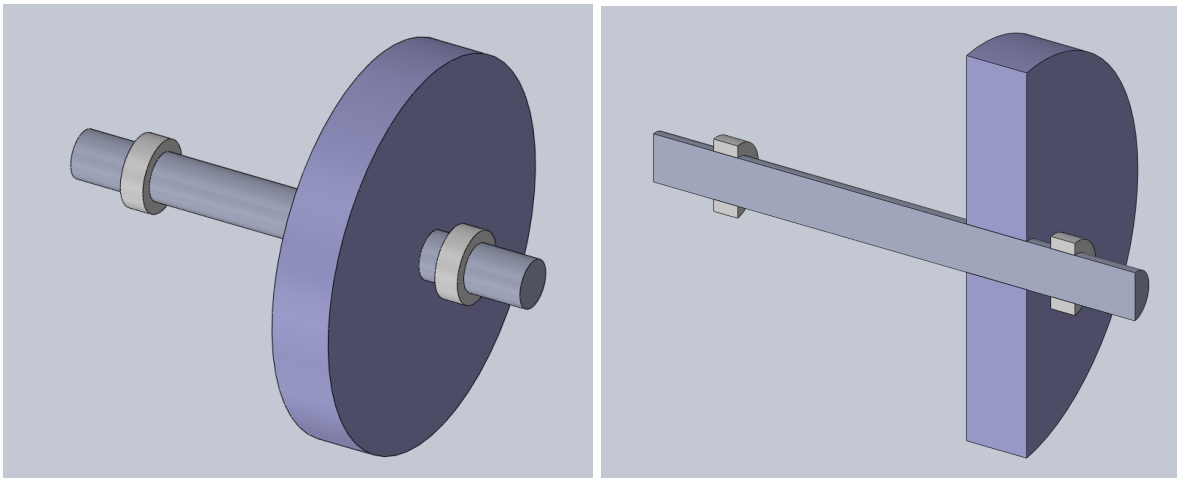

***Figure 10**: Isolated and section view of output shaft and gear E4/D4*

The reduction gear, along with its associated gears and bearings, may be assembled independently and mounted to the gearbox's baseplate before any other components are added. Each of the other three shafts must then be assembled within the housing, adding gears and clamping collars as the shaft is inserted. Large access ports must therefore be included in the gearbox housing to allow for easy assembly. These access ports can also be used for any repairs, replacements, or lubrication that may be required during the life of the gearbox.

2.6.3 Speeds and Loads

Using the tabulated angular speeds and torques ω, T calculated previously in section 6.1, the power transferred through each gear can be determined, along with a rough estimation of losses accumulated with each gear. Furthermore, an estimate of lifespan can be determined by examining the expected daily use cycle of the gearbox.

Before performing detailed analysis, a simulation using an online gearbox generator was conducted to validate the tabulated gear velocities [7]. For simplicity, gears with the same teeth and radii were used as the same gear as discussed in the previous section. The simulation has limited input speeds so angular velocities were scaled down. In the simulation, electric input is given by gear 0, diesel input is given by gear 4, and output is given by gear 3. The layout is seen below in **Figure 11**.

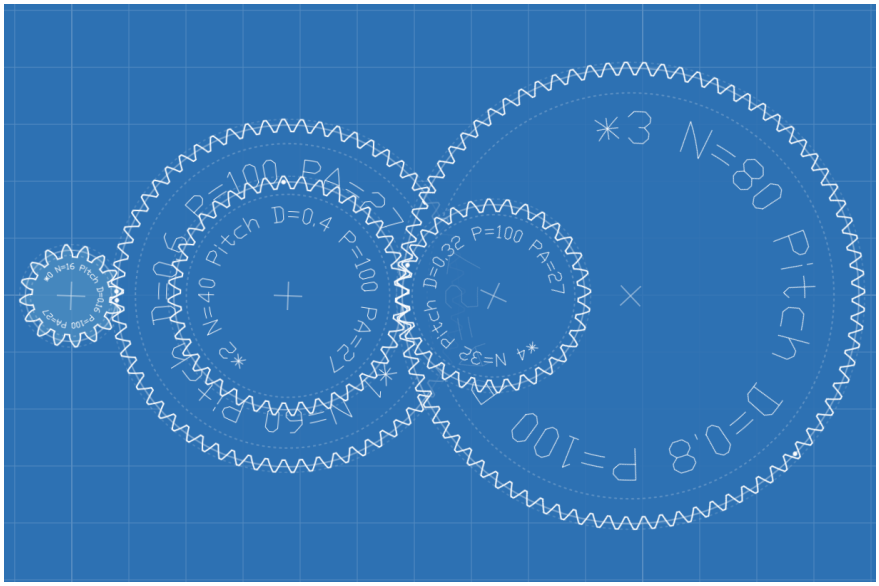

***Figure 11**: Simulation of chosen gears [7]*

Using the data from Table 5, power transferred between each gear, and applied to each shaft can be calculated using the following relation.

$$P = \omega T$$

Applying the simplifications to reduce the number of gears and shafts, the torque and power on the equivalent simplified model can be found by superimposing the torque and power transmitted through the original model. The power transmitted at each gear, along with the simplifications are shown below.

$$\omega_2 = \omega_{E2} = \omega_{D2} = \omega_{E3D3}$$

$$\omega_4 = \omega_{E4} = \omega_{D4}$$

$$P_{E1} = T_{E1}\omega_{E1} \quad , \quad P_{D1} = T_{D1}\omega_{D1}$$

$$P_{E2} = T_{E2}\omega_2 \quad , \quad P_{D2} = T_{D2}\omega_2$$

$$P_{E3D3} = (T_{E3} + T_{D3})\omega_2$$

$$P_{E4D4} = (T_{E4} + T_{D4})\omega_4$$

To determine the power transmitted through each shaft, the power of each attached gear is superimposed onto the shaft.

$$P_{SE} = P_{E1}$$

$$P_{SD} = P_{D1}$$

$$P_{S2} = P_{E2} + P_{D2}$$

$$P_{S4} = P_{E4D4}$$

Where:

$P_{SE} = Power\ transmitted\ to\ Electric\ input\ shaft,$
$P_{SD} = Power\ transmitted\ to\ Diesel\ input\ shaft,,$
$P_{S2} = Reduction\ Shaft,$
$P_{S4} = Output\ shaft$

The results of power calculations for each gear are tabulated below in **Tables 8** and **9**.

Table 8: *Power transmitted to each gear*

Gear Name	Power [kW]
P_E1	1500
P_D1	2500
P_E2	1500
P_D2	2500
P_E3D3	4000
P_E4D4	4000

Table 9: *Power transmitted to each shaft*

Shaft Name	Power [kW]
P_SE	1500
P_SD	2500
P_S2	4000
P_S5	4000

2.6.4 Gearbox Efficiency

To obtain an estimate of gearbox efficiency, we can examine all areas where losses are expected to occur. For this gearbox, losses are expected from gear meshing, friction at bearings, and friction at dynamic seals located on the rotating shafts. This means that total gearbox

efficiency can be calculated by multiplying bearing efficiency η_{brg} gear meshing efficiency η_{grm}, and seal efficiency η_{seal}, raised to the power of N components.

$$\eta_{total} = \eta_{brg}^{N_{brg}} \cdot \eta_{grm}^{N_{grm}} \cdot \eta_{seal}^{N_{seal}}$$

However, a simplification will be made, undertaking the assumptions that an efficiency of $\eta_{mesh} = 0.99$ applied at each meshing gear accounts for bearing losses and seal losses associated with each meshing set. Examining the design, there are 3 meshing sets, tabulated in **Table 10.** Conducting this calculation yields the following total efficiency.

$$\eta_{mesh}^{N} = \eta_{total} = 97.03\%$$

According to these calculations, our gearbox will perform above the rated specifications, resulting in an output power of 3881kW of the required 3800 kW.

Table 10: *Tabulating efficiency of each meshing pair* [8].

Meshing Pair	Efficiency [%]
E1-E2	0.99
D1-D2	0.99
E3D3-E4D4	0.99

The gearbox is expected to operate at a daily cyclical load specified in **Table 11**. This daily usage distribution is visualized in **Figure 12**.

Table 11: *Daily usage distribution*

Activity	Percent Usage	Power [kW]
Full Power	5%	3800
Slow Speed Transit	12%	800
High Speed Transit	23%	1400
Moored	30%	0
Stand-by	30%	0

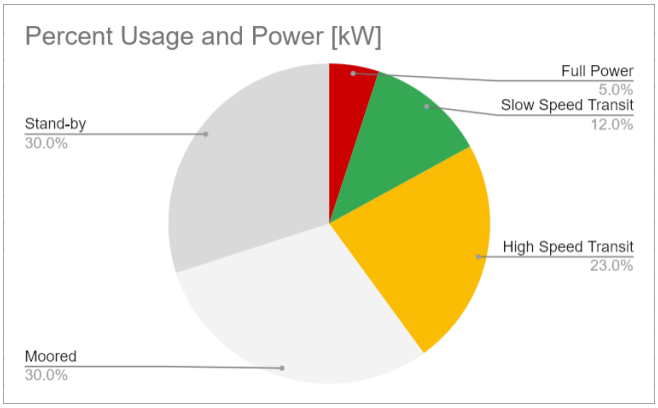

Figure 12: *Graphical representation of daily usage distribution*

The power experienced by each gear component, and shaft component during each loading case are tabulated in **Table 12**, **Table 13**, and visualized in **Figure 13**

Table 12: *Power experienced by each gear during each loading case.*

Gear	Full Power	HS Transit	SS Transit
P_E1	1500	1400	800
P_D1	2500	0	0
P_E2	1500	1400	800
P_D2	2500	0	0
P_E3D3	4000	1400	800
P_E4D4	4000	1400	800

Table 13: *Power experienced by each shaft during each loading case.*

Shaft	Full Power	HS Transit	SS Transit
P_SE	1500	1400	800
P_SD	2500	0	0
P_S2	4000	1400	800
P_S5	4000	1400	800

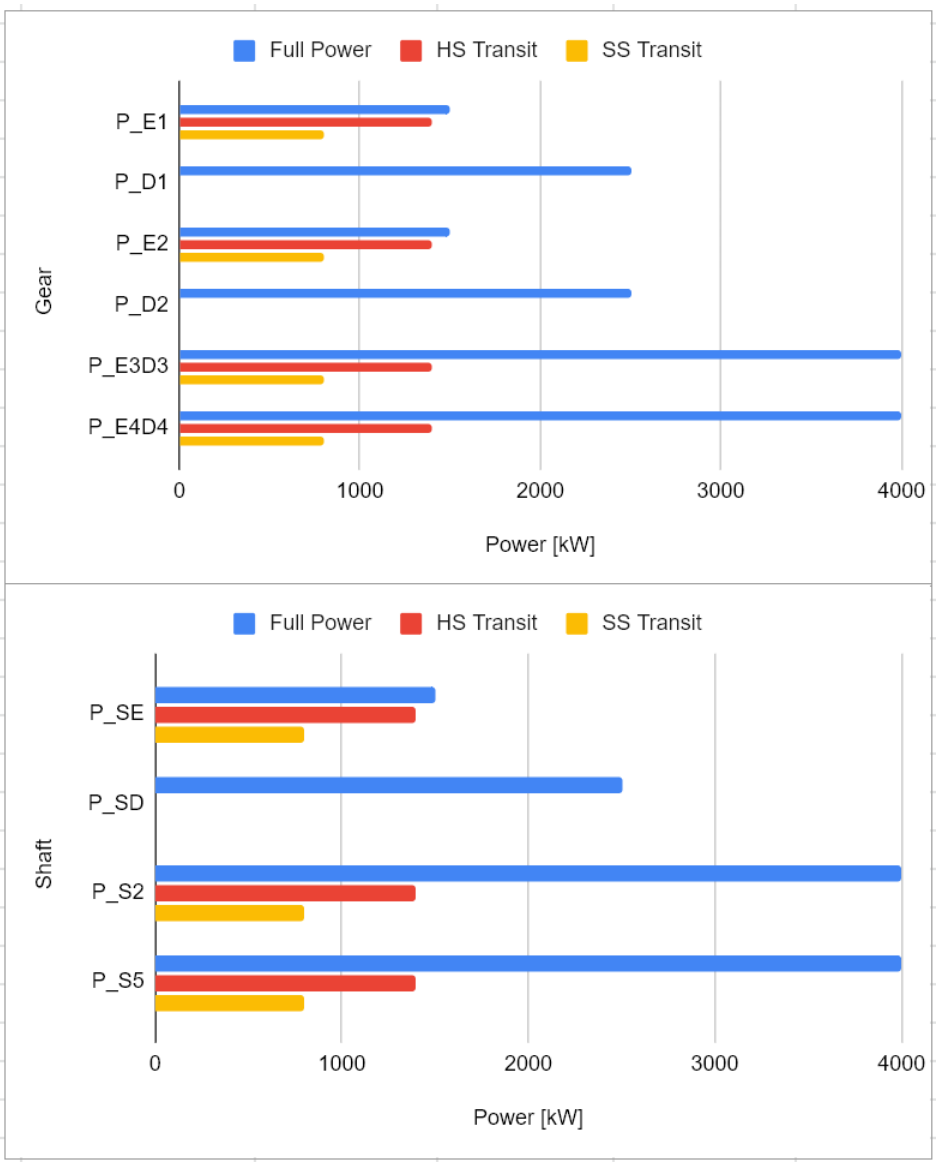

Figure 13: *Power transmitted by each gear (top) and each shaft (bottom) during each loading case.*

3 Design Stage Two: Qualitative Gearbox Elements

The following section will outline the more detailed design of gear box elements and features. This design omits rigorous stress and fatigue calculations and focuses on the qualitative features required to mount and locate components.

3.1 Preliminary Design Gearbox Layout

This section describes the preliminary design of the various components that comprise the gearbox, including—but not limited to—gears, shafts, seals, and bearings.

3.1.1 Gears

The gear design remains the same, and spur gears are selected as the gear type. Preliminary estimates for each gear diameter is summarized in **Table 14** below, allowing for preliminary sizing of bearings, seals and housing.

***Table 14**: Gear Diameters*

Gear Name	Diameter D [m]
E1	0.16
E2	0.6
D1	0.32
D2	0.4
E3/D3	0.4
E4/D4	0.8

3.1.2 Bearings

The rationale and motives behind bearing selection is discussed in section 8, along with the discussion of shafts.

3.1.3 Couplings

The gearbox is designed to interface with three external shafts. The Electric Input, Diesel Input, and Output shaft. The preliminary shaft diameter has been calculated to be 55mm (see

section 8). Additionally, each of these shafts has a required speed and torque, tabulated in table 13.

Table 15: *Coupling speed and torque requirements*

Gear Name	Speed [rpm]	Torque [in.-lb]
E1	3000	42259
D1	1000	211295
E4/D4	400	316942

Searching on McMaster-Carr, there are many shafts capable of sustaining the required operating speeds, but there are no couplings available for a 55mm shaft diameter that can sustain 317,000 in-lbs of torque. The closest available coupling is a High-Torque Set Screw Flexible Shaft Coupling that has a max speed of 6,000 rpm, and max torque of 14,000 in-lbs. An image is shown in **Figure 14** [9].

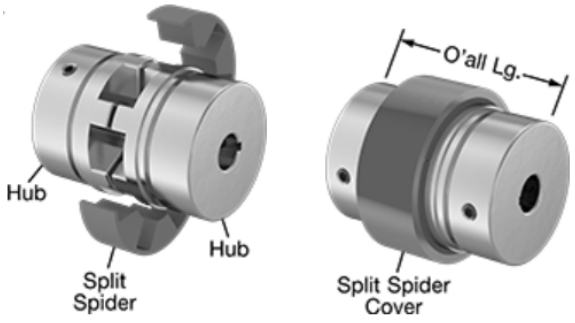

Figure 14: *High-Torque Set Screw Flexible Shaft Couplings [9]*

Due to this limitation, a custom machined coupling will be fabricated, discussed in section 4.5.1.

3.1.4 Seals

Rotary seals are selected to retain oil and grease within the gearbox, ensuring lubrication does not leak, as well as minimizing dirt, oil and water ingress. The gearbox designed in this report is not designed to undergo high pressures, so extra care is not required in seal selection. Preliminary shaft diameter has been calculated to be 55mm (see section 8). A bore-sealing spring-loaded rotary shaft seal has been selected to meet these requirements (**Figure 15)**. The

datasheet for this part states that a retaining ring is only required if subjected to pressures of 145 psi, so the seal can simply be press-fit into a specified bore. [9]

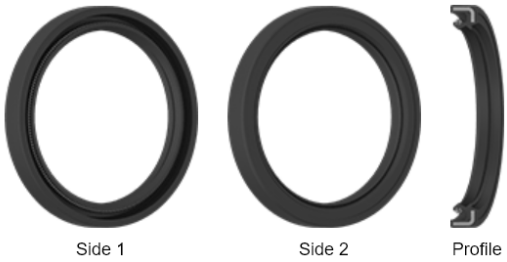

Figure 15: *Bore-Sealing Spring-Loaded Rotary Shaft Seals with Wiper Lip. [9]*

3.1.2 Preliminary Gearbox Layout

Gearbox layout and shaft placement is constrained by the center-to-center distances between each gear. The reduction shaft is used as the origin, as the diesel input, electric input, and output all interface directly with the reduction shaft. These constraints are tabulated in **Table 16**, using the preliminary diameters tabulated in **Table 12**. In addition, the shafts must not interfere with any of the spur gears.

Table 16: *Shaft positioning constraints, defined by center-to-center gear distance.*

Mating Gear Radius [m]		Reduction Gear Radius [m]		Center-to-center Distance
E1 (Electric Input)	0.08	E2	0.3	0.38
D1 (Diesel Input)	0.16	D2	0.2	0.36
E4/D4 (Output)	0.4	E3/D3	0.2	0.6

For a compact geometric design, the output shaft and reduction shaft both have the largest gear diameters, so they are configured along a horizontal plane. The input Electric and Diesel shafts are offset by 50 degrees in both directions. The shaft positioning is shown in **Figure 16.**

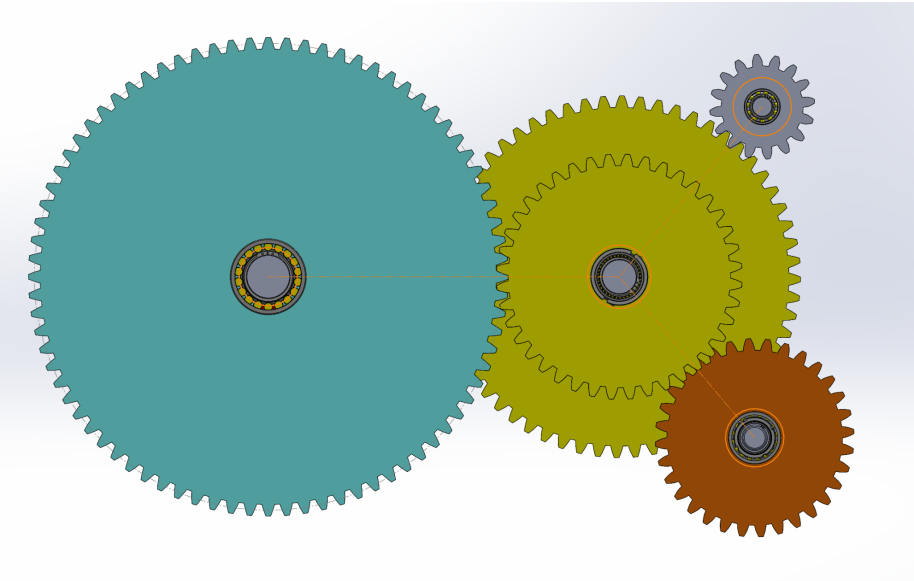

Figure 16: *Shaft positioning, constrained by center-to-center gear distance.*

3.1.3 Assembly Process

As the shaft diameters have not yet been specified, the bearings size has not been finalized, and installation procedures for mounting bearings to the shafts may entail cold conditions, or use heat expansion. In this preliminary design, the gears are axially located on the shaft with a two-piece collar assembly.

The preliminary assembly process for the prime mover input shaft is as follows:

1. Slide D1 onto diesel input shaft
    a. Install two-piece collar to hold the shaft in place
2. Mount the locating bearing onto the shaft
    a. Identify the locating shaft end by the threads.
    b. Mount the the bearing onto the threaded end
    c. Thread the locknut onto the end of the shaft, up to the specified torque rating.
3. Mount the non-locating bearing onto the shaft
    a. Once the bearing is mounted, secure the bearing to the shaft with a snap ring.

The preliminary assembly process for the electric input shaft is as follows:

1. Mount the locating bearing onto the shaft.
    a. Identify the locating shaft by locating the threaded end.
    b. Mount the bearing onto the threaded end.
    c. Thread the locknut onto the end of the shaft, up to the specified torque.
2. Mount the non-locating bearing onto the shaft.
    a. Once the bearing is mounted, secure the bearing to the shaft with a snap ring.

The preliminary assembly process for the reduction shaft is as follows:

1. Mount E3/D3 onto the shaft.
2. Mount the *reduction shaft spacer* onto the shaft.
3. Mount E2 onto the shaft
    a. Secure E2 with the two-piece shaft collar.
4. Mount the locating bearing onto the shaft.
    a. Identify the locating bearing with the threaded end.
    b. Mount the bearing onto the threaded end.
    c. Secure the locating bearing with the locknut, up to the specified torque.
5. Mount D2 onto the shaft.
    a. Slide D2 onto the shaft.
    b. Secure D2 in place with the two-piece shaft collar.
6. Mount the non-locating bearing onto the shaft.
    a. Once the bearing is mounted, secure the bearing to the shaft with a snap ring.

The preliminary assembly process for the output shaft is as follows:

1. Mount E4/D4 onto the Shaft
2. Mount the non-locating bearing onto the shaft.
    a. Secure the bearing with a snap ring
3. Mount the locating bearing onto the shaft.
    a. Secure the locating bearing with the locknut, up to the specified torque.

Gearbox assembly centers on the main Housing component (large, grey piece in **Figure 17**). The order of assembly is critical to ensure that the gears and shafts do not obstruct the

installation of other subassemblies. The assembly includes two access hatches, which are covered during operation by the two orange covers also shown in **Figure 17.**

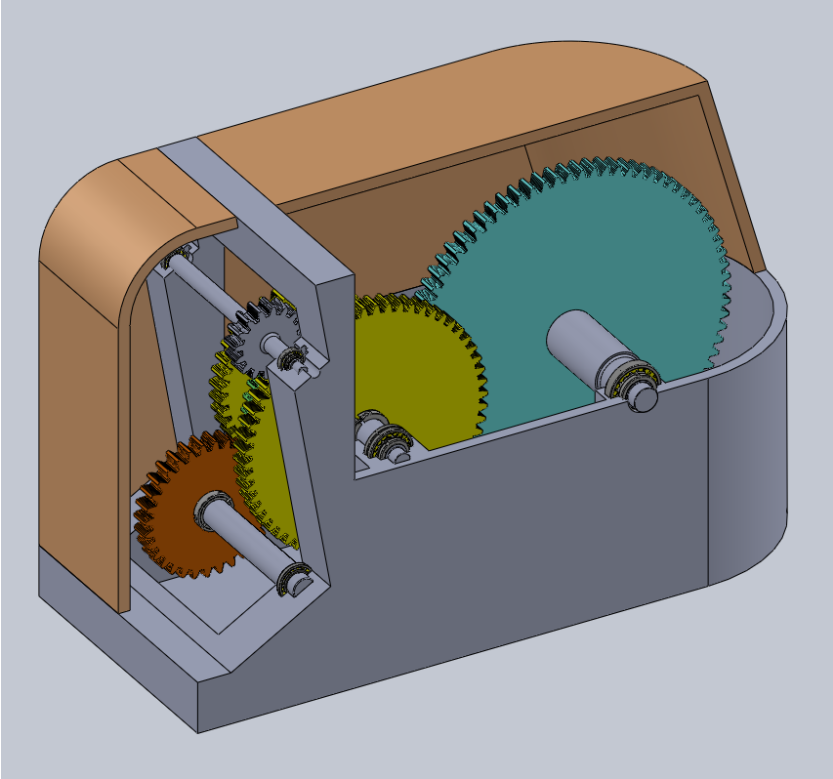

Figure 17: *Partial section view of preliminary gearbox design*

1. Install the **Prime Mover Input Shaft**.
    a. Lower the subassembly from above through the left-most access hatch
    b. Both bearings are captured by the geometry of the housing.
2. Install the **Reduction Shaft**.
    a. Lower the subassembly from above through the right-most access hatch
    b. Both bearings are captured by the geometry of the housing.
3. Install the **Output Shaft**.
    a. Lower the subassembly from above through the right-most access hatch
    b. Both bearings are captured by the geometry of the housing.
4. Install the **Electric Input Shaft**.
    a. Lower the subassembly from above through the left-most access hatch

b. Both bearings are captured by the geometry of the housing.

5. Install the **Hatch Covers**.
    a. Locate rotary shaft seals on the input and output shafts where they enter/leave the gearbox.
    b. Secure both access hatch covers to the main housing using bolts.
    c. Once installed, the hatch covers also help to retain the bearings' positions.

3.1.4 Areas Requiring Failure Analysis

Different components in the gearbox will experience greater stresses than others due to the nature of the applied loading and geometrical variance. An analysis of the critical points where gear failure is most likely to occur is conducted in this section. Failure analysis of each shaft is conducted in section 8.

When analyzing gears, failure is most likely to occur at the teeth or the keyhole. Tooth failure can occur by bending stress, or surface stress. Bending failure is likely to occur at the root of the tooth, where the fillet radius presents a stress concentration, while surface failure is likely to occur at the surface of the tooth, resulting in pitting and spalling.

For preliminary analysis, gear width and tooth geometry is assumed to be uniform across each gear. After identifying which gears are most likely to experience the highest stress, adjustments can be made to the geometry to increase resistance to failure. To identify the most likely candidates for failure, the force applied at each tooth interface is examined by multiplying the torque by the pitch radius. Individual force summation is conducted for the electric power transfer system, and the primary mover power transfer system. In addition, the number of cycles experienced by each tooth is a major factor, as faster rotating gears will experience more cycles, and more wear. This data is shown in **Table 16**. Because E3/D3 and E4/D4 have merged into 1 gear, the forces at these gears have been superimposed, displayed in **Table 17.**

Table 16: *Individual force summation for respective diesel and electric power systems.*

Gear Name	Radius r [m]	Torque T [Nm]	Cycles/Second	Force at Tooth [N]
E1	0.08	4775	314.1592654	382
E2	0.3	17905	83.7758041	5371
E3	0.2	17905	83.7758041	3581
E4	0.4	35810	41.88790205	14324
D1	0.16	23873	104.7197551	3820
D2	0.2	29842	83.7758041	5968
D3	0.2	29842	83.7758041	5968
D4	0.4	59683	41.88790205	23873

Table 17: *Superimposed force summation of condensed gearbox.*

Gear Name	Radius r [m]	Torque T [Nm]	Cycles/Second	Force at Tooth [N]
E1	0.08	4775	314.1592654	382
E2	0.3	17905	83.7758041	5371
D1	0.16	23873	104.7197551	3820
D2	0.2	29842	83.7758041	5968
E3/D3	0.2	47746	83.7758041	9549
E4/D4	0.4	95493	41.88790205	38197

Examining this data, it can be observed that the greatest force occurs at the output gear E4/D4, with a tangential force of 38kN followed by E3/D3, with a tangential force of 9.5kN. This aligns with intuition. As each speed reduction occurs, the corresponding force increases, culminating to a maximum force at the output. Additionally, E1 will experience the most cycles over the gearbox's lifespan, but the force is relatively low, so it can be dismissed as non-critical. With this information, these gears will have to be reinforced to ensure even stress distribution between these high-force gears, and the lower-force gears.

Analysis of critical failure points on the shafts will be discussed in section 8.

3.1.5 Housing

The main housing piece is bolted directly to the bed frame within the vessel. Both hatch covers then bolt to the main housing piece once the internal gear mechanism has been assembled (**Figure 18**).

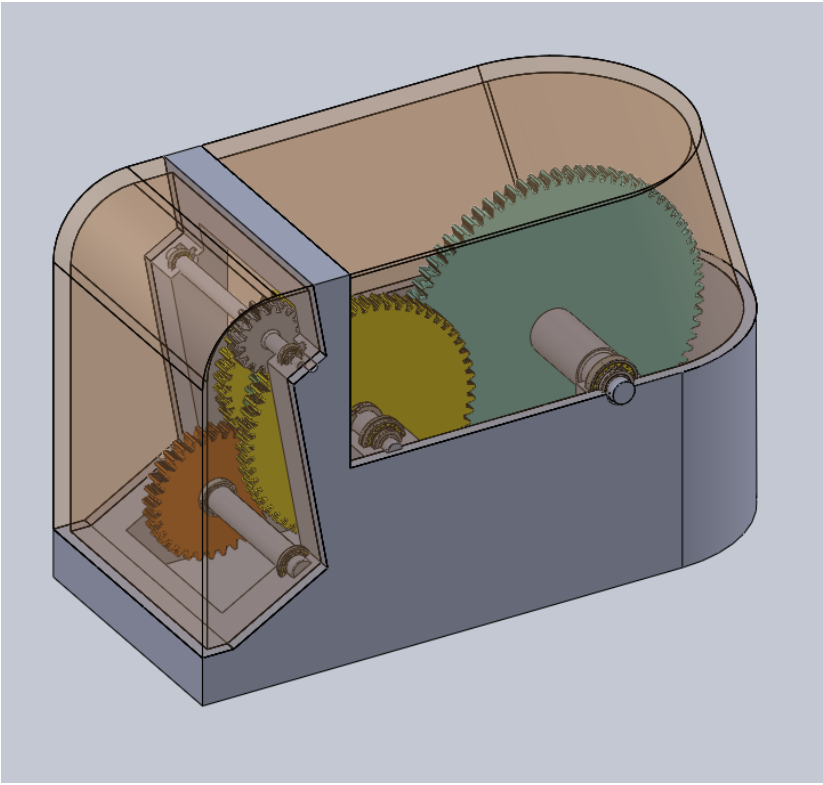

Figure 18: Preliminary housing assembly design

Each bearing incorporated in the design of the gearbox is captured by cavities in the main housing piece and its two hatch covers. **Figure 19** shows one of these bearings once it has been installed, along with its associated shaft and gear, in the main housing piece. Matching locating features can be found on the hatch covers as well, which fully capture the bearings once the covers are installed. The locating features on the main housing piece are arranged so that all bearings, shafts, and gears are held in place by their own weight until the hatch covers are installed. Rotary shaft seals are also located on the input and output shafts where they enter or leave the gearbox. These seals prevent leakage from the interior or contamination from the exterior.

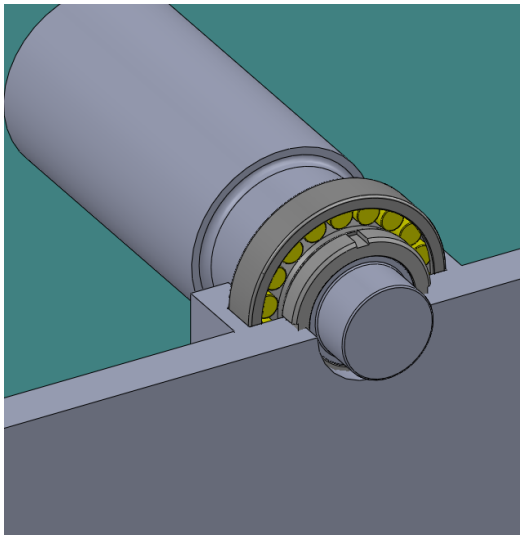

Figure 19: *Bearing and locating feature in main housing piece*

Together, the two hatches provide sufficient access to the housing's interior to install the gears and shafts (see Section 7.3).

3.2 Preliminary Design for Shafts

This section will outline the preliminary design of shafts, bearings, and other locating components affixed to the shafts. These initial designs are mainly qualitative in nature and represent the design principles being followed. Specific details (ie: dimensions, bearing selection) to refine these designs will be determined after more detailed fatigue and component specification analysis is completed.

3.2.1 Prime Mover Input Shaft

The first shaft to be discussed is the prime mover input shaft. As previously discussed, this shaft is provided input from the Diesel prime mover motor and turns gear D1. The following sections will outline the shaft design, discuss initial bearing selection for the shaft, outline areas of failure concern, and derive load equations.

The prime mover input shaft must be designed to transmit a maximum of 2500 kW at 1000 RPM. Using these constraints, it is possible to estimate the preliminary shaft diameter using the equation below.

$$d = \sqrt[3]{\frac{16*T}{\pi\tau}}\ [10]$$

Where T is the maximum torque of 23873 Nm and τ is the max shear stress of Type 316 stainless steel. τ for steels is considered to be roughly 0.75 times the ultimate tensile strength. For 315 stainless steel the ultimate tensile strength is 621 MPa, which leads to a value of 465.75 MPa for the shear stress [11]. Using the value of torque and converting the shear stress to pascals gives the following diameter.

$$d = \sqrt[3]{\frac{16(23873\ Nm)}{\pi(465.75x10^{6}Pa)}} = 63.9mm$$

Rounding this value up to the nearest 5 millimeters provides a preliminary value of a 65mm diameter for the prime mover input shaft diameter.

A preliminary drawing of this shaft can was created using Solidworks 3D modeling software. The model includes seats for two deep groove ball bearings, threading for a lock nut, a keyway to attach the prime mover pinion gear, a shoulder to seat this gear, a groove to seat a c-clip for the non-locating bearing, and a shoulder for this bearing to sit against. This drawing is seen in **Figure 20** and the model with critical features labeled in **Figure 21.**

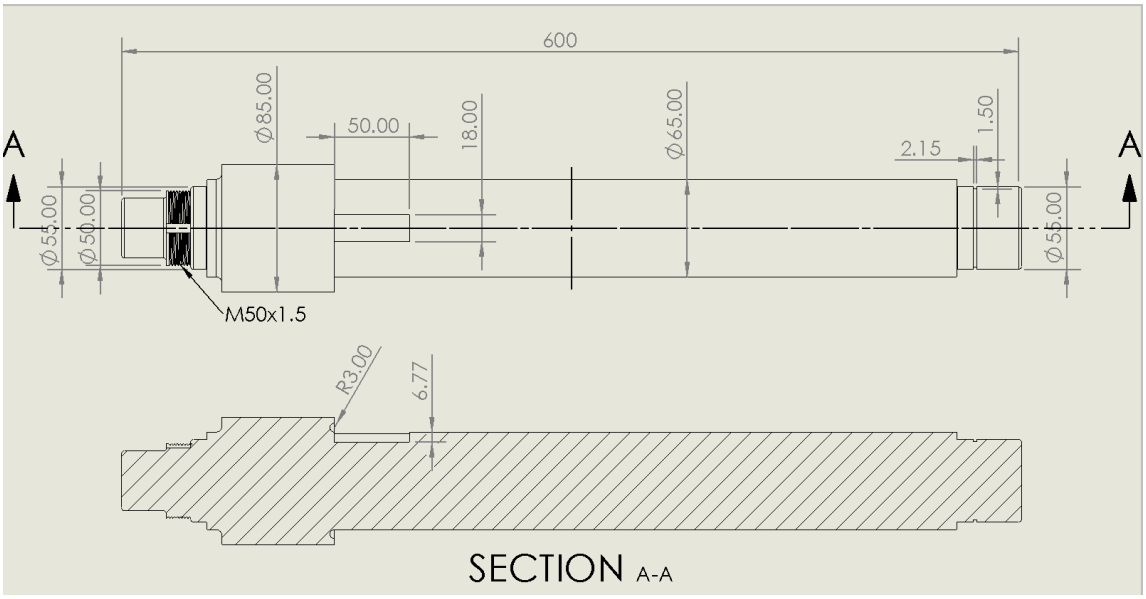

Figure 20: *Preliminary Dimensions for Prime Mover Input Shaft (Units in mm)*

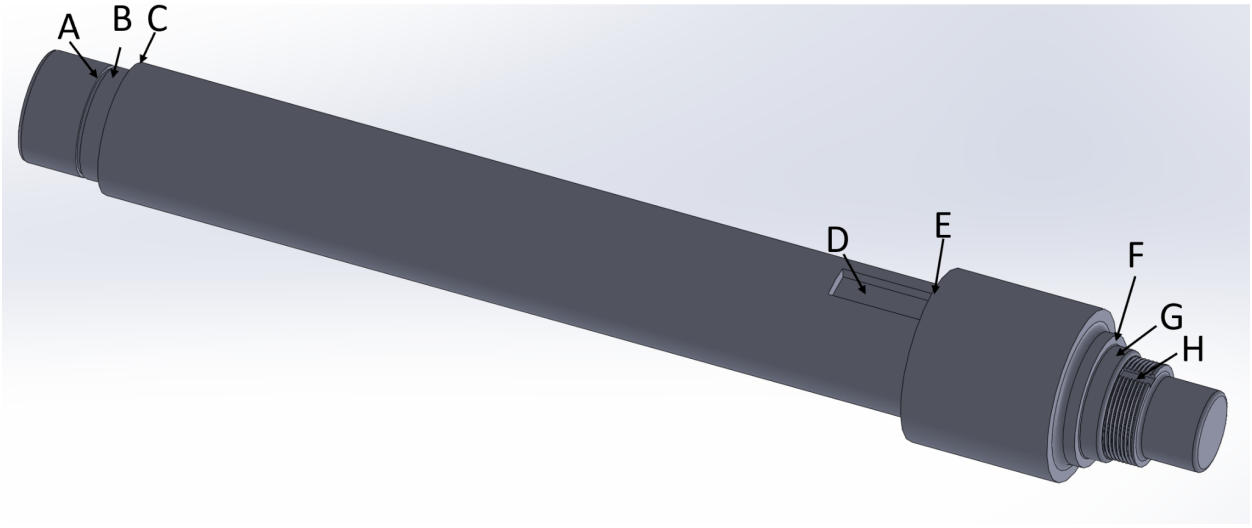

Figure 21: *Preliminary Prime Mover Input Shaft Model*

The critical features labeled above are described below in **Table 18:**

Table 18: *Feature list for diesel input shaft*

Label	Feature
A	Retaining ring groove
B	Floating deep groove ball bearing seat
C	Floating deep groove ball bearing abutment shoulder
D	Gear D1 keyway
E	Gear D1 Shoulder
F	Locating deep groove ball bearing abutment shoulder
G	Locating deep groove ball bearing seat
H	M50x1.5 external thread for bearing retaining lock nut

The initial bearing style chosen for this shaft were deep groove roller bearings. This decision was based off recommended configurations for input shafts by "Rolling Bearings in Industrial Gear Boxes" seen below in **Figure 22** [11].

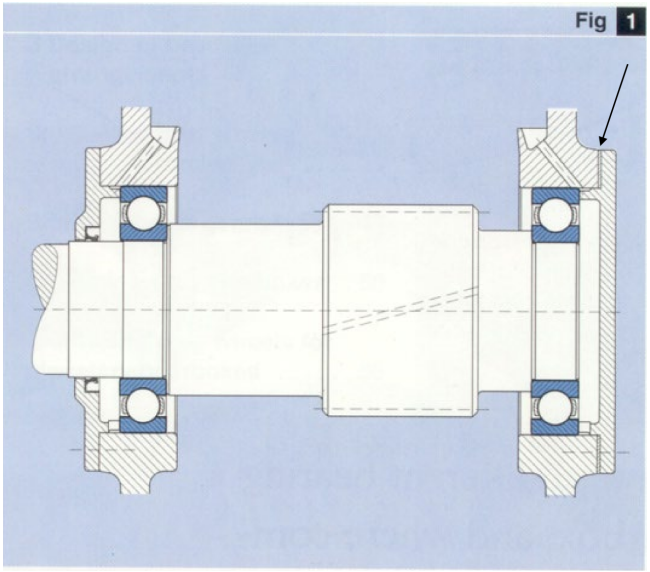

Figure 22: *Recommended Bearing Selection for Input Shafts [11]*

This bearing selection is ideal for the high speed and light axial loads placed on this shaft by the prime mover. The bearings initially selected for this application are SKF 16011 deep groove bearings with a 55mm bore diameter. The bearings required abutments are seen pictured below in **Figure 23.**

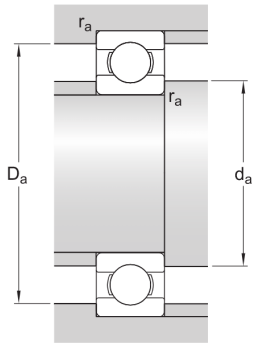

Abutment dimensions

d_a	min. 58.2 mm	Diameter of shaft abutment
D_a	max. 86.8 mm	Diameter of housing abutment
r_a	max. 0.6 mm	Radius of shaft or housing fillet

Figure 23: *Abutment Dimensions for Prime Mover input Shaft [12]*

As seen in the shaft drawing in **Figure 23**, the bearing seats onto the shaft at locations of corresponding diameter of the bore. The abutments the bearings sit against are 65mm which is over the minimum required diameter. The fillets on this abutment were also designed to match the maximum radius of shaft fillets specified by the bearing to ensure tight seating with limited stress concentration.

To mount the fixed bearing, a M50x1.5 lock nut and spring lock washer are used. This nut threads directly onto the shaft and the spring lock washer's tab sits in a slot machine in the shaft. This configuration is seen below in **Figure 24.**

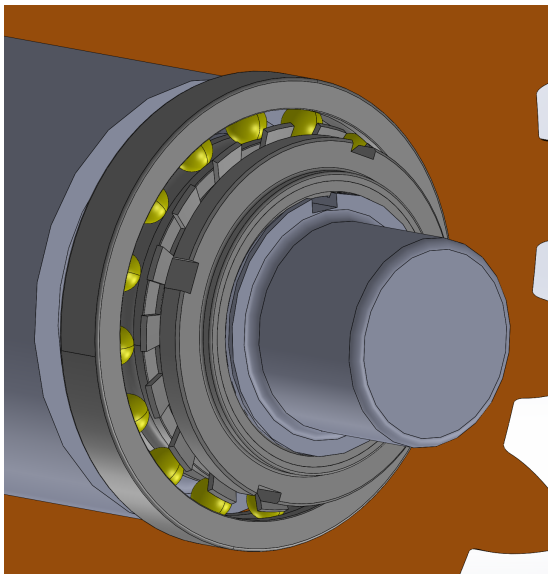

Figure 24: *Fixed Bearing Mounted with Lock Nut and Spring Lock Washer*

To mount the floating bearing, a retaining ring was placed in a groove next to the bearing. The ring used is a standard stainless steel c-clip for a shaft diameter of 55mm sold by McMaster Carr. Dimensions for the groove seen in the drawing above were determined by recommended dimensions on McMaster Carr. The floating bearing configuration is seen below in **Figure 25.**

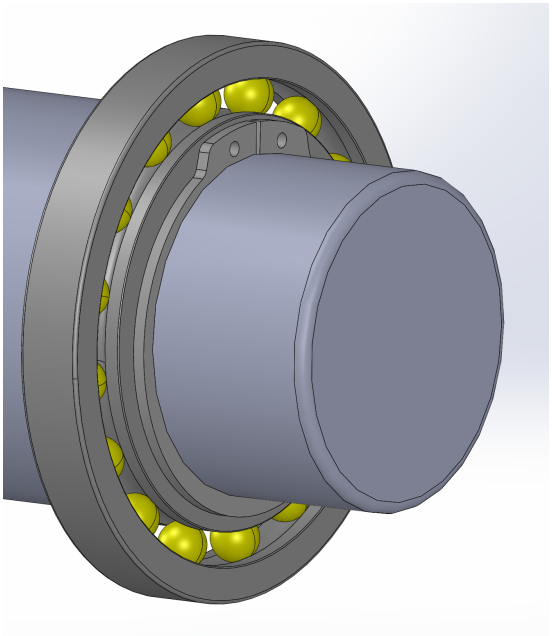

Figure 25: *Floating Bearing Mounted with Retaining Ring*

The gear, previously label D1, is mounted to the shaft by a keyway, shoulder, and a shaft collar. The keyways dimensions seen in the drawing above were determined by recommended key sizes for shaft diameters found in “Machine Design” [11]. One one side, the gear is held by a 10mm shoulder. As seen in the section view of the shaft drawing, the shoulder has 3mm radius undercut grooves to limit the stress concentration while still ensuring a flat face for the gear to seat against. The other side of the gear is held in place by a stainless steel clamping two piece shaft collar for 65mm shafts sold by McMaster Carr. This gear affixing arrangement is seen with the gear itself omitted for clarity below in **Figure 26.**

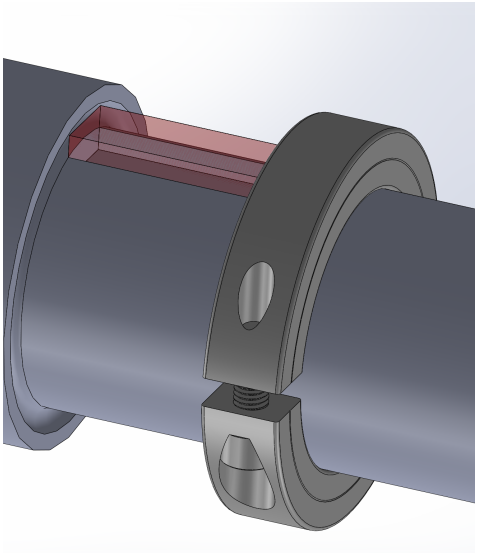

Figure 26: *Gear Affixing Arrangement*

Altogether, the shaft with its gear, bearings, and locating components is seen below in **Figure 27** with a section view seen in **Figure 28.**

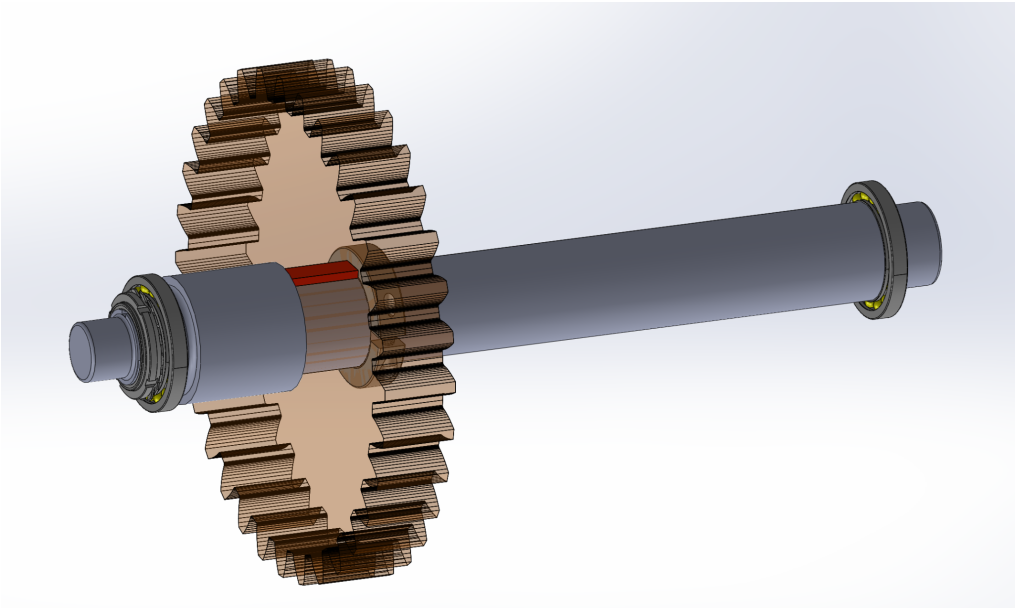

Figure 27: *Prime Mover Input Shaft Arrangement*

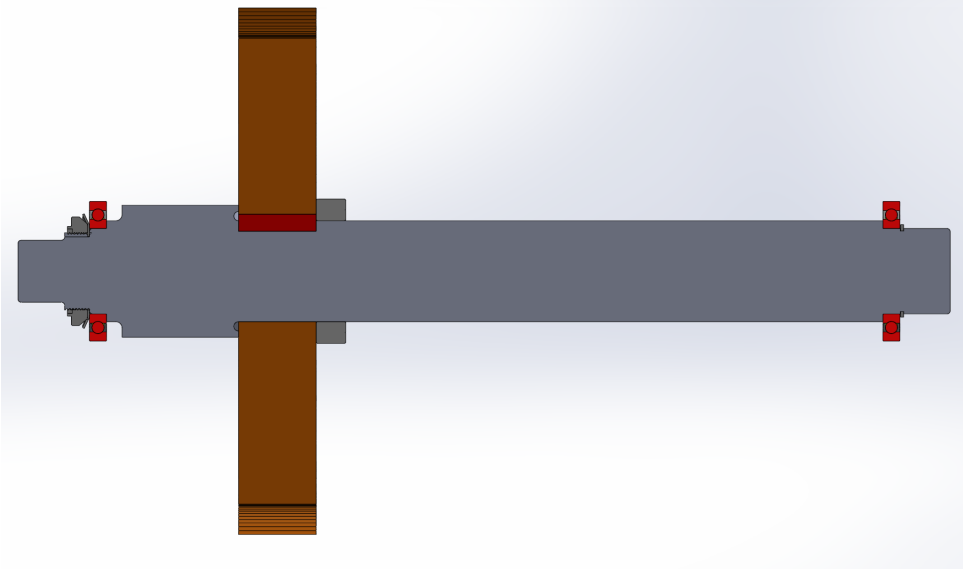

Figure 28: *Section View of Prime Mover Input Shaft Arrangement*

The major areas requiring failure analysis on the prime mover input shaft are labeled below in **Figure 29.**

Figure 29: *Areas of Stress Concentration on Diesel Input Shaft*

A cylindrical shaft is most likely to fail at the point of a stress raiser. A stress raiser commonly occurs when the diameter of the shaft is abruptly changed. In the prime mover input shaft there are three relevant areas where this occurs as seen labeled above in **Figure 29.** Locations 1 and 3 are at the corners of the bearing seat and shoulder abutments. Due to the need to seat bearings in these locations, fillet sizes are limited by the bearing specifications. This leads to an abrupt size change with only small fillets to ease stress concentration. Location 2 is of less concern due to the undercut fillets on the gear shoulder. However, the sharp angles of the key way and this location should be noted.

All three of these areas should be analyzed closer using fatigue and load calculations accounting for the gearboxes planned use cases. These calculations, if the design is successful, will reveal a lifetime of the part within a factor of safety of the desired lifetime. If by doing these analyses it is deemed that there is possibility of failure, changes must be made to the shaft design. Changes that may be required to decrease stress include increasing shaft diameter and increasing fillet radius. It should be noted that either of these changes if applied to locations 1 or 3 will require alterations to the bearings selected.

3.2.2 Electric Motor Input Shaft

Next, the same analysis completed for the prime mover input shaft will be completed for the electric input shaft. As previously discussed, this shaft is provided input from the electric motor and turns gear E1. Features that are similar to the diesel input shaft will be discussed in less detail.

Similarly to the diesel input shaft, the electric motor input shaft diameter can be estimated from maximum shear stress and torque. With a torque of 4774 Nm and the same max shear stress of 465.75 MPa, the diameter of the shaft can be calculated as follows:

$$d = \sqrt[3]{\frac{16(4774\ Nm)}{\pi(465.75x10^{6}Pa)}} = 37.37mm$$

Which can then be rounded up to 40mm to make it easier to source bearings.

Again, the electric motor input shaft is very similar to the diesel input shaft but with one major difference. Since the electric input shaft has a small diameter, the pinion gear can be machined right into the shaft instead of coupling the gear to the shaft with a keyed joint. A model of electric shaft assembly can be observed in **Figure 30.**

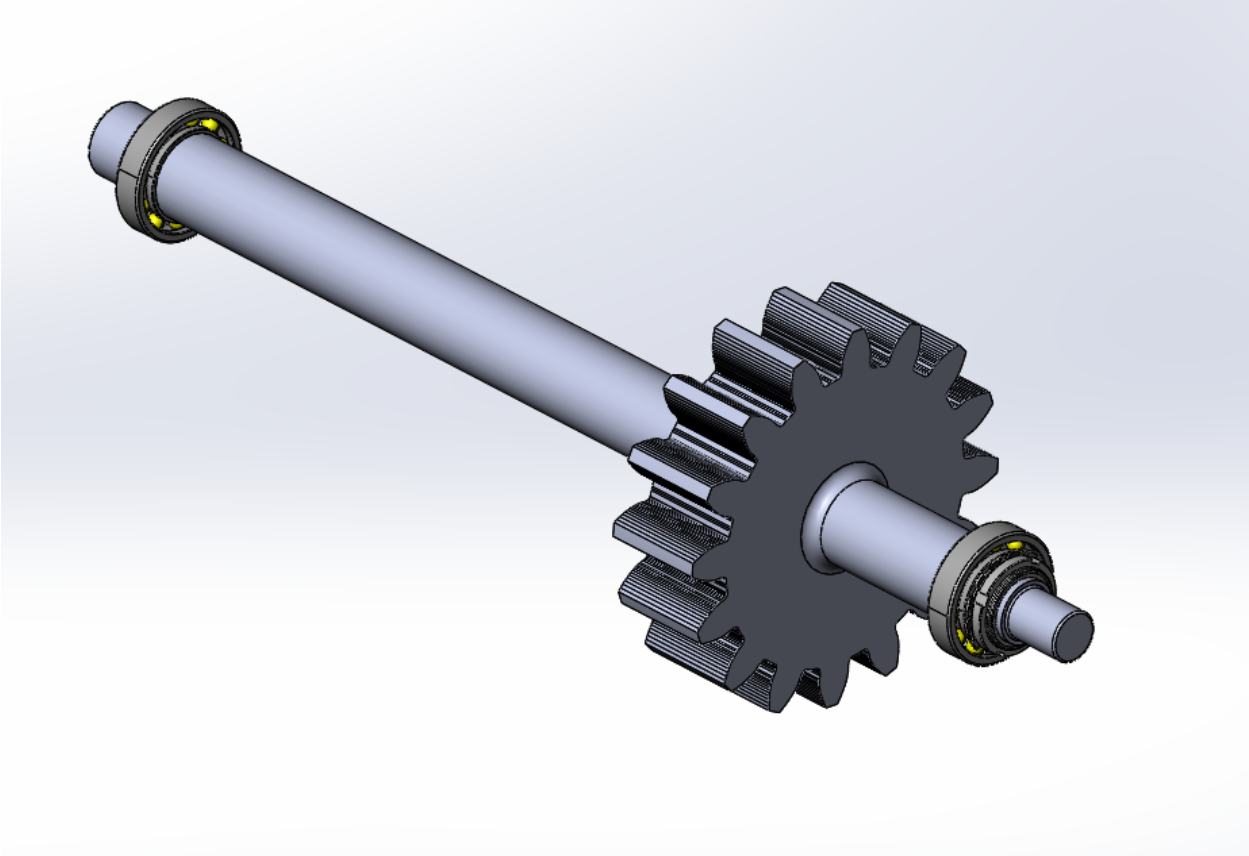

Figure 30: *Electric input shaft assembly*

Then by looking at the shaft itself, the mounting features for each of the elements can be analyzed. An isometric view of the part with its features labeled in **Table 19** can be observed in **Figure 31.**

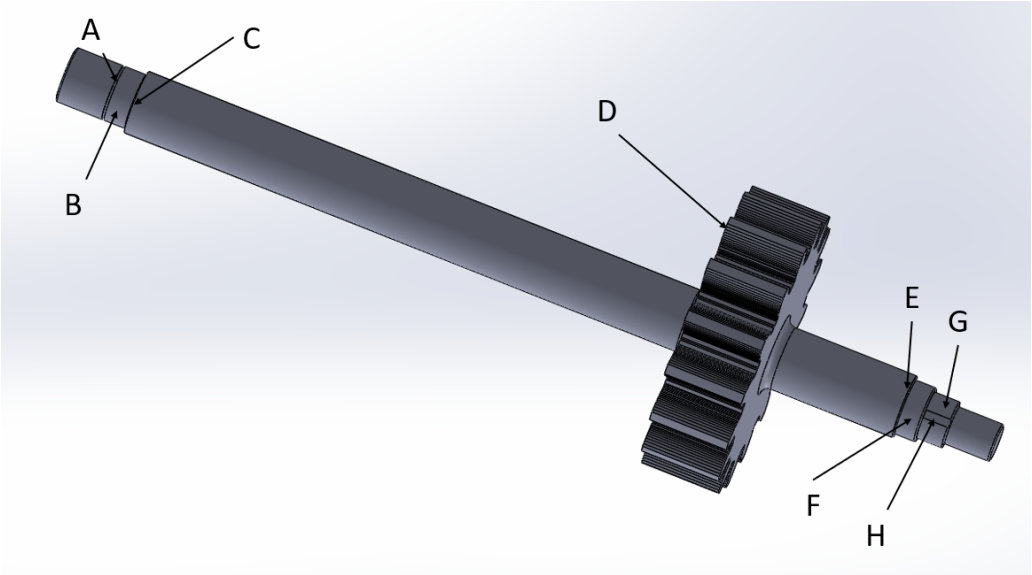

***Figure 31**: Electric motor input shaft features*

***Table 19:** Feature list for electric input shaft*

Label	Feature
A	Retaining ring groove
B	Floating deep groove ball bearing seat
C	Floating deep groove ball bearing abutment shoulder
D	Machined pinion-shaft
E	Locating deep groove ball bearing abutment shoulder
F	Locating deep groove ball bearing seat
G	M30x1.5 external thread for bearing retaining lock nut
H	Groove for spring washer attachment

An engineering drawing was also created for the electric input shaft showing the preliminary dimensions of relevant features. This drawing can be consulted in **Figure 32**.

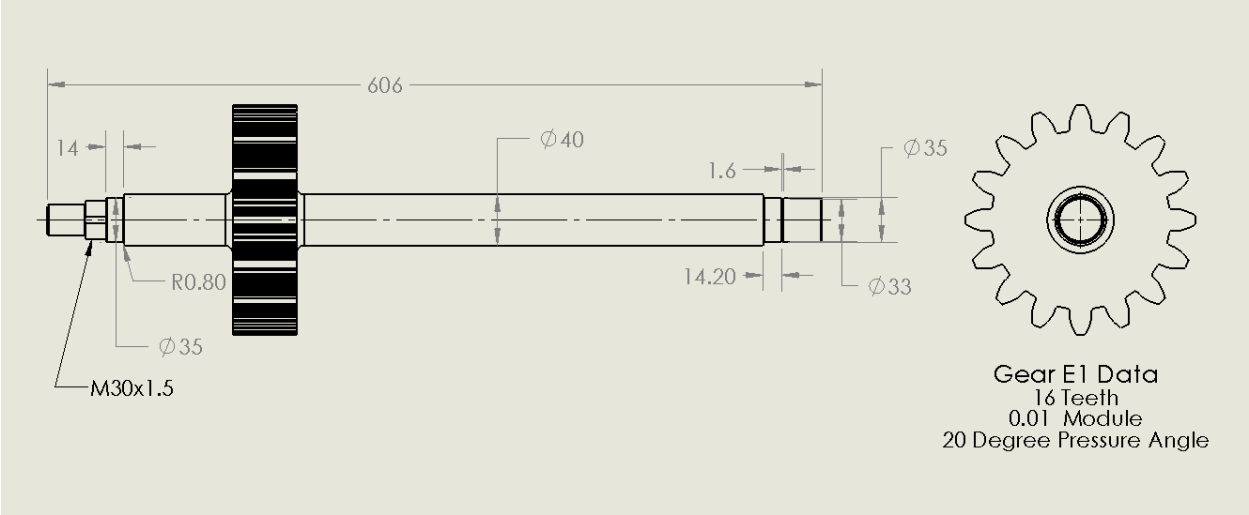

***Figure 32**: Electric motor input shaft engineering drawing (Dimensions in mm)*

Each of the design choices made in the creation of the electric input shaft were based on research and sources similar to the diesel input shaft. The bearings used for this shaft are deep groove ball bearings, which is the same as the diesel input shaft as they are one recommended configuration for input shafts that have more speed and less torque. The dimensions for the ball bearings used in this preliminary design are provided in **Figure 33**.

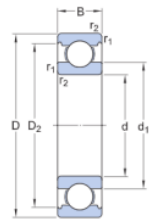

Dimensions

d	35 mm	Bore diameter
D	62 mm	Outside diameter
B	14 mm	Width
d_1	≈ 43.75 mm	Shoulder diameter
D_2	≈ 55.61 mm	Recess diameter
$r_{1,2}$	min. 1 mm	Chamfer dimension

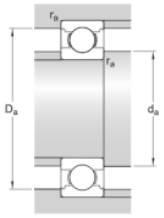

Abutment dimensions

d_a	min. 39.6 mm	Diameter of shaft abutment
D_a	max. 57.4 mm	Diameter of housing abutment
r_a	max. 1 mm	Radius of shaft or housing fillet

Figure 33: *Deep groove ball bearings dimensions for electric input shaft [12]*

Dimensions of note are the diameters of shaft abutment and the radius of shaft fillet. These dimensions were accounted for in the shaft design as the shoulder of the shaft that abuts the bearing is 40mm which is larger than the minimum diameter of 39.6mm. The radius of the shaft fillet at that shoulder is also set at 0.8mm which is less than the max of 1mm.

The securing of the locating and free bearing for the input electrical shaft is the same as the diesel input shaft as described in section 8.1.1 but with different sized retaining rings and lock nuts. The locating bearing is secured with a M30x1.5 lock nut and locking washer from Mcmaster-Carr, while the floating bearing is secured with a 35mm retaining ring that is spaced 0.2mm from the bearing to allow for thermal expansion.

As discussed in the prime mover shaft analysis, failure in cylindrical shafts is likely to occur at stress risers. There are four relevant areas where this occurs and are labeled in **Figure 34** below.

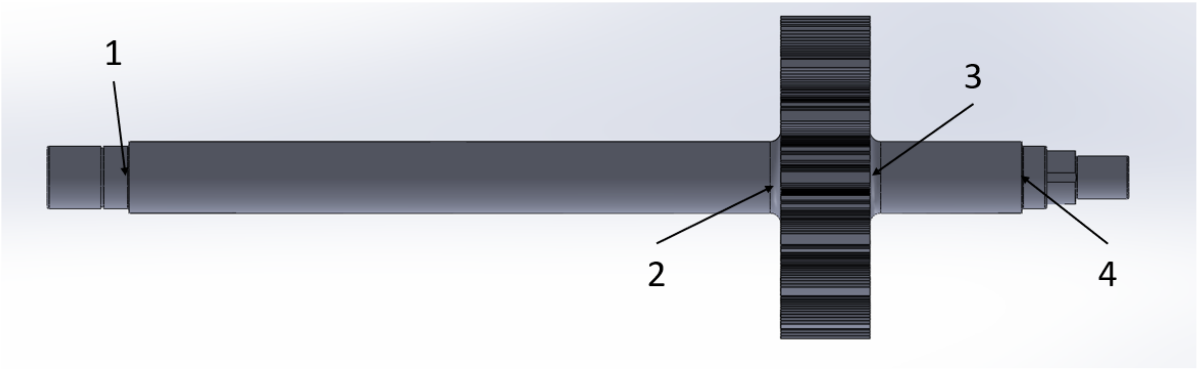

***Figure 34**: Areas of stress concentration on electrical input shaft*

Areas 1 and 4 are likely the largest source of stress as they are the shoulder which the bearings abut against. The bearings are designed to carry the majority of the radial load experienced by the shaft and are therefore an integral part of the shaft. With large loads comes large stresses which in turn can cause failure. Seeing as the shoulder is a stress concentration it is important to look at an area with high stress that is then also increased by stress concentrations. Areas 2 and 3 are also of interest for failure analysis as they also see a dramatic change in shaft diameter that leads to a stress concentration. This is then coupled with the stress caused by the meshing of gears near these points that create forces and thus induce stresses. As discussed in the prime mover shaft analysis, if calculations determine these areas to limit the life of the shaft below required, then design changes will need to be made.

3.2.3 Reduction Shaft

The next shaft to be analyzed is the reduction shaft. This shaft takes input into gears E2 and D2 from the two input shafts and provides a single output through gear E3/D3. For simplicity, design principles from other shafts that are applied again will be discussed in less detail.

The reduction shaft, spinning at lower speeds than the two input shafts, is under higher torque. As such, the preliminary shaft diameter was increased to 70mm from the 65mm diameter determined for the prime mover input shaft. A preliminary drawing of this shaft and CAD model outlining critical features is seen below in **Figures 35** and **36.**

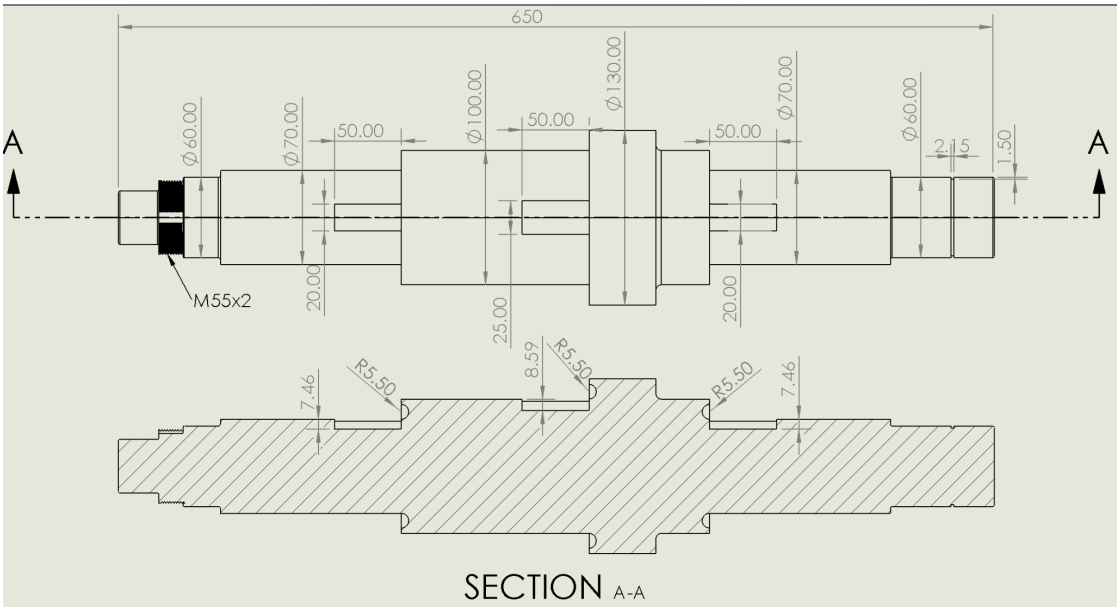

Figure 35: *Preliminary Dimensions for Reduction Shaft (Units in mm)*

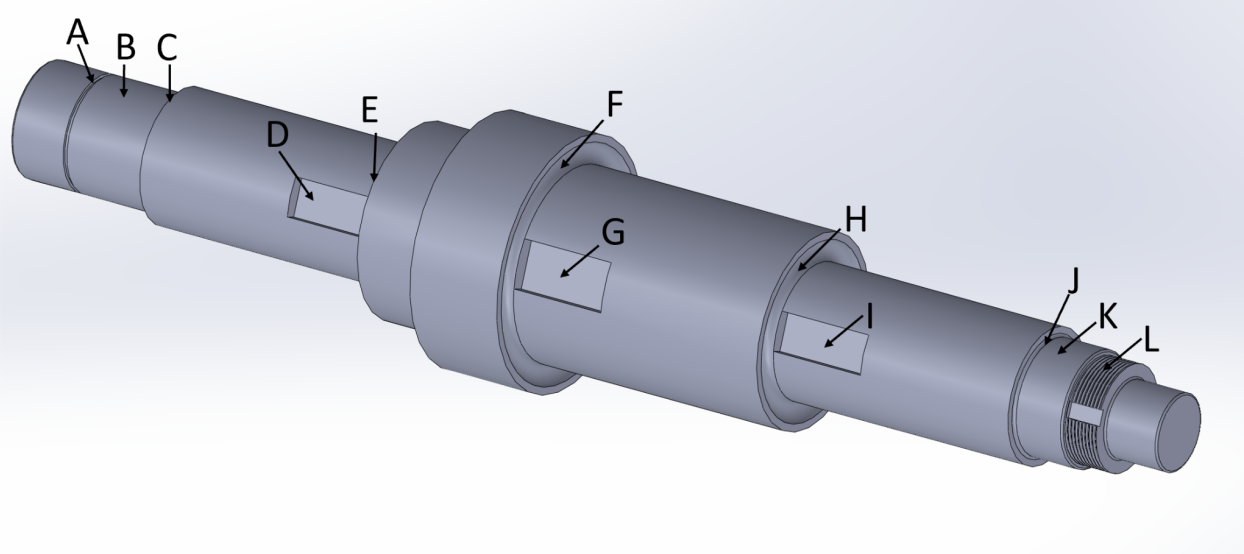

Figure 36: *Preliminary Reduction Shaft Model*

The critical features labeled above are described below in **Table 20**

Table 20: *Feature list for reduction shaft*

Label	Feature
A	Retaining ring groove
B	Bearing seat
C	Bearing abutment shoulder
D	Gear D2 key way
E	Gear D2 shoulder
F	Gear E3/D3 shoulder
G	Gear E3/D3 key way
H	Gear E2 shoulder
I	Gear E2 key way
J	Bearing abutment shoulder
K	Bearing seat
L	Lock nut threads

The initial bearing styes selected for this shaft is a floating CARB bearing and a fixed spherical roller bearing. This decision was based off recommended configurations for intermediate shafts by “Rolling Bearings in Industrial Gear Boxes” seen below in **Figure 37** [11].

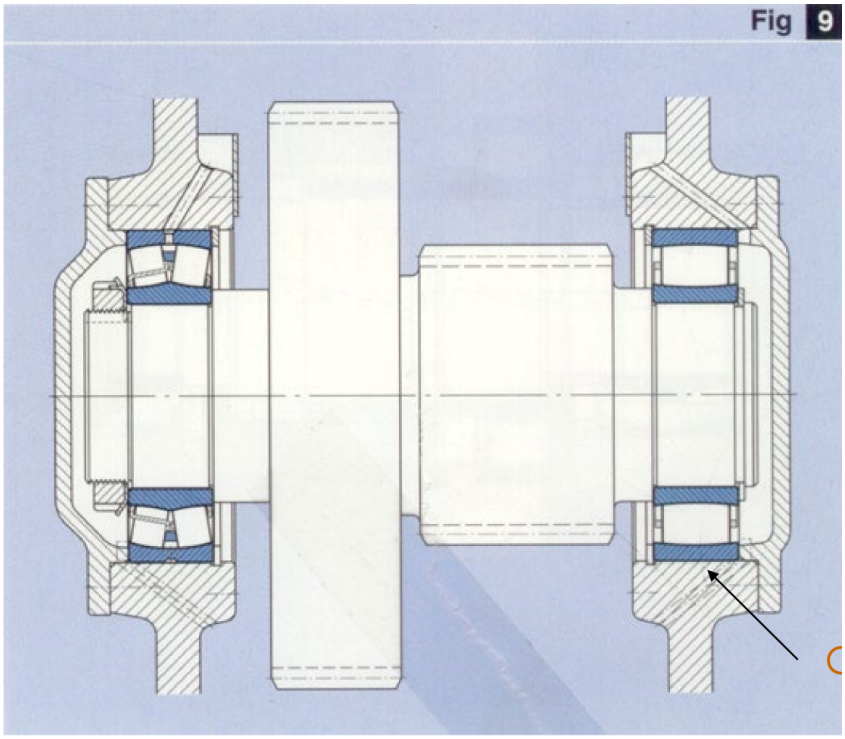

Figure 37: *Recommended Bearing Selection for Intermediate Shafts [11]*

This bearing configuration is ideal for the increased torques of the reduction shaft and the floating CARB bearing allows for angular misalignment that may occur due to multiple inputs into one shaft. The bearings initially selected for this shaft are SKF 22212 Spherical roller bearings with a 60mm bore diameter and a SKF C 6912V CARB bearings with a 60mm bore diameter. The bearings required abutment diameters are seen below in **Figures 38** and **39**.

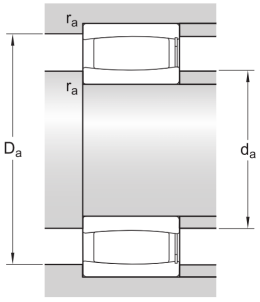

Abutment dimensions

d_a	min. 64.6 mm	Diameter of shaft abutment
d_a	max. 72 mm	Diameter of shaft abutment
D_a	max. 80.4 mm	Abutment diameter housing
r_a	max. 1 mm	Radius of fillet

Figure 38: *Abutment Dimensions for Reduction Shaft CARB Bearing [12]*

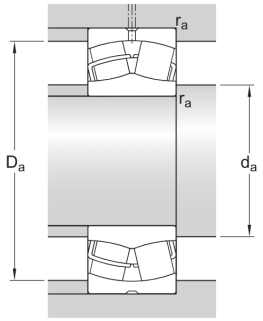

Abutment dimensions

d_a	min. 69 mm	Diameter of shaft abutment
D_a	max. 101 mm	Diameter of housing abutment
r_a	max. 1.5 mm	Radius of fillet

Figure 39: *Abutment Dimensions for Reduction Shaft Spherical Roller Bearing [12]*

As seen in the shaft drawing above, the shaft seats, and abutment diameters correspond to those required by the bearings. The floating and fixed bearings are affixed in the same manner as the diesel input shaft. A M55x2 lock nut and spring washer holds the fixed spherical roller bearing in place and a 60mm retaining ring holds the floating CARB bearing. As previously, these components were sourced from McMaster Carr.

The gears mounted on this shaft are E2, D2, and E3/D3. Gears E2 and D2 are mounted in the same manner as the prime mover input shaft gear D1. This was achieved by using a key way (with dimensions determined from “Machine Design”), a shoulder with undercut grooves, and a shaft clamp for 70mm shafts sold by McMaster Carr. The central gear E3/D3 is mounted similarly, with the exception of the shaft clamp. Due the 100mm shaft size at this gear’s location, a large enough shaft clamp could not be purchased. Instead, a custom machined stainless steel shaft collar will be used to separate gear E3/D3 from gear E2. The mounting of this gear and the collar design are seen below in **Figures 40** and **41**.

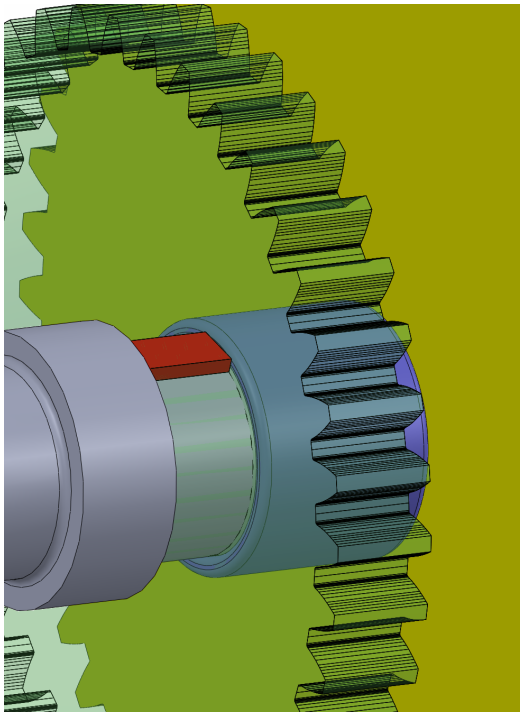

Figure 40: *Gear E3/D3 Mounting*

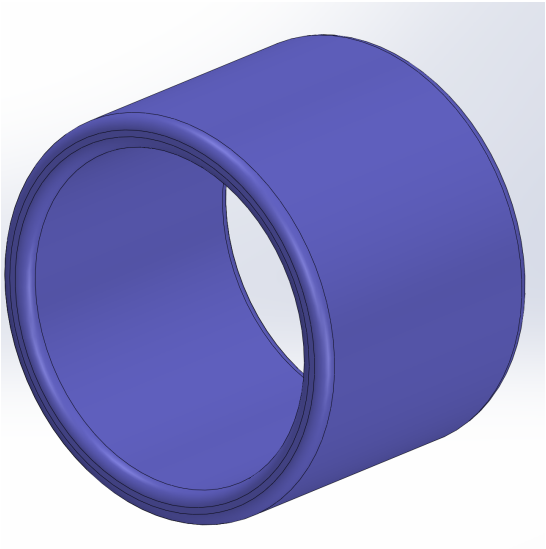

Figure 41: *Reduction Shaft Collar*

Alltogather, the shaft with its gear, bearings, and locating components is seen below in **Figure 42** with a section view seen in **Figure 43.**

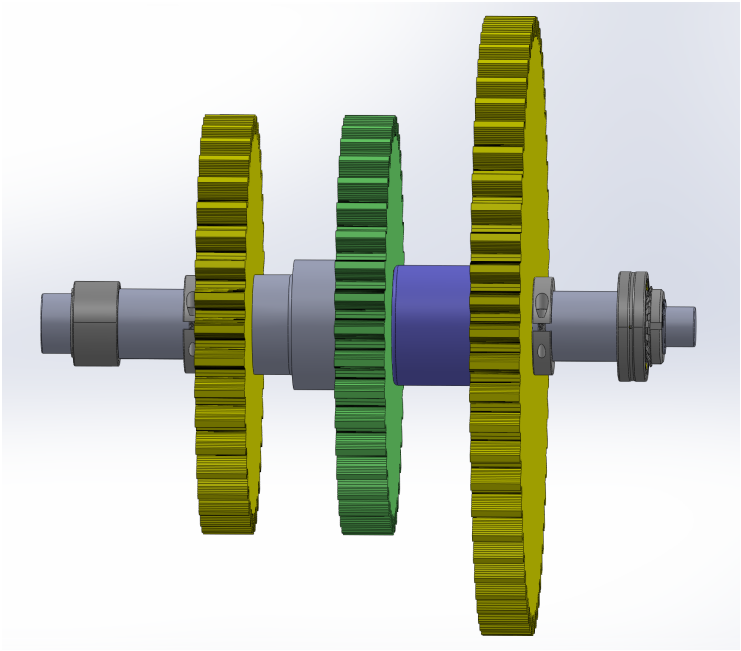

Figure 42: *Reduction Shaft Arrangement*

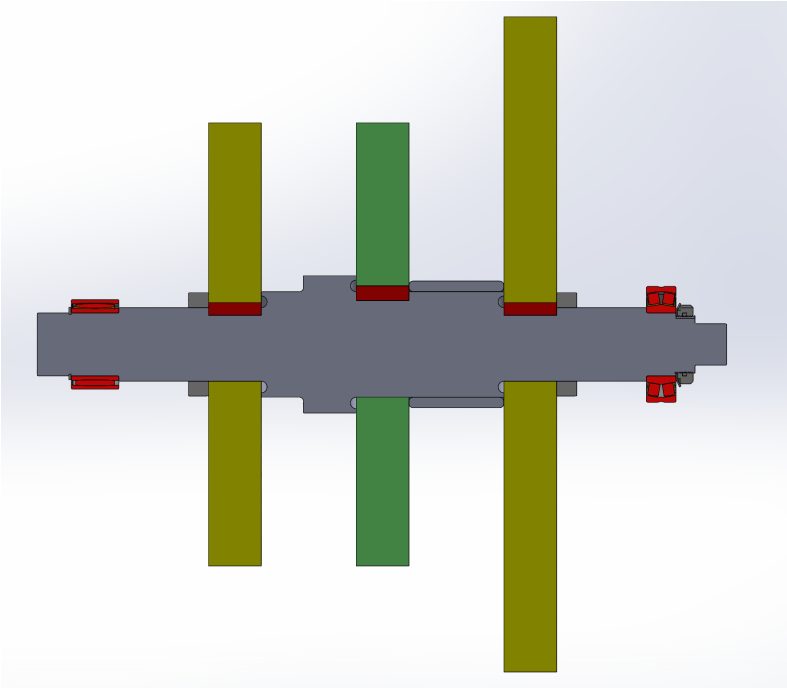

Figure 43: *Section View of Reduction Shaft Arrangement*

As discussed in the prime mover shaft analysis, failure in cylindrical shafts is likely to occur at stress risers. There are five relevant areas where this occurs and are labeled in **Figure 44** below.

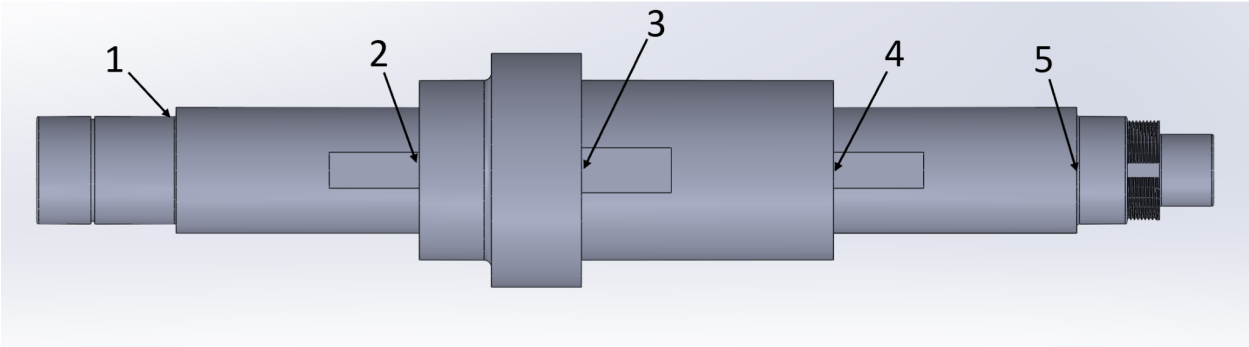

Figure 44: *Areas of stress concentration on Reduction Shaft*

Locations 1 and 5 exist at the corner between the bearing seats and abutment shoulders. While locations 2, 3, and 5 exist at the corners of gear seating shoulders. As before, the major area of concern at the gear seating shoulders is at the corners of the key ways.

3.2.4 Output Shaft

The final shaft to be discussed is the output shaft. This shaft takes input from the reduction shaft into gear D4/E4 and provides output to the propeller. As previous, areas with similar design principles will be discussed in less detail.

Similarly to the diesel input shaft, the electric motor input shaft diameter can be estimated from maximum shear stress and torque. With a torque of 90718Nm and the same max shear stress of 465.75 MPa, the diameter of the shaft can be calculated as follows:

$$d = \sqrt[3]{\frac{16(90718Nm)}{\pi(465.75x10^{6}Pa)}} = 99.73mm$$

Again, this value was rounded up, this time to 100mm. A preliminary drawing of this shaft is seen below in **Figure 45** and a CAD model with critical features is seen below in **Figure 46.**

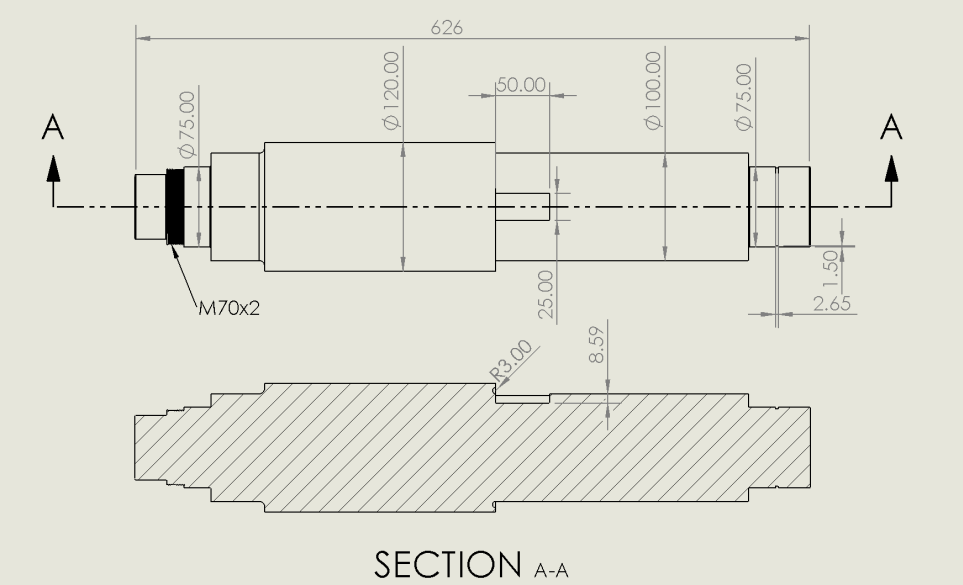

Figure 45: *Preliminary Dimensions for Output Shaft (Units in mm)*

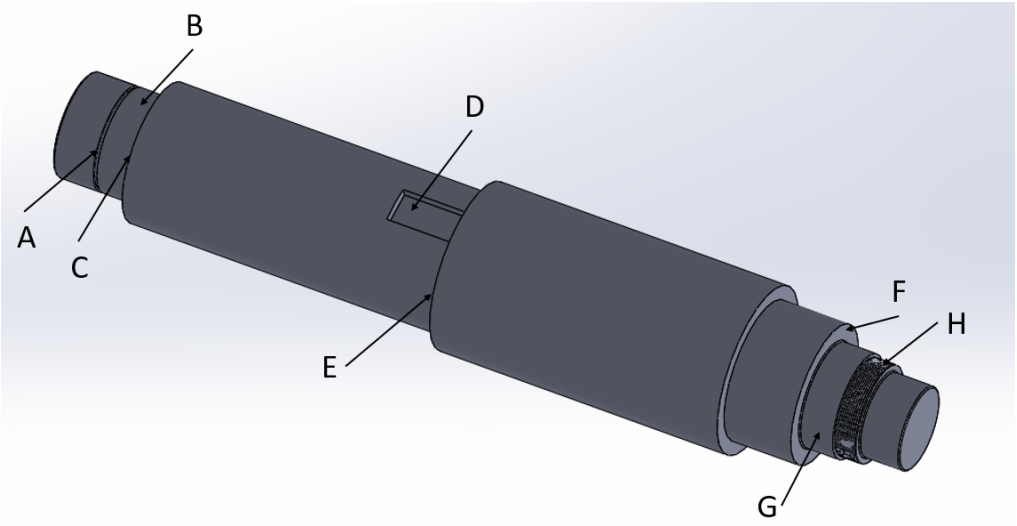

Figure 46: *Preliminary Output Shaft Model*

The critical features labeled above are described below in **Table 21:**

Table 21: *Feature list for output shaft*

Label	Feature
A	Retaining ring groove
B	Floating cylindrical roller bearing seat
C	Floating cylindrical roller bearing abutment shoulder
D	Gear E4/D4 keyway
E	Gear E4/D4 shoulder
F	Locating cylindrical roller bearing abutment shoulder
G	Locating cylindrical roller bearing seat
H	M70x2 external thread for bearing retaining locknut

The initial bearing style selected for this shaft are cylindrical roller bearings. This design choice was made knowing that this shaft has low axial load, high radial load, and low speeds. Cylindrical roller bearings are a suitable bearing style for these criteria as they are better designed for radial loads than ball bearings, and are simple to mount and dismount. This design choice was also made in part by the bearing configuration recommendation seen in the Machine Design textbook written by Norton and shown in **Figure 47** [11].

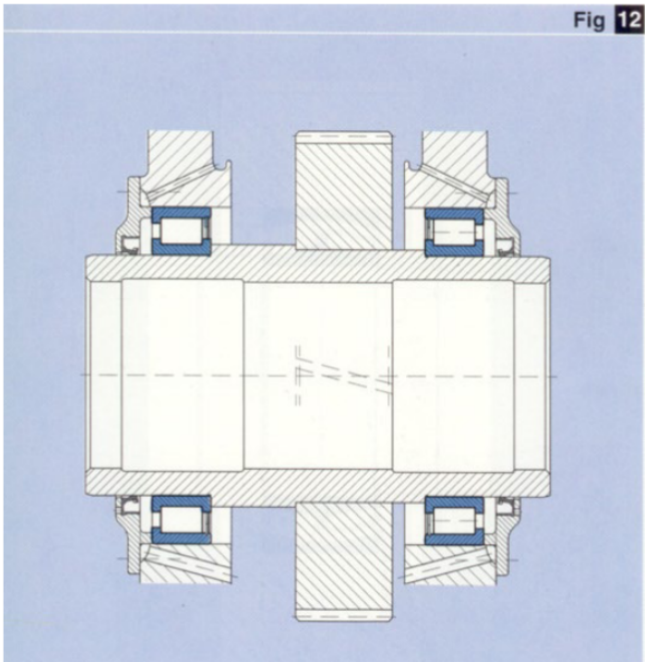

Figure 47: *Output shaft bearing configuration using cylindrical roller bearings [11]*

For the preliminary output shaft design, the specific type of roller bearing chosen was NU roller bearings. Similar to the input shaft design with ball bearings, NU roller bearings are non locating and can accommodate axial displacement in both directions which is important for dealing with thermal expansion. The dimensions for the preliminary SKF NU cylindrical roller bearings chosen are shown below in **Figure 48.** Like all the other shafts, the minimum and maximum abutment dimensions were utilized in the shaft design to properly seat the bearings.

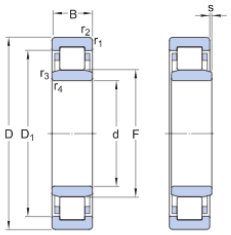

Dimensions

d	75 mm	Bore diameter
D	130 mm	Outside diameter
B	25 mm	Width
D_1	≈ 113.3 mm	Shoulder diameter of outer ring
F	88.5 mm	Raceway diameter of inner ring
$r_{1,2}$	min. 1.5 mm	Chamfer dimension
$r_{3,4}$	min. 1.5 mm	Chamfer dimension
s	max. 1.2 mm	Permissible axial displacement

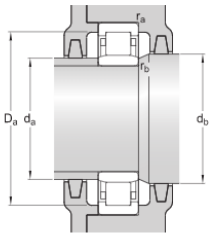

Abutment dimensions

d_a	min. 84 mm	Diameter of spacer sleeve
d_a	max. 86 mm	Diameter of spacer sleeve
d_b	min. 91 mm	Diameter of shaft abutment
D_a	max. 121.5 mm	Diameter of housing abutment
r_a	max. 1.5 mm	Radius of fillet
r_b	max. 1.5 mm	Radius of fillet

***Figure 48**: SKF NU cylindrical roller bearing dimensions for output shaft [12]*

The gear mounted on this shaft is E4/D4. This gear is mounted through a key way, and shoulder with designs as described previously for the prime mover input shaft and the reduction shaft. The difference with the gear mounting on this gear is the use of a 100mm set screw collar to hold the other side. As was the issue with the reduction shaft, 100mm shaft clamps cannot be purchased from McMaster Carr so this alternate method is required. The mounting of this gear and the set screw collar is seen below in **Figure 49.**

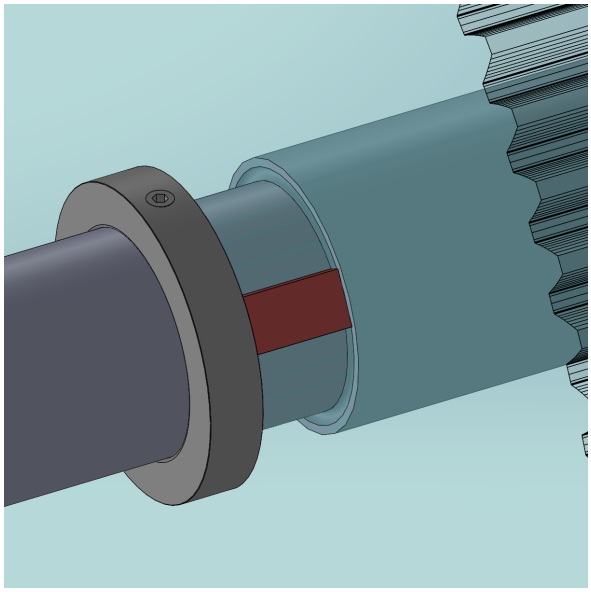

Figure 49: *Gear E4/D4 Mounting*

Altogether, the shaft with its gear, bearings, and locating components is seen below in **Figure 50** with a section view seen in **Figure 51.**

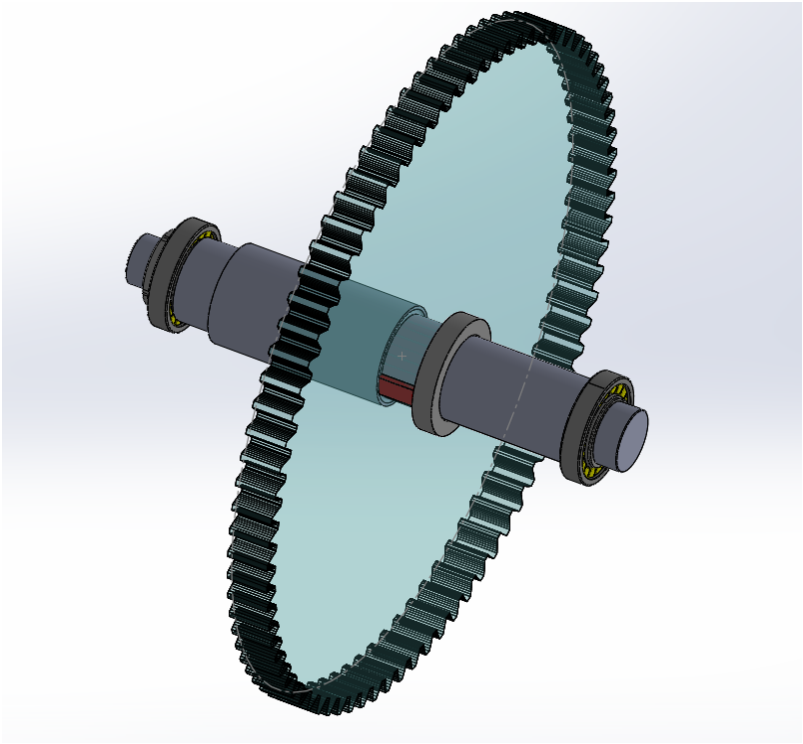

Figure 50: *Output Shaft Arrangement*

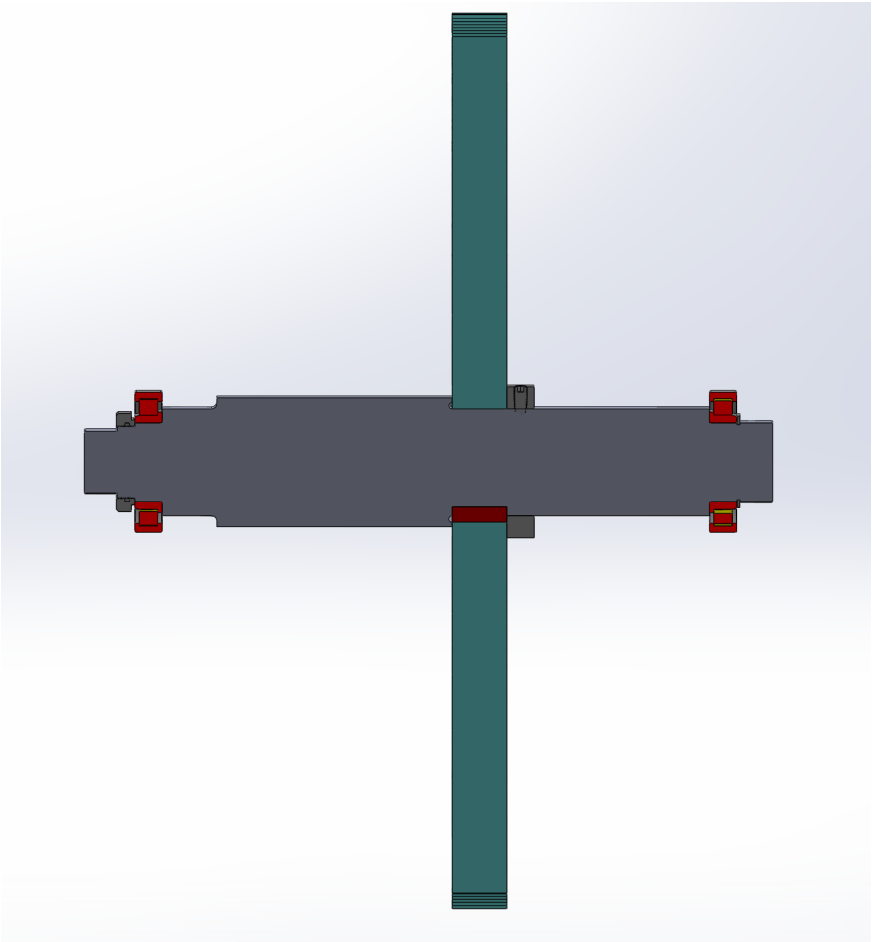

Figure 51: *Section View of Output Shaft Arrangement*

As discussed in the prime mover shaft analysis, failure in cylindrical shafts is likely to occur at stress risers. There are five relevant areas where this occurs and are labeled in **Figure 52** below.

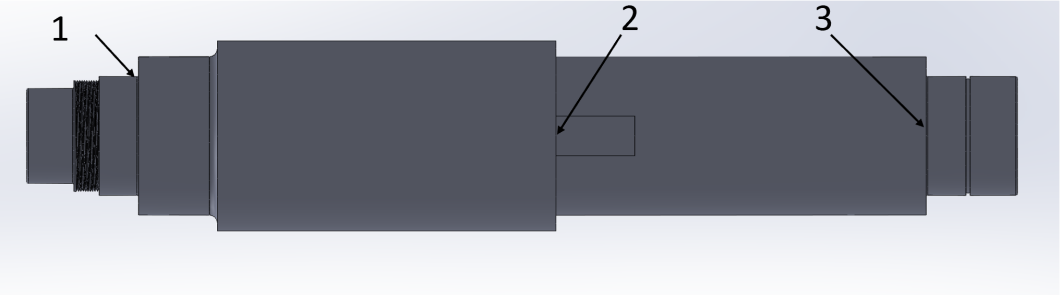

Figure 52*: Areas of stress concentration on Output shaft*

Locations 1 and 3 exist at the corner between the bearing seats and abutment shoulders. While location 2 exists at the corners of gear seating shoulders. As before, the major area of concern at the gear seating shoulders is at the corners of the key ways. Analysis for this shaft will be very similar to previous shafts.

4 Design Stage Three: Failure Analysis and Sizing

The following section will build on the qualitative design by performing required stress and fatigue calculations. These calculations will be used to resize components to ensure operation within a desired safety factor. Along with re-sizing, certain aspects will be refined to both accommodate new component dimensions and to improve operation.

4.1 Detailed Gear Design

The main consideration for the detailed gear design is fatigue from cyclical loading, and the bending and surface stresses associated with daily operation. To finalize the design, the bending stresses surface stresses were calculated, and compared to the associated bending and surface strength of the material. The gears were then scaled, by adjusting the module and face-width until the stresses fell within reasonable values with respect to the fatigue strength. After several iterations, a final module was selected, defining the radii of each gear, and the overall size of the gearbox. The final selected gear radii were relatively large, and no two-piece collars were available in the proper size. To accommodate this, the axial locating method to affix the gears to each shaft has been changed from a two-piece collar assembly to a set-screw. The set-screw is driven into the key, through a collar machined directly onto the gear, visible in **Figure 53**. This is discussed in more detail under **Detailed Shaft Design**. The final gear specifications are tabulated in **Table 22**, and a final summary of the gear parameters is tabulated in **Table 23**.

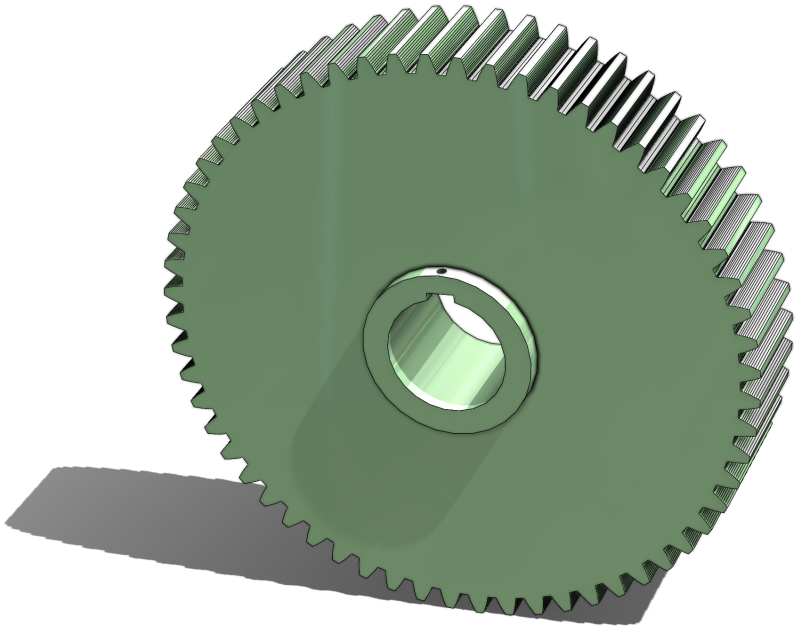

Figure 53: *E2 Gear, with set-screw collar visible.*

Table 22: *Gear specifications*

Module m [mm]	20
Face Width [mm]	240
Pressure Angle [degrees]	20
Material	A5 Steel

Table 23: *Summary of Gear Parameters*

Gear Name	Teeth Number N	Radius r [m]	Module m	Speed w	Torque T	Power [W]	Cycles at Low Speed	Cycles at High Speed	Cycles at Full Power
E1	24	0.24	0.02	314	4775	1500000	2.37E+09	7.25E+09	1.58E+09
D1	48	0.48	0.02	105	23873	2500000	0.00E+00	2.42E+09	5.26E+08
E2	60	0.6	0.02	126	11937	1500000	9.46E+08	2.90E+09	6.31E+08
D2	40	0.4	0.02	126	19894	2500000	9.46E+08	2.90E+09	6.31E+08
E3D3	30	0.3	0.02	126	31831	4000000	9.46E+08	2.90E+09	6.31E+08
E4D4	90	0.9	0.02	42	95493	4000000	3.15E+08	9.67E+08	2.10E+08

4.1.1 Fatigue Strength of Gears

Before calculating stresses, the fatigue strength is calculated, and then the safety factor can be calculated.

Bending Fatigue, Safety Factor

$$SF_{bending} = \frac{S_f}{\sigma_b}$$

Surface Fatigue, Safety Factor:

$$SF_{surface} = \left(\frac{S_{fc}}{\sigma_c}\right)^2$$

4.1.2 Bending Fatigue Factors

The bending strength is given by the following relationship.

$$S_{fb} = \frac{K_L}{K_T K_R} S'_{fb}$$

Where

$S'_{fb} = uncorrected\ bending - fatigue\ strength$

$K_L = lifetime\ correction\ factor$

$K_T = temperature\ correction\ factor$

$K_R = reliability\ correction\ factor$

The uncorrected material strength S'_{fb} is the static strength of the material, found in table 12-20 $S'_{fb} = 340MPa$ [Maybe we should include scans of these tables in the appendix? pg770]

The lifetime correction factor K_L is found by comparing the number of cycles each gear will undergo over their lifetime to the tested life of 10^7 cycles. The number of cycles each gear undergoes depends on the operational load profile of the system and the speed at which they operate at. Breaking down the load profiles allows for an analysis of each shaft and their subsequent gears. At full power, all the shafts are turning at their maximum speed. Since this load is only required at 5% of the total lifetime it is possible to convert that value to minutes by

multiplying 5% by 20 years by 365 days/year by 24 hours/day by 60 minutes/hour. This leads to the number of minutes running at full power as 525600. The total minutes at each running load profile was then calculated in excel and is shown in **Figure 54** below.

		Load Cycle in Minutes	
		Operation Time [years]	20
		Operational Time in minutes	10512000
Load Profile	Full Power	5% [minutes]	525600
	Slow Speed	12% [minutes]	1261440
	High Speed	23% [minutes]	2417760

Figure 54: *Total minutes of operation at each profile over 20 years*

Using these values it is then possible to determine the number of minutes each gear will be turning in operation. For the prime mover, it is only in use during full power so it will have an operational time of 525600 minutes. The rest of the shafts and gears will run at all three of the profiles or 4204800 minutes. The number of cycles each gear will experience is the product of the operational time and rotational speed in RPM. Since some of the gears will be spinning at lower speeds for the slow profile that must be compensated for. Assuming 250 rpm is the output shaft speed during slow speed transit, it is possible to get the speed of each of the other shafts using gear ratios. The reduction shaft has a rotational speed of 750 rpm at slow speed, and the electric input shaft has a rotational speed of 1875 at slow speed transit. Now that the speeds for each of the shafts (and the gears) is determined at each load profile, it is possible to sum the cycles of each shaft at the profiles to get the total number of revolutions. A representation of this equation would look like:

(Full power minutes * full power speed) + (Slow speed minutes * slow speed) = Total cycles

See Appendix B-6 for sample calculation.

Computing this equation for each of the gears gives the following values for total cycles experienced by each gear which is observed in **Table 24.**

Table 24: *Total cycles experienced by each gear over lifetime*

Gear	Total Cycles [10^6]
E1	11195.28
D1	525.6
E2	4478.111888
D2	4478.111888
E3D3	4478.111888
E4D4	1492.706773

With the number of cycles each gear is experiencing, the lifetime factor for bending fatigue can be calculated from Figure 12-24 in Norton. Where each gear experiences more than $3X10^6$ cycles and is used for critical service applications. The equation for the lifetime factor is then:

$$K_L = 1.6831N^{-0.0323}$$

Where N is the number of cycles experienced over the gears lifetime.

The temperature correction factor K_T is applied when the material is subjected to values greater than 250℉. Typically, gearboxes operate at approximately 60℃ above the ambient air temperature [17]. Therefore, the operating temperature is set at approximately 80℃ and a value of $K_T = 1$ is selected. The reliability correction factor K_R is taken from table 12-19 in Norton. Assuming a reliability of 99%, $K_R = 1$. The correction factors for each gear is tabulated in **Table 25**, and the fatigue strength for each gear is tabulated in **Table 26**. Sample hand-calculations are available in Appendix B-1.

Table 25: *Bending Fatigue Correction Factors*

Gear Name	K_L	K_T	K_R
E1	0.8492229525	1	1
D1	0.8798988298	1	1
E2	0.8747323453	1	1
D2	0.8747323453	1	1
E3D3	0.8747323453	1	1
E4D4	0.9063296803	1	1

Table 26: *Bending Gear Fatigue Strengths*

Gear Name	S_{fb}
E1	288.7358038
D1	299.1656021
E2	297.4089974
D2	297.4089974
E3D3	297.4089974
E4D4	308.1520913

4.1.3 Surface Fatigue Factors

The surface fatigue strength is given by the following relationship.

$$S_{fc} = \frac{C_L C_H}{C_T C_R} S'_{fc}$$

Where

$S'_{fc} = \ uncorrected\ surface\ fatigue\ strength$

$C_L = \ lifetime\ correction\ factor$

$C_H = \ hardness\ correction\ factor$

$C_T = \ temperature\ correction\ factor$

$C_R = \ reliability\ correction\ factor$

The uncorrected surface fatigue strength S'_{fc} found in table 12-21 of Norton, as $S'_{fc} = 1150Mpa$ [11]. C_L, C_T, *and* C_R are computed similarly to the corresponding bending correction factors, and C_H is a hardness factor that is introduced when the gear and pinion are made of different materials, which is not the case in this gearbox, therefore $C_H = 1$. The correction factors for each gear and pinion set are tabulated in **Table 27**, and the surface strength of each set are tabulated in **Table 28**, and sample hand calculations are available in Appendix B-2.

Table 27: *AGMA Surface fatigue correction factors.*

	Gear Name	C_R	C_T	C_L	C_H
Set 1	E1	1	1	0.7532125741	1
	E2	1	1	0.8010070744	1
Set 2	D1	1	1	0.7928703949	1
	D2	1	1	0.7928703949	1
Set 3	E3D3	1	1	0.7928703949	1
	E4D4	1	1	0.8431813505	1

Table 28: *AGMA Corrected Surface fatigue strengths*

	Gear Name	S_{fc}
Set 1	E1	866.1944602
	E2	921.1581356
Set 2	D1	911.8009541
	D2	911.8009541
Set 3	E3D3	911.8009541
	E4D4	969.6585531

4.1.4 Bending Fatigue Stress

Bending fatigue is caused by the tangential force W_t that occurs between meshing gear teeth. There is also a radial force W_r, dependent on the pressure angle ϕ. The tangential and radial force can be written with the following relationships.

$$W_t = \frac{T}{r}$$

And

$$W_r = W_t tan(\phi)$$

Where

$W_t = tangential\ force$

$W_r = radial\ force$

$T = torque\ transmitted\ by\ gear$

$r = gear\ radius$

$\phi = pressure\ angle$

The tangential and radial force experienced by each gear is tabulated in **Table 29**.

Table 29: *Contact forces on each gear*

Gear Name	Torque [Nm]	Radius [m]	Tangential Wt [N]	Radial Wr [N]
E1	4774.648293	0.24	19894.36789	7240.95774
D1	23873.24146	0.48	49735.91972	18102.39435
E2	11936.62073	0.6	19894.36789	7240.95774
D2	19894.36789	0.4	49735.91972	18102.39435
E3D3	31830.98862	0.3	106103.2954	38618.44128
E4D4	95492.96586	0.9	106103.2954	38618.44128

The bending stress experienced at the teeth can be expressed with the following relationship.

$$\sigma_b = \frac{W_t}{mFJ}\frac{K_a K_m}{K_v}K_s K_B K_I$$

Where

$W_t = tangential\ force$

$m = gear\ module$

$F = face\ -\ width$

$J = bending\ strength\ geometry\ factor$

$K_a = application\ factor$

$K_m = load\ distribution\ factor$

$K_v = dynamic\ factor$

$K_s = size\ factor$

$K_B = rim\ thickness\ factor$

$K_I = idler\ factor$

The tangential force W_t, gear module m, and face-width F are all closely related. An iterative approach was taken to select a module and face-width that resulted in a reasonable tangential force and bending stress that lay within the material strength. The bending strength geometry factor J was taken from the AGMA Bending Geometry factor, 20^o full-depth teeth with HPSTC loading table located in Norton. The application factor K_a was selected from Table 12-17 in Norton, assuming moderate shock on the output, a uniform driving machine for the gears driven by the electric motor, light shock for the gears driven by the prime mover. For the gears driven by both electric and prime mover, a ratio of ⅓ was applied to the application factors to reflect the proportional power from each driver. The load distribution factor K_m is applied to account for any axial misalignment that occurs between the mating teeth, and is more pronounced with larger face widths. Assuming a face width of 240mm, a load distribution factor was interpolated from Table 12-16 found in *"Machine Design"* [11]. The size factor K_s is applied when gears are very large. In this gearbox, $K_s = 1$. The rim thickness factor K_B is applied when spokes are introduced to the gears to reduce weight. No spokes are present in this gearbox, so $K_B = 1$. The idler gear factor K_I accounts for extra stresses when a gear is subjected

to loading from two separate gears. No gears in the gearbox are subjected to this condition, so $K_I = 1$ for all gears. The dynamic factor K_v is introduced to account for internally generated vibration loads, a function of pitch-line velocity and the index of the gears. The dynamic factor can be represented with the following relationship.

$$K_v = \left(\frac{A}{A+\sqrt{200V_t}}\right)^B$$

Where

$V_t = pitch\ line\ velocity$

$A = 50 + 56(1 - B)$

$B = \frac{(12-Q_v)^{2/3}}{4}$

$Q_v = 11$ (Marine Transmission quality index, Table 12-6) [11]

The bending stress correction factors are tabulated in **Table 30**.

Table G30: *AGMA Bending Stress correction factors*

Gear Name	K_V	K_m	K_a	K_s	K_B	K_I
E1	0.8089818712	1.777206704	1.25	1	1	1
D1	0.8414352645	1.777206704	1.5	1	1	1
E2	0.8089818712	1.777206704	1.25	1	1	1
D2	0.8317098115	1.777206704	1.5	1	1	1
E3D3	0.8469066774	1.777206704	1.66	1	1	1
E4D4	0.8469066774	1.777206704	1.66	1	1	1

Applying these correction factors, the bending stress for each gear is found, as well as the safety factor for bending fatigue, tabulated in **Table 31**. and **Table 32**. Sample hand calculations are available in Appendix B-1

Table 31: *Gear Bending Stresses*

Gear Name	$\sigma_b[MPa]$
E1	30.88613818
D1	83.46848754
E2	28.86689079
D2	82.00730987
E3D3	201.6763193
E4D4	183.6235556

Table 32: *Gear Bending Safety Factor*

Gear Name	$SF_{bending}$
E1	9.348394485
D1	3.584174231
E2	10.30277211
D2	3.626615699
E3D3	1.474684774
E4D4	1.678172989

4.1.5 Surface Fatigue Stress

Surface fatigue is caused by relative sliding and rolling between mating gear teeth. High levels of fatigue can result in spalling or pitting, resulting in material being removed from the tooth face. Surface fatigue can be monitored by regularly checking the lubrication bath for chips. The surface. The surface stresses can be expressed with the following relationship.

$$\sigma_c = C_P\sqrt{\frac{W_t}{FId}\frac{C_a C_m}{C_v}C_s C_f}$$

Where

$W_t = tangential\ force$

$F = face\ width$

$d = pitch\ diameter$

$I = surface\ geometry\ factor$

$C_P = elastic\ coefficient$

$C_a = application\ coefficient$

$C_m = lad\ distribution\ coefficient$

$C_v = dynamic\ factor$

$C_s = size\ factor$

$C_f = surface\ finish\ factor$

The surface geometry factor I takes into account the radii of curvature of the gear teeth and pressure angle. The AGMA definition for I is presented.

$$I = \frac{cos\phi}{(\frac{1}{\rho_p} \pm \frac{1}{\rho_g})d}$$

Where ρ_p and ρ_g are the radii of the pinion and gear respectively, and ϕ is the pressure angle. The elastic coefficient C_P accounts for differences in tooth materials. The AGMA definition for C_p is presented.

$$C_P = \sqrt{\frac{1}{\pi[(\frac{1-\nu_p^2}{E_p}) + (\frac{1-\nu_g^2}{E_g})]}}$$

Where ν_p, ν_g, E_p, E_g are the poisson's ratio and moduli of elasticity of the pinion and gear, respectively. The surface finish factor C_f accounts for unusually rough surface finishes. For this gearbox, a value of $C_f = 1$ is selected. Tabulated values of each coefficient for each gear-pinion set is shown in **Table 33**.

Table 33: *AGMA Surface Stress correction factors.*

	Gear Name	C_v	C_m	C_a	C_s	$C_P[\sqrt{MPa}]$ **2**	C_f
Set 1	E1	0.8089818712	1.777206704	1.25	1	191	1
	E2	0.8089818712	1.777206704	1.25	1	191	1
Set 2	D1	0.8414352645	1.777206704	1.5	1	191	1
	D2	0.8317098115	1.777206704	1.5	1	191	1
Set 3	E3D3	0.8469066774	1.777206704	1.66	1	191	1
	E4D4	0.8469066774	1.777206704	1.66	1	191	1

Applying these correction factors along with the selected gear parameters yields the surface stresses for each gear-pinion set, tabulated in **Table 34**, and the safety factors for each set are tabulated in **Table 35**. Sample calculations are available in Appendix B-2

Table 34: Gear surface stresses.

	Gear Name	$\sigma_c\ [MPa]$
Set 1	E1	365.5085658
	E2	231.1679145
Set 2	D1	431.9367495
	D2	475.9213864
Set 3	E3D3	829.7291661
	E4D4	479.0443574

Table 35: *Gear surface fatigue Safety Factor*

	Gear Name	$SF_{surface}$
Set 1	E1	5.61611103
	E2	15.87863897
Set 2	D1	4.456149711
	D2	3.670537307
Set 3	E3D3	1.207611866
	E4D4	4.097190972

4.2 Detailed Shaft Design

In order to ensure all shafts were able to meet their respective loading demands, a detailed analysis was conducted for each shaft. In each instance, key points where the shaft was likely to fail due to the presence of stress concentrations were identified. Once these points had been identified, the stresses in the location were determined in order to calculate the Von Mises stress. Next, the material and geometrical properties of the shaft were examined to determine the corrected fatigue limit as a function of constants C_{temp}, C_{size}, C_{reliab}, C_{Surf}, C_{load}, and the uncorrected fatigue strength S_e'. This fatigue limit was then compared to the von mises stress at each location in order to determine the factor of safety against fatigue failure, ensuring our design would last to at least the specified lifetime of the tug.

4.2.1 Shaft Design Process

Each shaft was designed using a similar process, as outlined below. First, the general analysis as outlined above was conducted. First, the bending moment at each point of interest was calculated by making a cut in the shaft at that point. Then, the bending stress was calculated using the following formula.

$$\sigma_b = \frac{-M_i c_i}{I}$$

Where M_i is the moment at a point of interest i, c is the radius at a point of interest i, and I is the second moment of area of the shaft. Next, torsion of the shaft was obtained from earlier gear calculations and used to find shear stress from the following relationship.

$$\tau_{torsion} = \frac{Tc}{J}$$

Where T is the shaft torque, c is the radius, and J is the polar moment of Area. Next, theoretical stress concentrations were determined at each location for both shear and bending moment loadings. Due to the fact that each shaft has different geometry, the specific relations used will be discussed in more detail in each shaft's specific section below. Once theoretical stress concentrations had been compiled for each location, they were used to find the fatigue stress concentrations K_f and $K_{f,S}$ for bending stress and shear, respectively. Theoretical stress concentrations are related to fatigue stress concentrations as follows.

$$K_f = 1 + q(K_t - 1)$$
$$K_{f,s} = 1 + q(K_{t,s} - 1)$$

Where the parameter q, known as the notch sensitivity, is given by the following relationship.

$$q = \frac{1}{1+\frac{\sqrt{a}}{\sqrt{r}}}$$

The quantity $\sqrt{a}$ is known as Neuber's constant, and is a material property. Using interpolation for 1045 Hot Rolled Steel, the Neuber constant was found to be 0.084732, which will be used in all calculations. Finally, the fatigue stress concentrations for shear and bending are known, and Von Mises stress can be calculated to be later compared with the endurance limit. The Von Mises stress is given by the following relation.

$$\sigma' = \sqrt{(K_f \sigma_{bending})^2 + 4(K_{f,s}\tau)^2}$$

This calculation was completed for each critical location on each shaft in order to determine if any locations on the shaft are subject to fatigue failure. Parameters were then varied until the desired results were obtained. In the case of shaft design, many design parameters had

been predetermined, leaving a few geometrical and material properties to be altered. These parameters included the total lengths of all shafts, the shaft radius at each point of interest, and the constants C_{temp}, C_{size}, C_{reliab}, C_{Surf}, C_{load}. The material chosen for all shafts was 1045 Hot Rolled Steel, with the following strength properties outlined in **table 36** below.

***Table 36**: 1045 Hot Rolled Steel Strength Properties*

Property	Strength (MPa)
S_{ut} (ultimate tensile strength)	556
S_e' (uncorrected fatigue strength)	282.5
S_y (yield strength)	310

Using the same material for all shafts reduces overall cost as the manufacturer would be able to order in bulk, as well as simplifying maintenance and design. The surface finish correction could be determined as follows.

$$C_{surf} \approx A(S_{ut})^{b}$$

Referencing table 6-3 of *"Machine Design"*, A is 57.7 and b is -0.718 for hot rolled steel. This results in a surface correction of 0.61. Next, since the gearbox operates at approximately 60℃ above the ambient temperature [17] which was assumed to be 20℃. This means that the gearbox operates at a temperature below 450℃, the temperature correction, C_{temp}, was set to 1. As discussed, all shafts are subjected to a combination of bending moment and torsional loading, so the load correction, C_{load}, was also set to 1. The reliability correction, C_r, was set to 0.814 via the assumption of 99% reliability [11]. Finally, the size correction was calculated as a function of the diameter d (in units of inches) at each point of interest as follows.

$$C_{size} = 0.869d^{-00.97}$$

We now have all the required information to compute corrected endurance strength and the factor of safety against fatigue failure at each point of interest on each shaft as follows.

$$S_e = C_{temp} C_{size} C_{surf} C_{rel} C_{load} S_e'$$

$$S_e = C_{size} * 0.61 * 0.814 * 282.5 MPa$$

$$S_e = 140.27255 * C_{size}$$

$$N_i = \frac{S_{e,i}}{\sigma_i'}$$

Where the index i indicates a quantity at a specific point of interest i. The endurance limit is simplified down to a function of its diameter at each point of interest to increase the speed at which subsequent calculations can be completed. Using this information, each point of interest on each shaft can be analyzed to determine the factor of safety. At this point in the design process, we entered an iterative stage where parameters were varied to achieve desired safety factors at each point of interest. For the purposes of this design, we strived to achieve factors of safety of at least 1.5 at each location of interest on each shaft. The subsequent sections will discuss the iterative process and specific calculations for each shaft.

4.2.2 Prime Mover Input Shaft

The prime mover input shaft, along with the electric motor input shaft and the output shaft were analyzed via one general free body diagram, as they all have essentially the same features but with slightly different geometries. This generalized free body diagram can be seen in **figure 55** below.

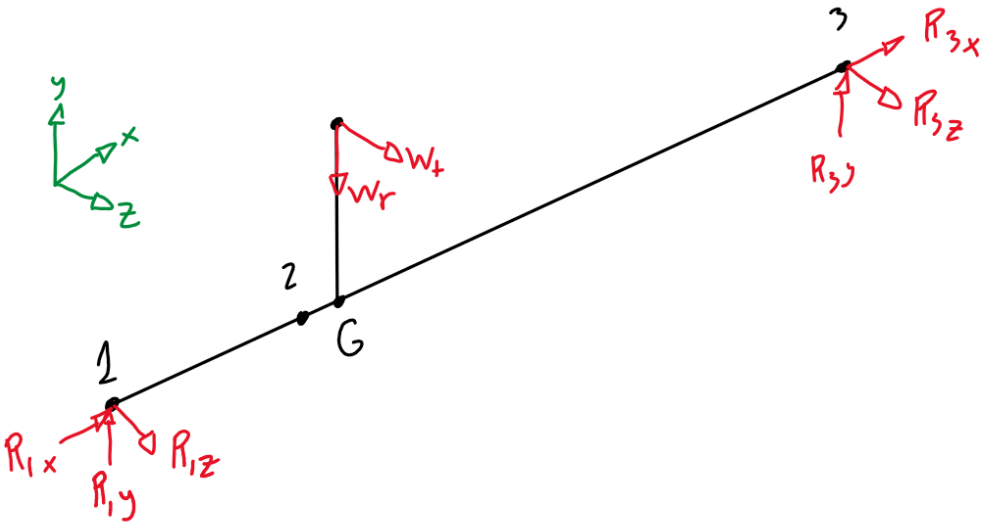

***Figure 55**: Generalized free body diagram for input and output shafts*

In this case, the reaction forces along the x direction are zero, leaving us with four equations and four unknowns. Furthermore, each of the three aforementioned shafts employs a consistent coordinate system, which measures the distance from one end of the shaft to each point of interest along each shaft. The prime mover input shaft drawing can be seen below in **Figure 56**.

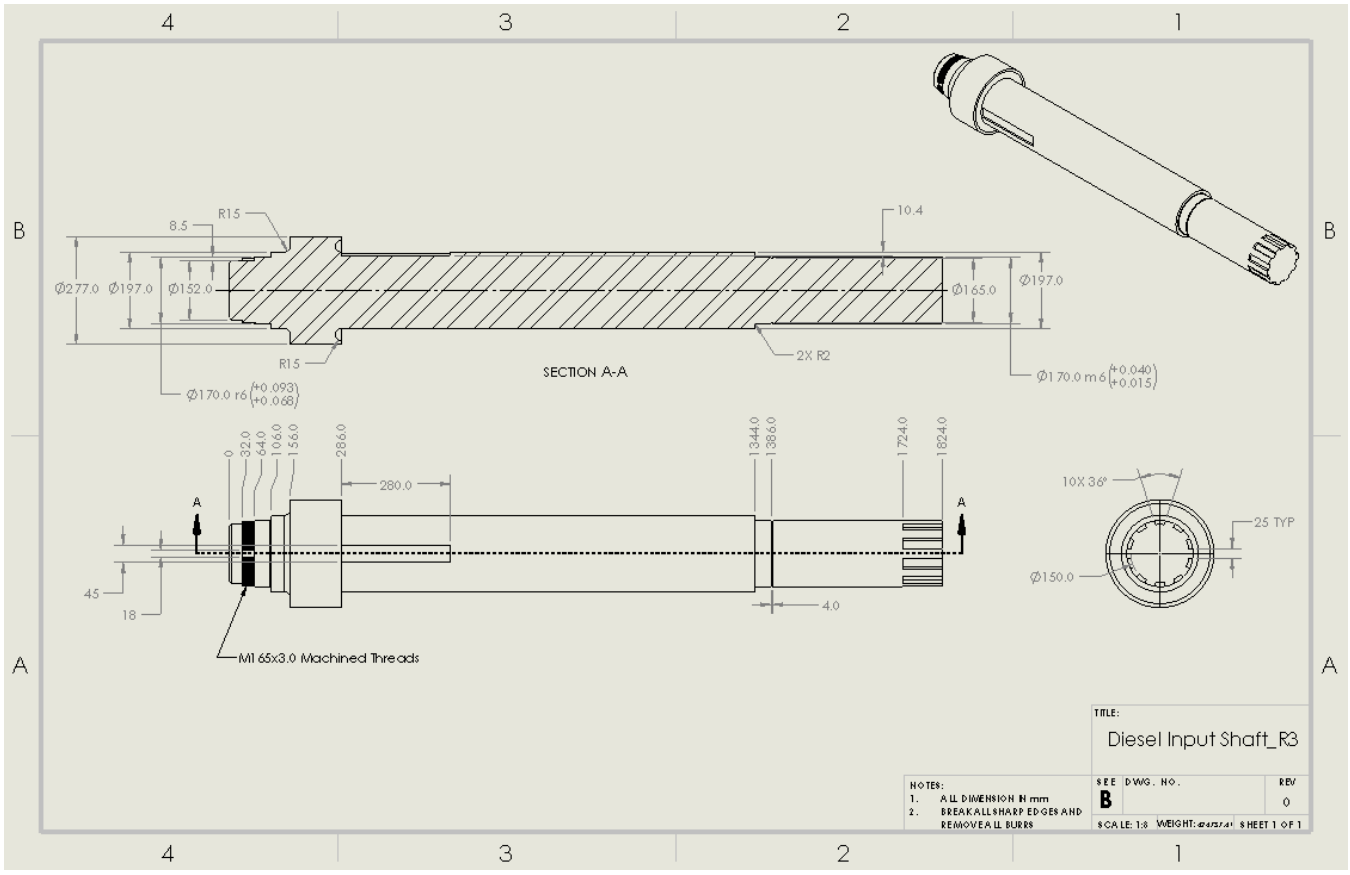

Figure 56: *Prime mover input shaft*

It should be noted that the bearing seats are toleranced with a fit tolerance. These tolerances are based on the seat tolerance document provided by SKF (see Appendix C) and are based on the size of the shaft as well as the force that the bearings are experiencing. More details about selection of the tolerances will be provided in the bearing section.

As mentioned, there are three points of interest that were selected for further failure analysis to due their respective propensities for stress concentrations to arise. These locations are areas with abrupt geometrical changes, and are indicated in **figure 57** below.

Figure 57: *Points of interest for prime mover input shaft*

Referencing the generalized free body diagram, the distance from point 1, which is considered to be the leftmost point of the shaft for this analysis, to points 2 and 3 are given by the following relationships.

$$d_2 = \frac{L}{4} - \frac{W}{2}$$

$$d_3 = L$$

Where L is the total length of the shaft of 1.2m, and W is the face width of the gears of 240mm. The length of the shaft was determined by ensuring that none of the gears overlap with any shafts, while the face width was determined as part of the gear stress calculations.

Using this information, the reaction forces at locations 1 and 3 were found, and are shown in **table 37** below.

Table 37*: Reaction loads for the prime mover input shaft*

Reaction	Load [N]
R_{1y}	13576.8
R_{1z}	-37301.9
R_{3y}	4525.6
R_{3z}	-12434.0

Next, the bending moment and torsion at each point of interest could be found. At the supports (locations 1 and 3), the bending moment is 0 Nm, whereas at location 2, the bending moment was 7145.26Nm. The torsion at each point was also calculated, and found to be 23873.24Nm at each of location 1, 2 and 3, due to each location having the same effective radius from the center of the shaft. For more detailed calculations, see Appendix B - Sample Hand Calculations.

With the Torsion and Moments determined for each location, the corresponding stresses associated with the loading were determined. Normal stress due to bending and shear stress due to torsion are defined as follows.

$$\sigma_b = \frac{-M_i c_i}{I}$$

$$\tau_{torsion} = \frac{Tc}{J}$$

These stresses were calculated at each point of interest on the shaft and are displayed in **table 37** below.

***Table 37**: Bending and torsional stresses in the diesel input shaft*

Point	Bending Stress (σ_b) [Pa]	Torsional Shear (τ_s) [Pa]
1	0	24747693.95
2	9519618.241	15903137.8
3	0	24747693.95

Next, theoretical stress concentrations were calculated. Examining the geometry of the prime mover input shaft in **figure 56** above, the radii of fillets along with changes of diameter for sudden changes were noted. These are tabulated in **table 38** below.

Table 38: *prime mover geometrical features at each location for theoretical stress concentrations*

Location	Diameter Ratio (D/d)	Fillet Radius [m]
1	1.158823529	0.002
2	1.406091371	0.015
3	1.158823529	0.0002

Using this data, theoretical stress concentrations can be calculated for bending and torsional stress for each type of abrupt geometrical feature. The theoretical stress concentration due to bending moment for this geometry is given by the following equation.

$$K_t = A\left(\frac{r}{d}\right)^b$$

Where r is the fillet radius, d is the smaller diameter of an abrupt diameter change, and constants A and b are functions of the diameter ratio D/d. These constants were found for diameter ratio at each location of interest via interpolation of **table 39** below.

Table 39: *Constants A and b as a function of diameter ratio D/d*

D/d	A	b
6	0.87868	-0.33243
3	0.89334	-0.3086
2	0.90879	-0.28598
1.5	0.93836	-0.25759
1.2	0.97098	-0.21796
1.1	0.9512	-0.23757
1.07	0.97527	-0.20958
1.05	0.98137	-0.19653
1.03	0.98061	-0.18381
1.02	0.96048	-0.17711
1.01	0.91938	-0.17032

This allowed for the calculation of the theoretical stress concentration for bending stress, which are shown in **Table 40** below

.

Table 40: *Theoretical stress concentrations for bending of the prime mover input shaft*

Location	Theoretical Stress Concentration for Bending
1	2.474259489
2	1.681448069
3	4.054551804

In a similar manner, the torsional shear stress concentration factors were found. These results are shown in **Table 41** below. For complete sample calculations, refer to Appendix B, or the attached spreadsheet.

Table 41: *Theoretical stress concentrations for torsional shear of the prime mover input shaft*

Location	Theoretical Stress Concentration for Torsional Shear
1	1.956241167
2	1.456584028
3	2.985730155

Once the theoretical stress concentrations were determined, they were then adjusted to their corresponding fatigue counterparts. For both types of theoretical stress concentrations, the fatigue concentrations can be determined via the following equation.

$$K_f = 1 + q(K_t - 1)$$

Where q is the notch sensitivity. The determination of the notch sensitivity was discussed in section 4.2.1 above, so the results for each location are tabulated below in **Table 42**.

Table 42: *Notch sensitivity for each location of interest*

Location	Notch Sensitivity
1	0.7680732491
2	0.9006900141
3	0.5115406914

Finally, the fatigue stress concentrations for bending, K_f, and torsional shear, K_{fs}, can be calculated. These results are shown for each location in **Table 43** below.

Table 43*: Fatigue stress concentrations for each point of interest on the prime mover input shaft*

Location	K_f	K_{fs}
1	2.132339276	1.73446326
2	1.613773471	1.411240675
3	2.562527542	2.015781776

The Von Mises stress at each location was then determined via the following formula.

$$\sigma' = \sqrt{(K_f \sigma_b)^2 + 4(K_{fs} \tau)^2}$$

The results of computing the Von Mises stress at each location is tabulated in **table 44** below.

Table 44: *Von Mises Stress at each location of interest on the prime mover input shaft*

Location	Von Mises Stress (σ') [MPa]
1	74.35
2	41.80
3	86.41

The only remaining portion of the fatigue analysis of the prime mover input shaft is now the determination of the corrected endurance limit of the shaft. Derived in section 4.2.1, the following relationship was used to determine this property.

$$S_e = 140.27255 * C_{size}$$

The size correction factor, C_{size} was left in variable form to reflect the fact that for each shaft has different sizes, and therefore different size correction factors. As mentioned earlier, no radius of any shaft in this design exceeds 10 inches, so the following formula for the size correction formula was used.

$$C_{size} = 0.869d^{-0.097}$$

In order to acknowledge the fact that each point of interest has a different local diameter, this calculation was completed for each point. The results of both the C_{size} calculation, and the subsequent determination of the endurance limit, S_e, are shown in **table 45** below.

Table 45: *Size correction factors and resulting endurance limits at each point of interest*

Location	C_{size}	S_e [MPa]
1	0.7224841256	101.34
2	0.7122273235	99.91
3	0.7224841256	101.34

Lastly, the factor of safety against fatigue failure was calculated for each location as the quotient of the local endurance limit and the local Von Mises stress. These results can be seen in **table 46** below. Notably, all safety factors are above 1, indicating our design is sufficient to undergo the determined loading conditions.

Table 46: *Factors of safety against fatigue failure at each point of interest of the P.M. input shaft*

Location	Factor of Safety
1	1.4
2	2.4
3	1.2

4.2.3 Electric Input Shaft

The drawing of the electric input shaft is shown in **Figure 58** below.

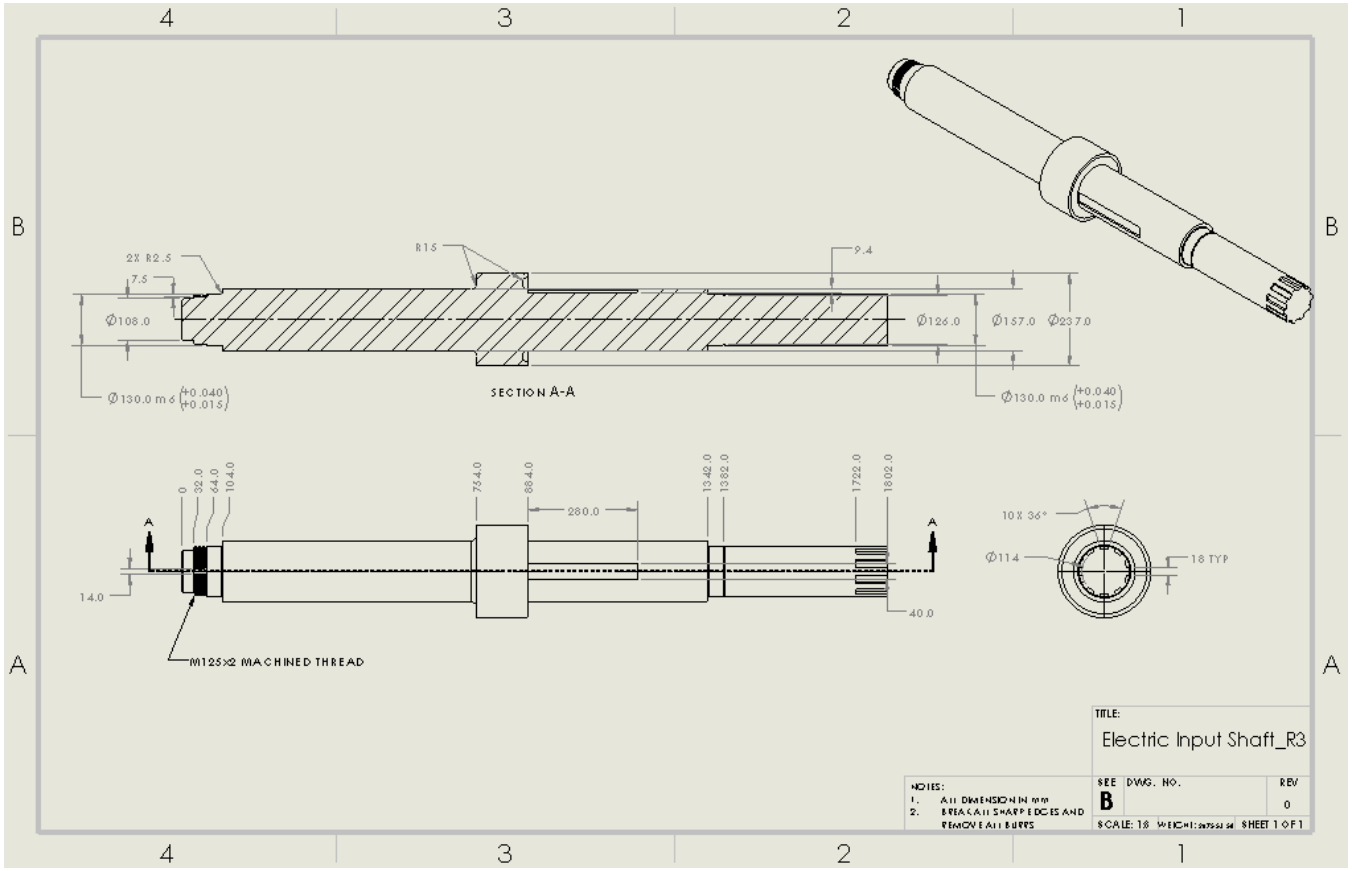

Figure 58: *Electric input shaft*

As mentioned in section 4.2.2 above, due to the similarities between the two input shafts and the output shafts, each shaft was analyzed via a generalized free body diagram with its geometrical parameters left in variable to account for differences in geometry between each of

the three shafts analyzed this way. Therefore, to avoid unnecessary redundancies, the relevant results of the calculations will be presented, without the derivations and explanations of each step. Specifically, each table of values provided in section 4.2.2 will have an equivalent counterpart in this section. With that said, the geometry of the shaft will have to be well defined to continue with the analysis. Reviewing **figure 59** below, the three points that were selected for failure analysis are labeled 1, 2, and 3.

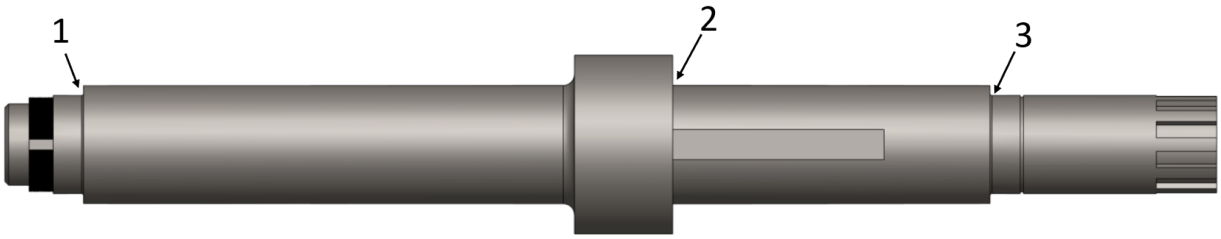

Figure 59: *Points of interest considered for failure analysis on the electric input shaft*

The distances to points 2 and 3 from point 1 on the electric input shaft are as follows.

$$d_2 = \frac{3L}{4} - \frac{W}{2}$$

$$d_3 = L$$

Where L is the length of the electric input shaft of 1.2m, and W is the common gear face width of 240mm. Proceeding with the same analysis as the prime mover input shaft, the bending moments and torques were calculated at each location of interest. These results are shown in **table 47** below.

Table 47: *Bending Moments and Torques at each location of interest on the electric input shaft*

Location	Bending Moment [Nm]	Torque [Nm]
1	0	4774.65
2	4128.37	4774.65
3	0	4774.65

From this information, the nominal shear stress due to torsion and the nominal normal stress due to bending was calculated at each location of interest. These results are displayed below in **table 48**.

Table 48: *Shear and normal stress at each location of the electric input shaft*

Location	Stress Due to Bending [Pa]	Shear Stress Due to Torsion [Pa]
1	0	11068313.19
2	10866259.89	6283657.991
3	0	11068313.19

Next, the theoretical stress concentrations for each type of loading (bending moment - K_t and torsion - K_{ts}) were determined using the same method as in section 4.2.2 above. The results are as follows in **Table 49**.

Table 49: *Theoretical stress concentrations in the electric input shaft*

Location	K_t	K_{ts}
1	2.237564572	1.81426531
2	1.607283498	1.416371296
3	3.679138425	2.794199187

Next, the associated fatigue stress concentration factors were determined by first finding the notch sensitivity, and then utilizing the same formula as in section 4.2.2. This yields the following results for the fatigue stress concentrations for torsional shear and normal stress due to bending moment, which are shown in **table 50** below.

Table 50: *Fatigue stress concentrations for electric input shaft*

Location	K_f	K_{fs}
1	1.974398545	1.64111316
2	1.546974182	1.375021469
3	2.445004336	1.967708716

Now that the fatigue stress concentrations are known at each location of interest, the Von Mises stresses at each location can be calculated in the same way as in section 4.2.2. The Von Mises stresses for each location of interest are tabulated in **Table 51** below.

Table 51: *Von Mises stresses at each location of interest on the electric input shaft*

Location	Von Mises Stress (σ') [MPa]
1	31.46158476
2	22.50616585
3	37.72270924

Now the focus of the analysis shifts to calculating the endurance limit of the shaft, which depends on the local size correction factor, C_{size}, as explained in section 4.2.1. Since no components of this shaft have a diameter greater than 10 inches, the calculation is the same as in section 4.2.2. The results for C_{size}, and subsequently the corrected endurance limit, S_e, are shown in **table 52** below.

Table 52: *Local size correction factors and endurance limits of the electric input shaft*

Location	C_{size}	S_e [MPa]
1	0.7415310646	104.0164533
2	0.7280808164	102.1297527
3	0.7415310646	104.0164533

Finally, the factors of safety against fatigue failure at each location of interest on the electric input shaft are tabulated in **table 53** below.

Table 53: *Local factors of safety against fatigue failure of the electric input shaft*

Location	Factor of Safety
1	3.3
2	4.5
3	2.8

As was the case with the prime mover input shaft, after design iteration, the factors of safety against fatigue failure are all greater than 1, indicating a robust design.

4.2.4 Reduction Shaft

The reduction shaft is the most complex shaft involved in our design. It houses the gears E2, D2, and E3/D3, so it has more shoulders and complex geometry features that give rise to stress concentrations. This can be seen in the drawing shown in **Figure 60** below.

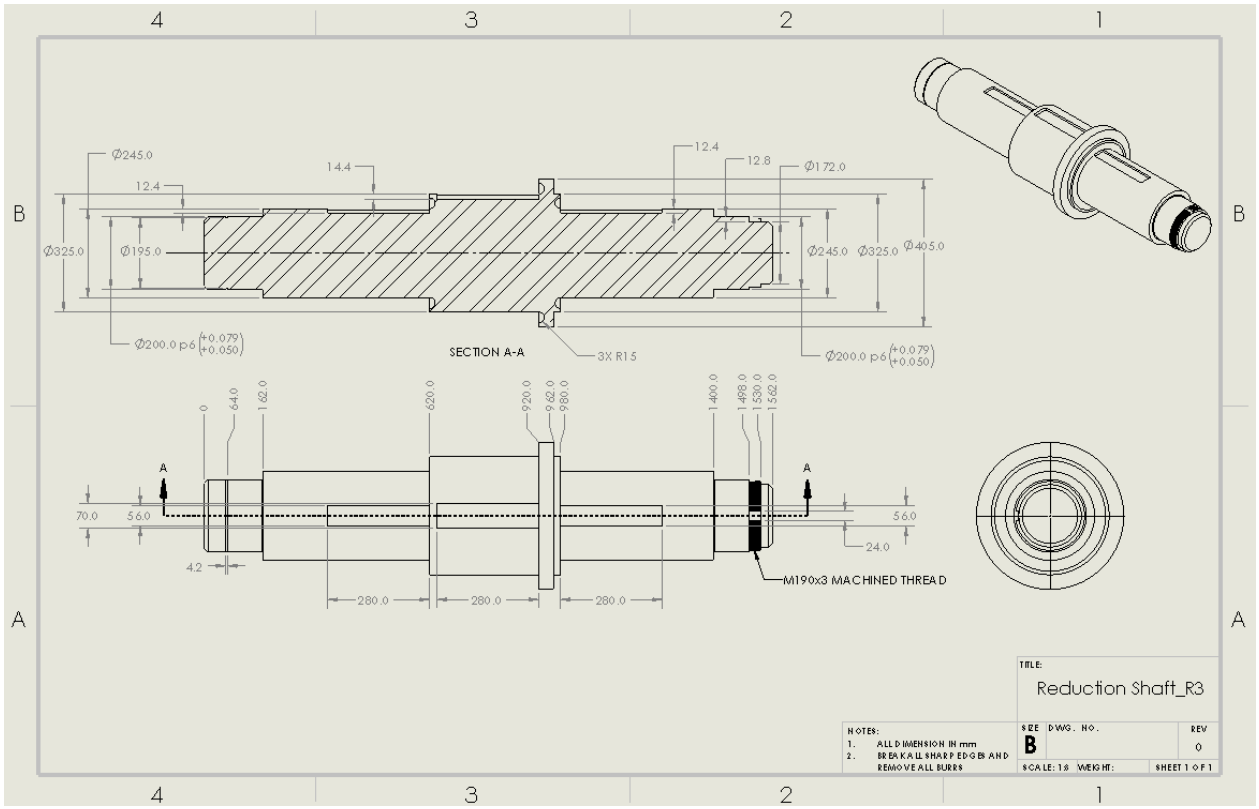

Figure 60: Drawing of the reduction shaft

Due to the more complex geometry and loading, the generalized free body diagram analysis of the electric input shaft, prime mover input shaft, and output shaft could not be applied. **Figure 61** below shows a two-dimensional view of the reduction shaft, labeled with the five locations of interest that were considered for fatigue failure analysis.

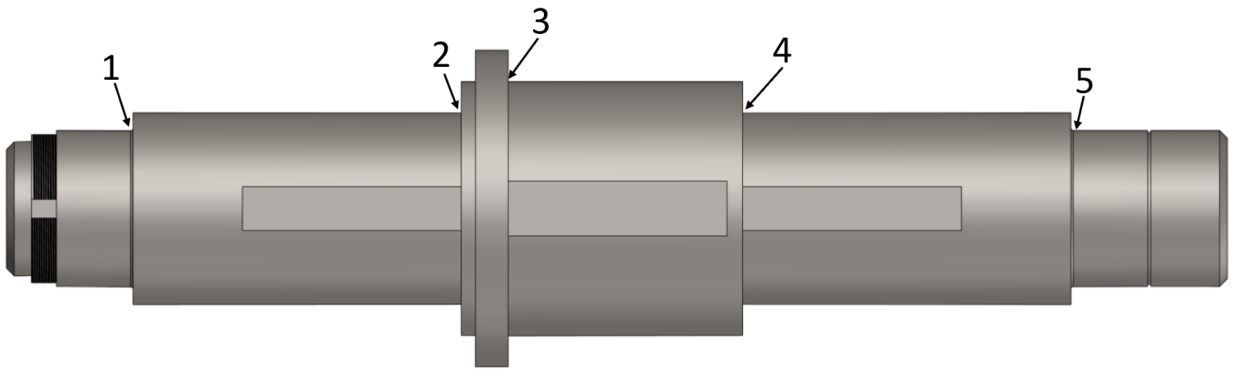

Figure 62: Locations of interest on the reduction shaft

Similar to the other shafts, the distances from the end point of the shaft (location 1) to each subsequent point of interest are important geometrical properties of the shaft, which are used in the calculation of the bending moment and torque at each point of the shaft. These distances are defined as follows.

$$d_1 = 0$$

$$d_2 = \frac{L}{4} + \frac{W}{2}$$

$$d_3 = \frac{L}{2} - \frac{W}{2}$$

$$d_4 = \frac{3L}{4} - \frac{W}{2}$$

$$d_5 = L$$

Where L is the length of the output shaft of 1.2m, and W is the common gear face width of 240mm. This point in the analysis differs from previous shafts. This is because the determination of the moments at each point of interest is more difficult than previous shafts due to the presence of more forces, and the fact that the net torque on the reduction shaft is 0. The latter statement imposes the requirement that in order to find the torque at each point of interest of the shaft, each section of the shaft must be analyzed. **Figure 63** below shows the free body diagram of the reduction shaft.

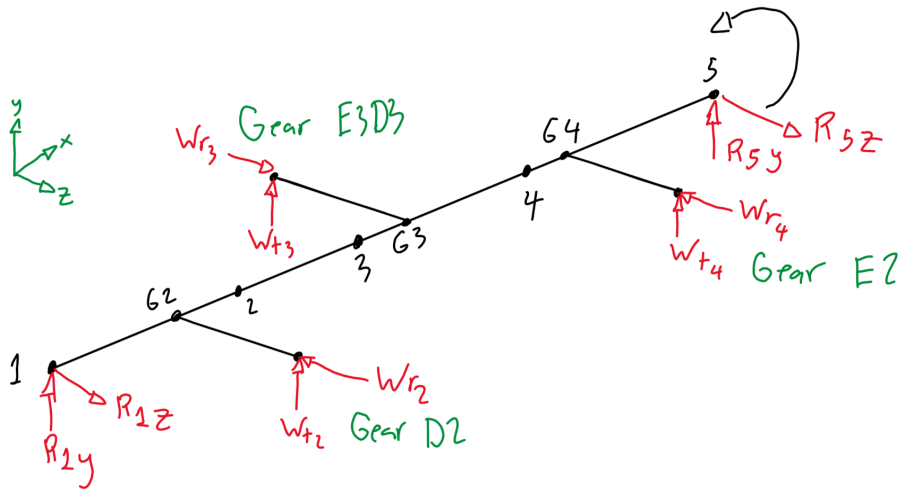

Figure 63: Free body diagram of the reduction shaft

To see the full hand calculations solving for the moments and torques at each point of interest, reference appendix B. The results of these calculations are tabulated below in **table 54**.

Table 54: Moments and torques at each point of interest on the reduction shaft

Location	Bending Moment [Nm]	Torque [Nm]
1	0	0
2	40071.29004	19894
3	42875.79656	19894
4	33998.38787	51725
5	0	0

From this point forward in the analysis, the same steps will be taken as for the other shafts. Therefore, derivation and explanation of formulae will be omitted in order to highlight the calculations and results to reduce redundancy between sections.

With the torques and moments known at each point of interest, the resulting nominal stresses they cause can be calculated. Specifically, the normal stress due to bending moment and the shear stress due to torsion are shown in **Table 55** below.

Table 55: Normal and shear stress at each point of interest on the reduction shaft

Location	Stress Due to Bending [Pa]	Shear Due to Torsion [Pa]
1	0	0
2	27754613.04	6889726.807
3	12722200.17	2951550.183
4	23548333.44	17913289.7
5	0	0

Using the same methods as for all other shafts, the theoretical stress concentrations for shear stress due to torsion, K_{ts}, and for normal stress due to bending, K_t, were calculated. These results are shown below in **Table 56**.

Table 56: Theoretical stress concentrations of each point of interest the reduction shaft

Location	K_t	K_{ts}
1	2.365279959	1.911524323
2	1.755818416	1.497254522
3	1.857285845	1.553474741
4	1.755818416	1.497254522
5	2.365279959	1.911524323

The theoretical stress concentrations were then converted to their fatigue counterparts, by first calculating the notch sensitivity, q, at each location, then following the same process as laid out in section 4.2.2. The fatigue stress concentrations K_f and K_{fs} are detailed in **table 57** below.

Table 57: Fatigue stress concentrations of each point of interest the reduction shaft

Location	K_f	K_{fs}
1	2.095248062	1.731238485
2	1.6807581	1.447872183
3	1.7721488	1.498509173
4	1.6807581	1.447872183
5	2.095248062	1.731238485

With the fatigue stress concentrations known, the Von Mises stress was calculated in the same manner as introduced in section 4.2.2, giving the following results shown in **table 58** below.

Table 58: Von Mises stresses of each point of interest the reduction shaft

Location	Von Mises Stress (σ') [MPa]
1	0
2	49.74573458
3	23.81160029
4	59.87114164
5	0

Again, the focus of the analysis shifts to calculating the endurance limit of the shaft, which depends on the local size correction factor, C_{size}, as explained in section 4.2.1. Since no components of this shaft have a diameter greater than 10 inches, the calculation is the same as in section 4.2.2. The results for C_{size}, and subsequently the corrected endurance limit, S_e, are shown in **table 59** below.

Table 60: *Local size correction factors and endurance limits of the reduction shaft*

Location	C_{size}	S_e [MPa]
1	0.7111839469	99.75958575
2	0.6973210002	97.81499487
3	0.678467687	95.17039255
4	0.6973210002	97.81499487
5	0.7111839469	99.75958575

Finally, the factors of safety against fatigue failure at each location of interest on the reduction shaft are tabulated in **table 61** below.

Table 61: *Factors of safety against fatigue failure at each point of interest of the output shaft*

Location	Factor of Safety
1	N/A
2	1.966299135
3	3.996807916
4	1.633758639
5	N/A

As was the case with all of the previous shafts, after design iteration, the factors of safety against fatigue failure are all greater than 1, indicating a robust design that is capable of withstanding the expected loading conditions it will be subjected to. Notably for this shaft, there was no bending moment or torque at either of the endpoints of the shaft (points 1 and 5). For this reason, there is no corresponding factor of safety against fatigue failure in these location as the SF would tend to infinity.

4.2.5 Output Shaft

The drawing of the electric input shaft is shown in **figure 64** below.

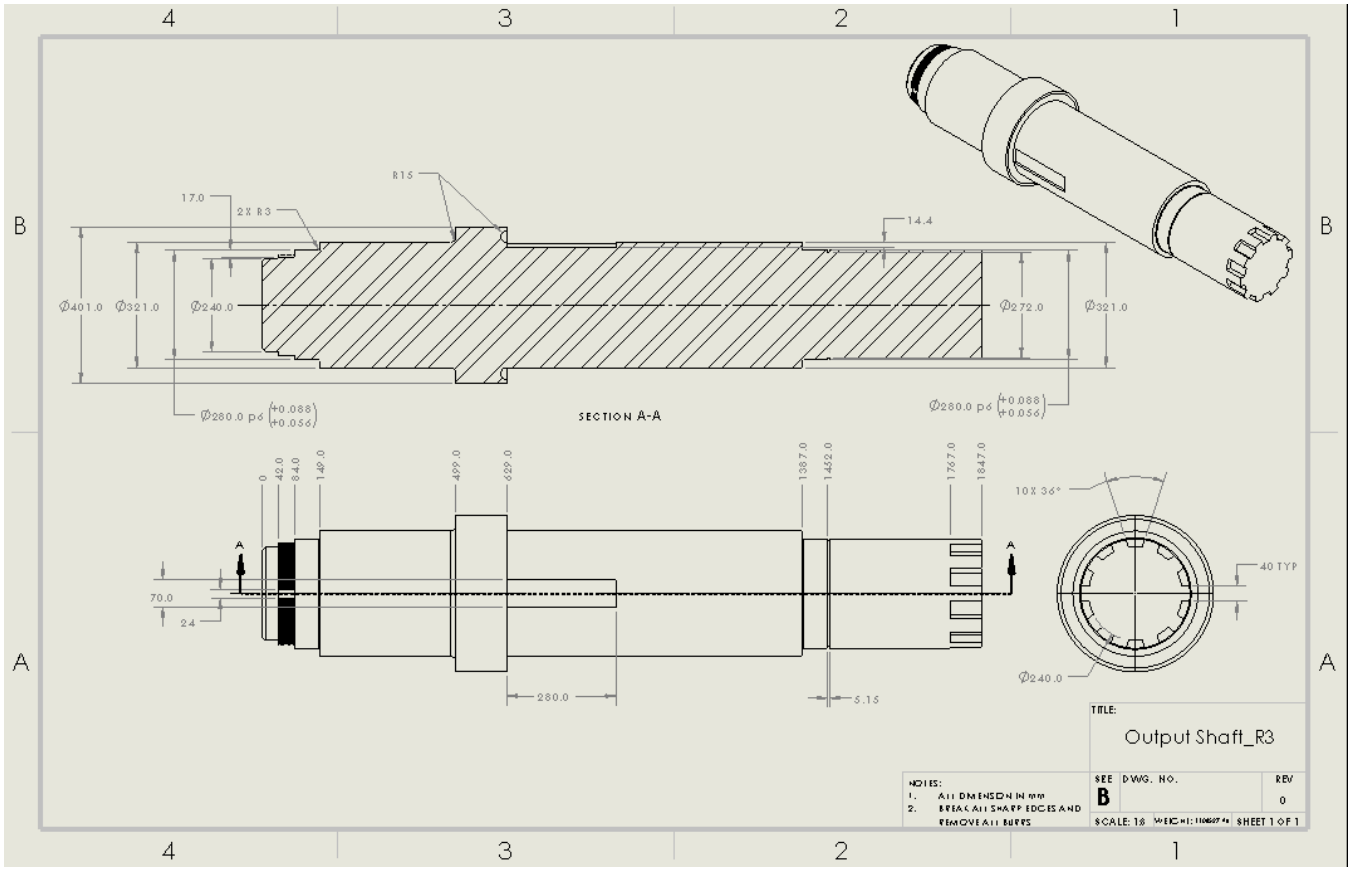

Figure 64: Drawing of the output shaft

As mentioned in section 4.2.2 above, due to the similarities between the two input shafts and the output shafts, each shaft was analyzed via a generalized free body diagram with its geometrical parameters left in variable to account for differences in geometry between each of the three shafts analyzed this way. Therefore, to avoid unnecessary redundancies, the relevant results of the calculations will be presented, without the derivations and explanations of each step. Specifically, each table of values provided in section 4.2.2 and 4.3.3 will have an equivalent counterpart in this section. With that said, the geometry of the shaft will have to be well defined to continue with the analysis. Reviewing **figure 65** below, the points of interest selected for fatigue failure analysis are labeled 1, 2, and 3.

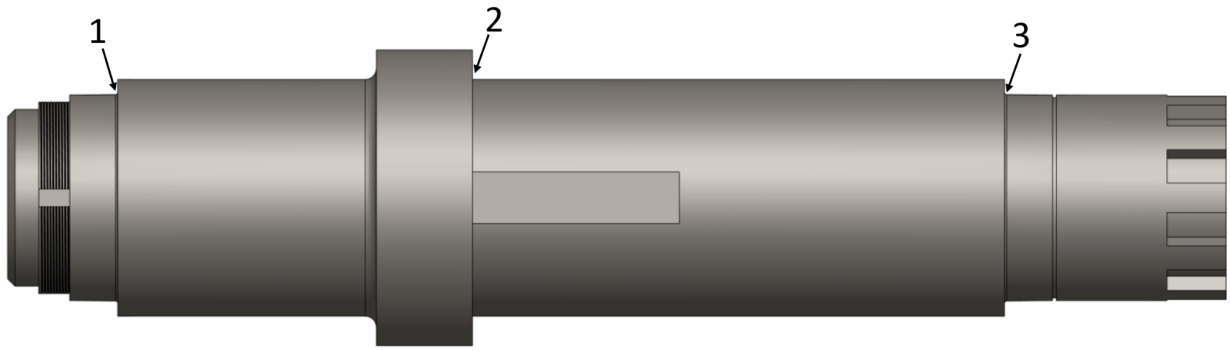

Figure 65: *points of interest selected for failure analysis on the output shaft*

The distances to points 2 and 3 from point 1 on the output shaft are as follows.

$$d_1 = 0$$

$$d_2 = \frac{L}{2} - \frac{W}{2}$$

$$d_3 = L$$

Where L is the length of the output shaft of 1.2m, and W is the common gear face width of 240mm. Proceeding with the same analysis as the prime mover input shaft and the electric input shaft, the bending moments and torques were calculated at each location of interest. These results are shown in **table 62** below.

Table 62: *Bending Moments and Torques at each location of interest on the output shaft*

Location	Bending Moment [Nm]	Torque [Nm]
1	0	95493
2	27099.1	95493
3	0	95493

From this information, the nominal shear stress due to torsion and the nominal normal stress due to bending was calculated at each location of interest. These results are displayed below in **table 63**.

Table 63: *Shear and normal stress at each location of the output shaft*

Location	Stress Due to Bending [Pa]	Shear Stress Due to Torsion [Pa]
1	0	22154777.76
2	8345249.132	14703691.93
3	0	22154777.76

Next, the theoretical stress concentrations for each type of loading (bending moment - K_t and torsion - K_{ts}) were determined using the same method as in section 4.2.2 above. The results are as follows in **Table 64**.

Table 64: Theoretical stress concentrations in the output shaft

Location	K_t	K_{ts}
1	2.520740705	1.98146966
2	2.62808493	2.108722917
3	2.520740705	1.98146966

Next, the associated fatigue stress concentration factors were determined by first finding the notch sensitivity, and then utilizing the same formula as in section 4.2.2. This yields the following results for the fatigue stress concentrations for torsional shear and normal stress due to bending moment, which are shown in **table 65** below.

Table 65: *Fatigue stress concentrations for output shaft*

Location	K_f	K_{fs}
1	2.219961004	1.787349683
2	2.306074152	1.889434154
3	2.219961004	1.787349683

Now that the fatigue stress concentrations are known at each location of interest, the Von Mises stresses at each location can be calculated in the same way as in section 4.2.2. The Von Mises stresses for each location of interest are tabulated in **Table 66** below.

Table 66: *Von Mises stresses at each location of interest on the output shaft*

Location	Von Mises Stress (σ') [MPa]
1	68.58632813
2	51.82492095
3	68.58632813

Now the focus of the analysis shifts to calculating the endurance limit of the shaft, which depends on the local size correction factor, C_{size}, as explained in section 4.2.1. Since no components of this shaft have a diameter greater than 10 inches, the calculation is the same as in section 4.2.2. The results for C_{size}, and subsequently the corrected endurance limit, S_e, are shown in **table 67** below.

Table 68: *Local size correction factors and endurance limits of the output shaft*

Location	C_{size}	S_e [MPa]
1	0.688347161	96.55621156
2	0.6792831886	95.28478504
3	0.688347161	96.55621156

Finally, the factors of safety against fatigue failure at each location of interest on the output shaft are tabulated in **table 69** below.

Table 69: *Factors of safety against fatigue failure at each point of interest of the output shaft*

Location	Factor of Safety
1	1.407805523
2	1.83859007
3	1.407805523

As was the case with all of the previous shafts, after design iteration, the factors of safety against fatigue failure are all greater than 1, indicating a robust design that is capable of withstanding the expected loading conditions it will be subjected to.

4.3 Detailed Bearing Selection

In order to mount all shafts, bearings are selected to sustain the loading carried by the shafts. Due to the exclusive use of spur gear, there are no axial loads that the bearings must withstand. For this reason, cylindrical roller bearings are used. The bearing load P is calculated for each bearing location from the free body diagram and corresponding equations established in section 4.2. With these loads established, bearings are selected that withstand the load with a safety factor of 1.5. Lifespan calculations are also completed for the bearings on each shaft in accordance with the provided design specifications, specifically regarding the percentage of time the prime mover and the electric motor will be running over a 20 year lifespan. In addition, the bearing seat tolerance was also chosen based on the ratio of total load with respect to the dynamic load rating of the bearing. Once the bearing has been selected, the total load on that bearing can be divided by dynamic load rating to give a value. That value can be compared to the table in Appendix C to find the suitable fit tolerance for the shaft.

4.3.2 Electric Motor Input Shaft Bearings

Figure 66 below shows the locations of the bearings used on this shaft, which are labeled 1 and 3.

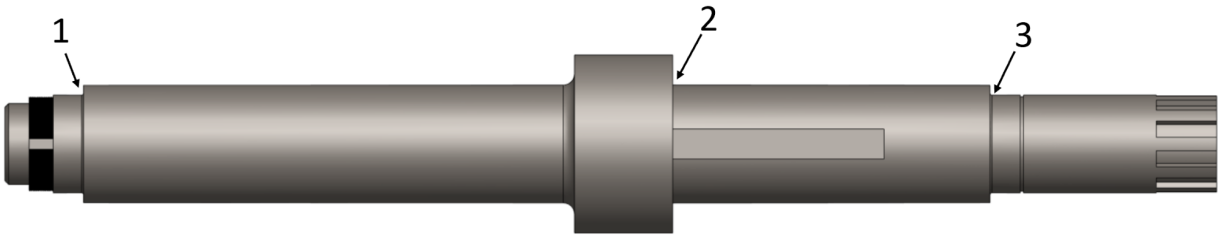

Figure 66: *Electric motor input shaft with bearing locations (1 and 4)*

Previously in section 4.2, the reactions at these bearing seats were calculated. Below in **table 70**, the reaction loads for the electric input shaft are seen.

Table 70: *Reaction loads for electric input shaft*

Location	Reaction Load
A_y	1810.24
A_z	-4973.59
B_y	5430.72
B_z	-14920.78

These reactions are related to the loads felt by the bearings via the following equation.

$$P = VXF_R + YF_A$$

Where P is the equivalent dynamic bearing load, F_R is the radial force component, F_A is the axial force component, V is the rotational factor, X is the radial load factor, and Y is the radial load factor. In this case, the axial force would be any reaction force at the bearing location in the x direction of the established coordinate system. Notably, there are no reaction forces in this direction, resulting in that term dropping out of the equation, and X, the radial load factor, being set to 1. Lastly, the rotational factor is also set to 1 due to the fact that the selected bearing is "conventional", which is characterized by its inner race rotating [11]. Substituting these values and using the fact that the axial force component is 0, we arrive at the following simple equation relating equivalent dynamic bearing load to the radial force experienced.

$$P = F_R$$

At each bearing, F_R is the resultant force in the radial direction. This means that the radial force can be related to the defined reactions from the free body diagram as follows.

$$F_{R1} = \sqrt{A_y^{\,2} + A_Z^{\,2}}$$

$$F_{R4} = \sqrt{B_y^{\,2} + B_z^{\,2}}$$

Where F_{R1} is the radial load at location A (or bearing 1 on figure X), and F_{R4} is the radial load at location B (or bearing 4 on figure X). Computing these dynamic loads results in a bearing load of 5292.79 N and 15878.36 N at bearing location 1 and bearing location 4, respectively. With these values determined, the basic lifetime rating, L_{10}, and the hours of operation, L_{10h}, can be determined as follows.

$$L_{10} = \left(\frac{C}{P}\right)^p$$

$$L_{10h} = \frac{10^6}{60n} L_{10}$$

The constant C, is the dynamic load rating of the bearing. Cylindrical roller bearings are chosen for their ability to withstand large radial loads and minimal axial loads. In accordance with the basic lifetime rating equation, the exponent p is set to 10/3 due to the use of cylindrical roller bearings [11].

An iterative design process is conducted to select a bearing with a sufficient lifespan. The design specifications indicate that the electric input shaft will be operational for approximately 40% of the tug's 20 year total lifespan, equating to 70,080 hours of operation. To ensure reliability, a factor of safety of 1.5 is applied to account for any potential increase in operational time beyond the specified 40%. This results in a total "expected designed lifespan" of 105,120 hours. After careful consideration, the NU 226 ECM cylindrical roller bearings are selected due to their dynamic load rating of C = 415,000 N.

The load profile of the electric input shaft is also taken into account when determining the hours of operation, L10h. It is determined that for 70% of its run time, the shaft rotates at 3000 rpm, and for the remaining 30% of the time, it rotates at 1875 rpm. The hours of operation for the bearing at location 4 are calculated as a weighted average of both speeds based on the amount of time the shaft sustains each speed. This calculation is demonstrated below for the bearing at location 3.

$$L_{10h} = L_{10h,3000rpm} * 70\% + L_{10h,1875rpm} * 30\%$$

$$L_{10h} = \left(\frac{10^6}{60*3000\ rpm} * 70\% + \frac{10^6}{60*1875\ rpm} * 30\%\right) * \left(\frac{415{,}000N}{15878.36N}\right)^{10/3}$$

$$L_{10h} = 347337\ hours$$

We can see that the hours of operation is greater than our expected designed lifespan, meaning that the bearing will outlast our design targets. Specifically, the safety factor associated with bearing failure, given by the following formula, is 3.3 for this bearing.

$$SF = \frac{Hours\ of\ Operation}{Designed\ Lifespan} = 3.3$$

Through similar analysis, it was determined that the hours of operation of the bearing at location 1 one to be 13525563.5 hours providing a safety factor of 128.7.

4.3.1 Prime Mover Input Shaft Bearings

Given the fact that the diesel shaft only experiences loading for 5% of the tug's total lifetime of 20 years, bearings are selected to last for at least 8760 hours before safety factors are applied. With a factor of safety of 1.5 applied, the diesel shaft bearings are designed to last for 13,140 hours. The angular speed of the diesel input shaft is determined to be 104.7 rad/s, or 60,000 rotations per hour. With this data, the expected cycles over 13,140 hours can be calculated, to ensure the selected bearings are capable of withstanding the loading over their lifespans. a final number of cycles is calculated as 788.4×10^6. As is consistent for all shafts throughout the design, there are no axial loads, only radial loads, simplifying the analysis. The load P experienced by a bearing is given by the following formula, where V is the rotational

factor, F_R is the radial force, F_A is the axial force, and X and Y are the radial and axial load factors, respectively.

$$P = VXF_R + YF_A$$

$$P = VXF_R$$

Furthermore, both the axial load factor and the rotational factor are 1. This further simplifies the analysis of the force experienced by the bearing. **Figure 67** below shows the prime mover input shaft, where the locations 1 and 3 are where bearings will be mounted.

Figure 67: *Locations of bearings on prime mover input shaft (1 and 3)*

Loading in each of the bearing locations is determined via the free body diagram in section X above. From the static equilibrium equations established via the free body diagram, locations 1 and 2 experience a bearing load of 39695.9 N and 13231.97 N, respectively. Using the bearing load and the design lifespan, bearings were selected to meet the requirements. A NU 1034 ML cylindrical roller bearing was selected from SKF [13]. They specify a C value of 320,000, allowing for the calculation of the basic life rating, L_{10} as follows.

$$L_{10} = \left(\frac{C}{P}\right)^p$$

Using the provided C value and p = 10/3, the basic lifespan is determined to be 1050×10^6 cycles. This provides a respectable factor of safety of 1.3 for the bearing at location 1, and 51.9 for the bearing at location 3.

4.3.3 Reduction Shaft Bearings

The reduction shaft turns whenever either the electric input shaft, or the prime mover input shaft turns. Therefore, as per the provided design specifications, since the electric input

shaft runs for 40% of the 20 year lifespan, this equates to an estimated lifetime of 70,800 hours. When a factor of safety of 1.5 is then applied to account for variance of estimated run time, the design life is asserted to be 105,120 hours. However, for 5% of the lifespan, the reduction shaft will be powered by both the prime mover input shaft and the electric motor input shaft. Specifically, for 70% of its running time, the reduction shaft will experience an angular speed of 1200 rpm, while for the remaining 30% the angular speed will be 750 rpm. The loads at each of the bearings were also calculated using the static equilibrium equations established from the free body diagram of the shaft in section X. Specifically, bearings will be mounted at locations 1 and 5 on the shaft as shown in **figure 68** below.

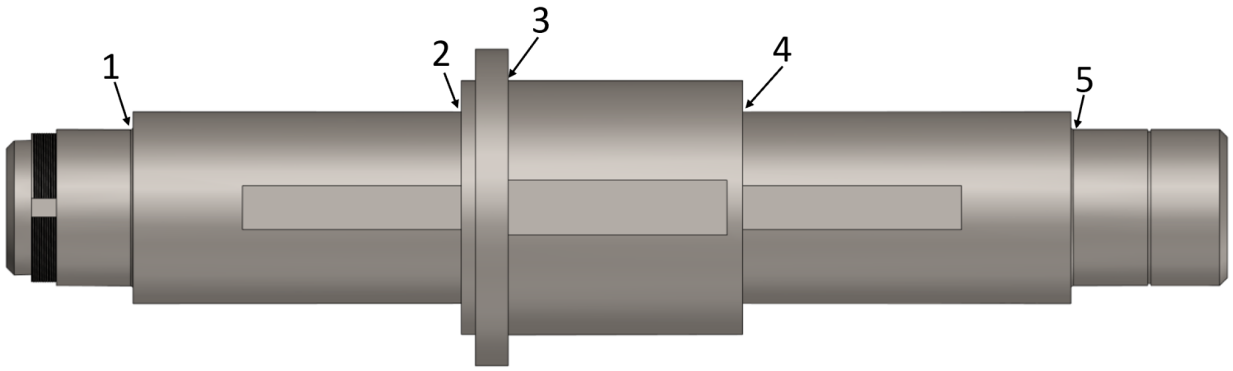

Figure 68: *Reduction shaft bearing locations (1 and 5)*

The bearing loads, P, are again calculated at each bearing location and found to be 95407.8N and 80948.5N at locations 1 and 5, respectively. With the design lifespan and the bearing loads, the NU 2240 ECML roller bearings were selected [13]. They specify a C value of 1,370,000, allowing for the calculation of the hours of operation value, L_{10h}. Similarly to the electric input shaft, the L_{10h} value was calculated as a sum of the percentage of the time at maximum angular speed and the percentage of the time at the lower angular speed as shown below.

$$L_{10h} = \left(\frac{10^6}{60*1200\,rpm} * 70\% + \frac{10^6}{60*750\,rpm} * 30\%\right)L_{10}$$

Completing this calculation, the operational hours are found to be 117942.8 h and 203980.2 h at locations 1 and 5, respectively. Comparing these values with the asserted design life of 105,120 hours, the design exhibits safety factors of 1.12 at location 1 and 1.9 at location 5.

4.3.4 Output Shaft Bearings

The output shaft has the exact same lifespan parameters as the reduction shaft, as it is under power for the same time period. However, the bearings experience different loads, and the angular speed of the shaft is significantly smaller than that of the reduction shaft. The output shaft also shares the property that for 70% of its running time it undergoes a larger angular speed of 700 rpm and 250 rpm for the remaining 30%. Continuing with the same process as for the previous shafts, the design lifespan was found to be 40% of 20 years, or 70,800 hours. Again applying a 1.5 factor of safety gives a designed life of 105,120 hours. **Figure 69** below shows the locations where bearings will be mounted on the output shaft, specifically locations 1 and 3.

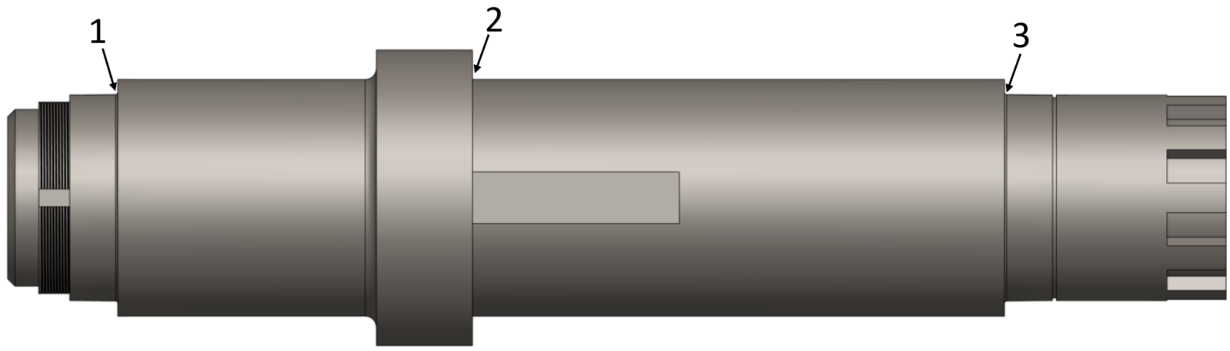

Figure 69: *Output shaft bearing locations (1 and 3)*

Evaluating the equations of static equilibrium to determine the reaction loads at locations 1 and 3 gives bearing loads of 56456.4N at location 1 and location 2. From this information in combination with the designed lifespan, the NU 1056 ML cylindrical roller bearings from SKF were chosen [14]. These bearings specify a C value of 765,000, allowing for the calculation of the hours of operation, L_{10h} in a similar manner to the previous shafts.

$$L_{10h} = \left(\frac{10^6}{60*400\ rpm} * 70\% + \frac{10^6}{60*250\ rpm} * 30\%\right)L_{10}$$

Calculating the hours of operation gives 291629.8769 hours for both bearings, resulting in a factor of safety of 2.8 for each bearing.

4.4 Detailed Housing Design

The gearbox housing was designed using two main structural components, a tub and a lid (see **Figure 70** and **71**). The seam between these two components is horizontal and crosses the axis of each shaft in order to provide a simple yet secure mount for all bearings. Each bearing is supported by the wall of the housing below and encased by the wall of the housing above. Housing abutments prevent movement toward the interior of the gearbox while cover plates with additional abutments prevent outward motion (**Figures 72** and **73**). Where input or output shafts are required to leave the gearbox, these cover plates include additional o-rings to seal the interior of the gearbox from the environment.

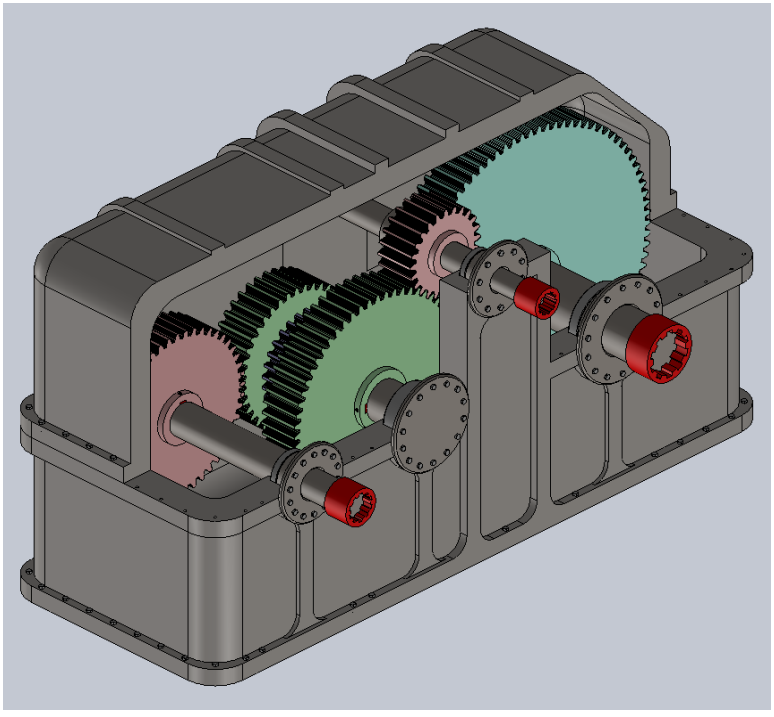

Figure 70: *Partial section view of full gearbox assembly*

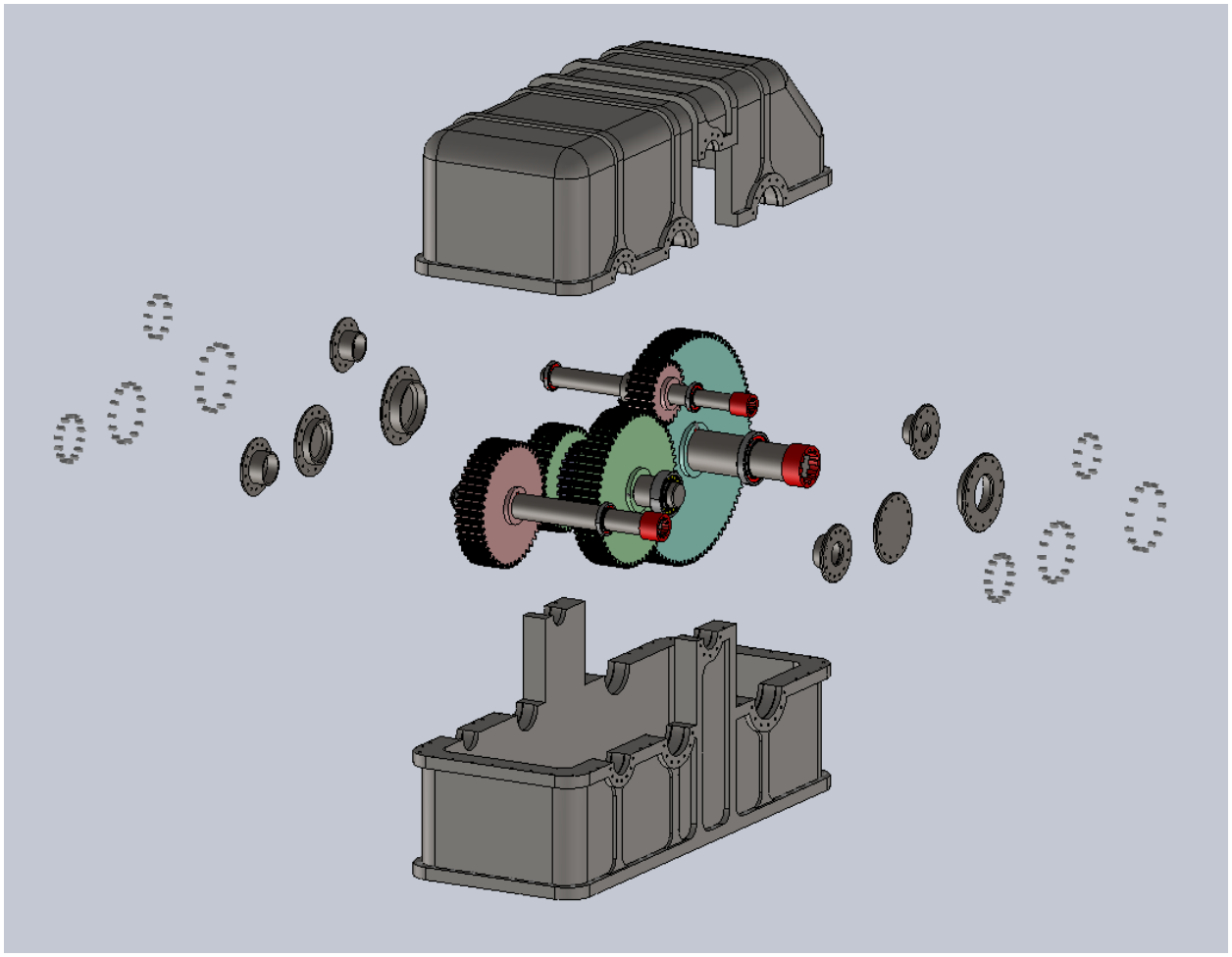

Figure 71: Exploded view of full gearbox assembly

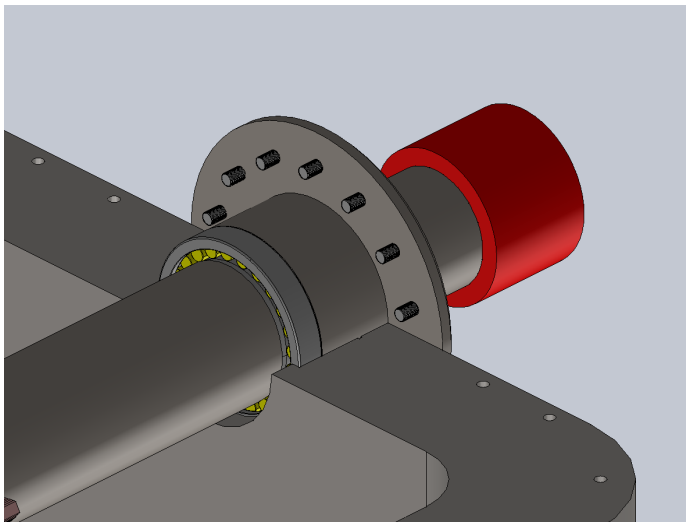

Figure 72: *Section view of the diesel input shafts where it enters the gearbox*

Figure 73: *Section view of the electric input shaft where it enters the gearbox*

The gearbox housing is mounted to the frame of the vessel using thirty-eight ¾-26 hex head screws arrayed around the perimeter of the tub's footprint. Similarly, the housing lid is secured to the housing tub using another thirty-eight ¾-26 hex head screws.

When fully assembled, the gearbox is 4.1 meters long, 1.6 meters wide, and 2.2 meters tall, resulting in an overall displaced volume of $14.43m^3$. The internal gear mechanisms are arranged such that both input shafts and the output shaft enter the gearbox on the same side (Figure 70).

During routine maintenance, the gears' bearings may be exposed by removing the shaft covers, allowing for convenient lubrication access. For work that requires access to the gears or shafts themselves, the housing lid may be removed. Given their arrangement within the gearbox, each shaft subassembly is stable and secure enough for maintenance even without the presence of the housing lid.

4.5 Secondary Gearbox Elements

4.5.1 Couplings

The initial design idea for the couplings was to source prefabricated ones that could withstand the forces observed by the system. It was quickly discovered that no coupling found online would work for this application and instead this gearbox would require custom fabricated ones. A simple yet effective type of coupling are spline couplings. They are very commonly used in transmission as they can transmit very high torques and would be ideal for use in a gearbox. The decided upon coupling type was a parallel key spline which was used in both the inputs as

well as the output shaft. Engineering drawings for all the couples can be observed in **Figures 74**, **75**, and **76** below.

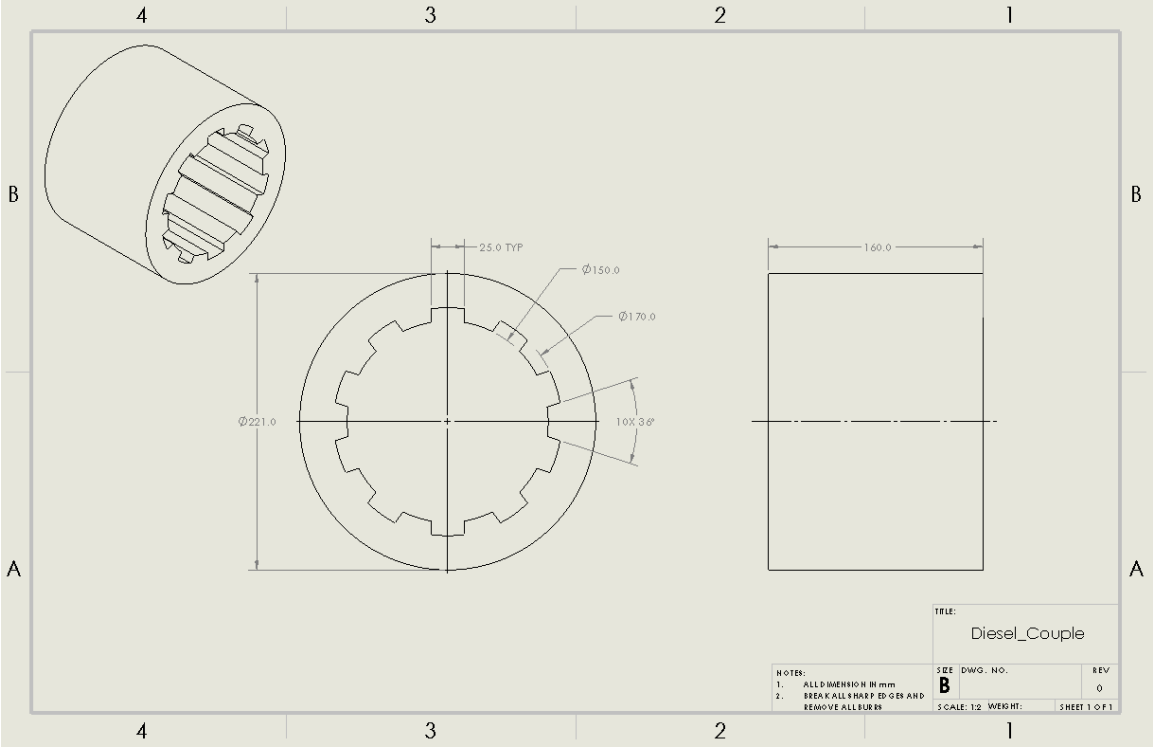

Figure 74: *Diesel power coupling*

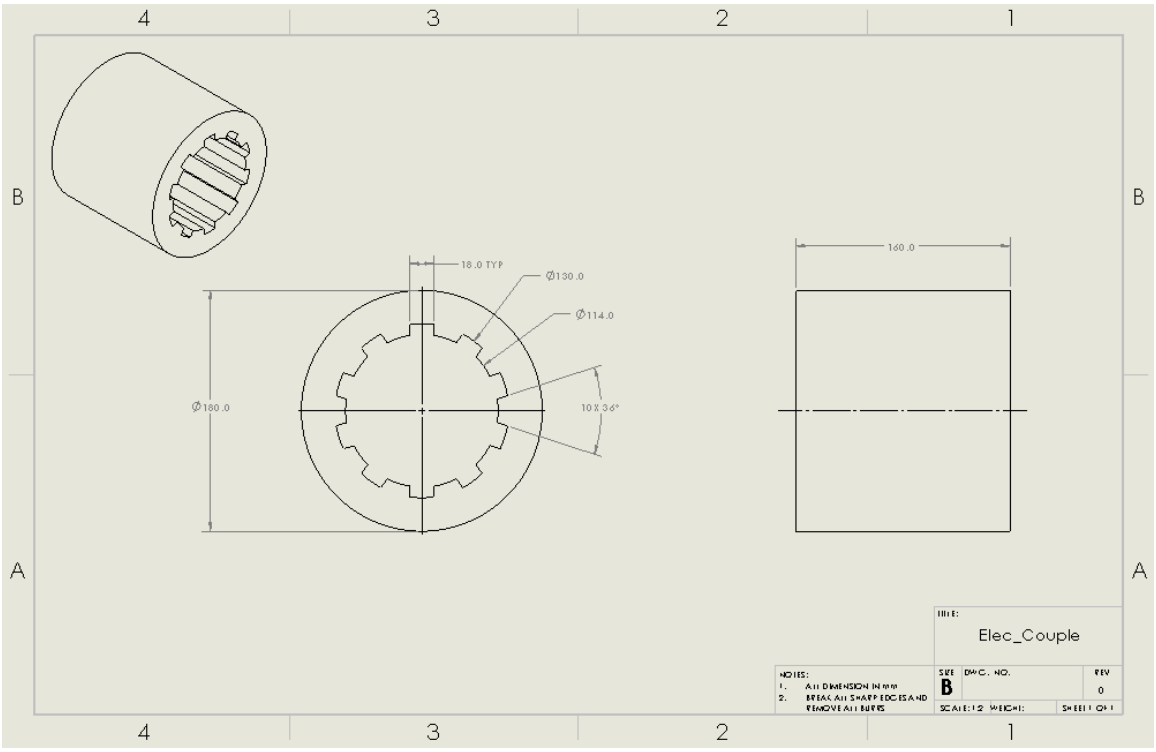

Figure 75: *Electric power coupling*

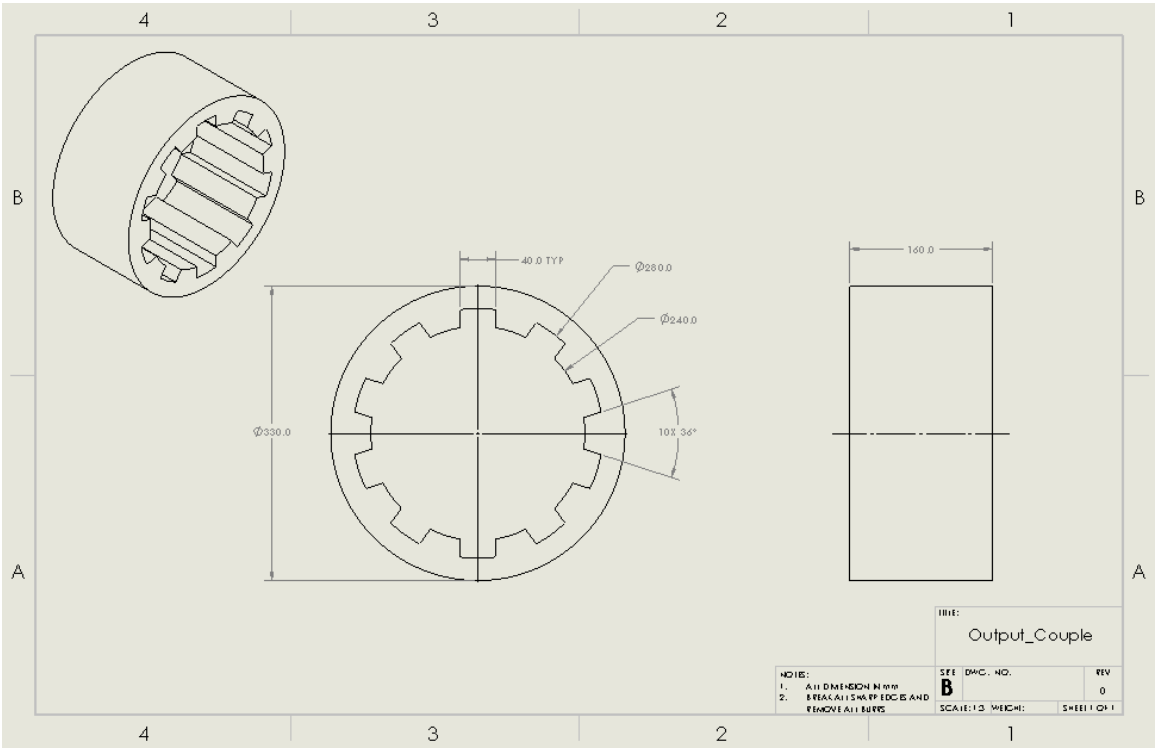

Figure 76: *Output coupling*

The couplings are to be manufactured from 1045 hot rolled steel, the same material as the shaft. This way the coupling and the shaft have the same strength and will wear evenly.

4.5.2 Keys

As previously discussed, each of the gears will be mounted to their respective shafts by using keyways and keys. Keyed connections are a very useful and common way to transmit high torque between gears and shafts. Since this gearbox will undergo high torque loads it was decided that a keyed connection would be a suitable method of power transmission. The rectangular keys that are used in this design are based on the ISO/R773 - Js9 standard for metric keyways [19]. Based on this standard, custom fabricated keys were designed since it is not common to source keys online of the size necessary for this application. A drawing showing these keys is displayed below in **Figure 77.**

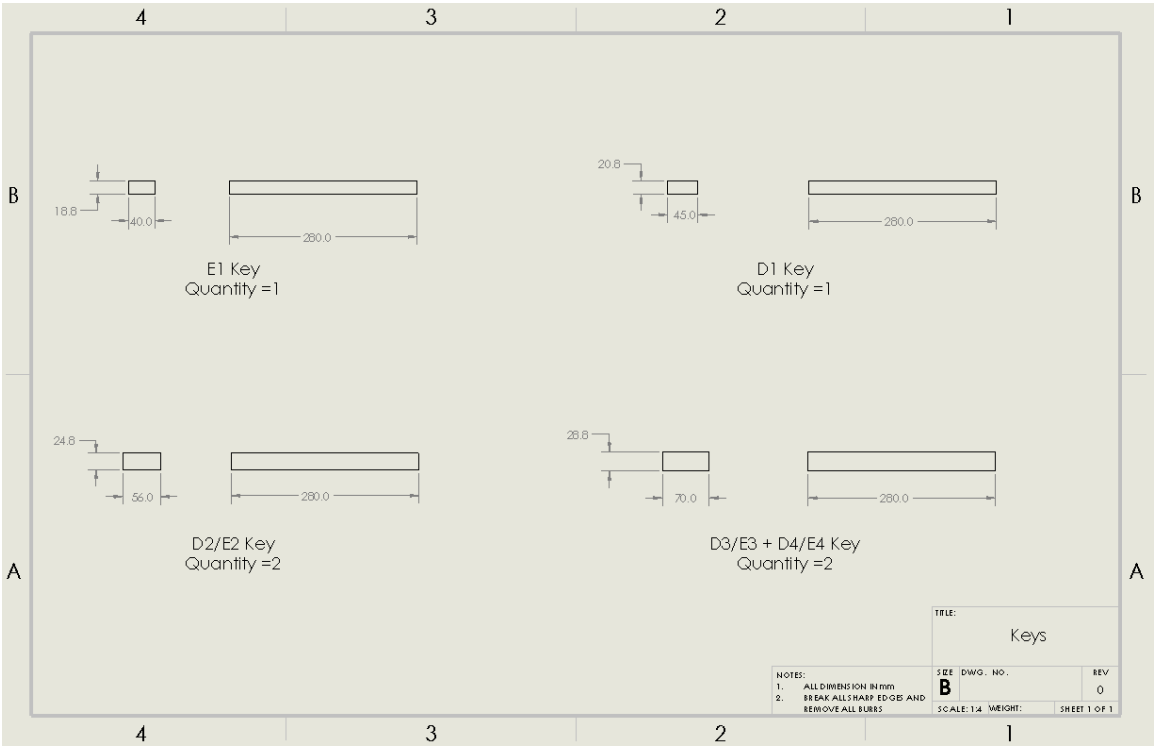

Figure 77: Drawings for custom keys

The keys will also be manufactured from 1045 hot rolled steel to best perform with the shafts of the same material.

4.6 Assembly

The gearbox is composed of many subassemblies that are interconnected to create one functional assembly. The full assembly has the ability to be moved and secured to the desired application using its associated housing. By removing the housing, the gearbox can be separated into its subassemblies for repairs and maintenance. Looking at each of the subassemblies it is observed that they are all composed of the same parts that are required for a proper gearbox. These parts include the shaft, gears, bearings, lock nut, spring washer, retaining ring, set screws, and keys. Each subassembly will be analyzed in the further sections.

4.6.1 Diesel Input Subassembly

The diesel input subassembly supports the diesel input shaft and gear. An exploded drawing view of this assembly is shown in **Figure 78** below with the bill of materials included [BOM].

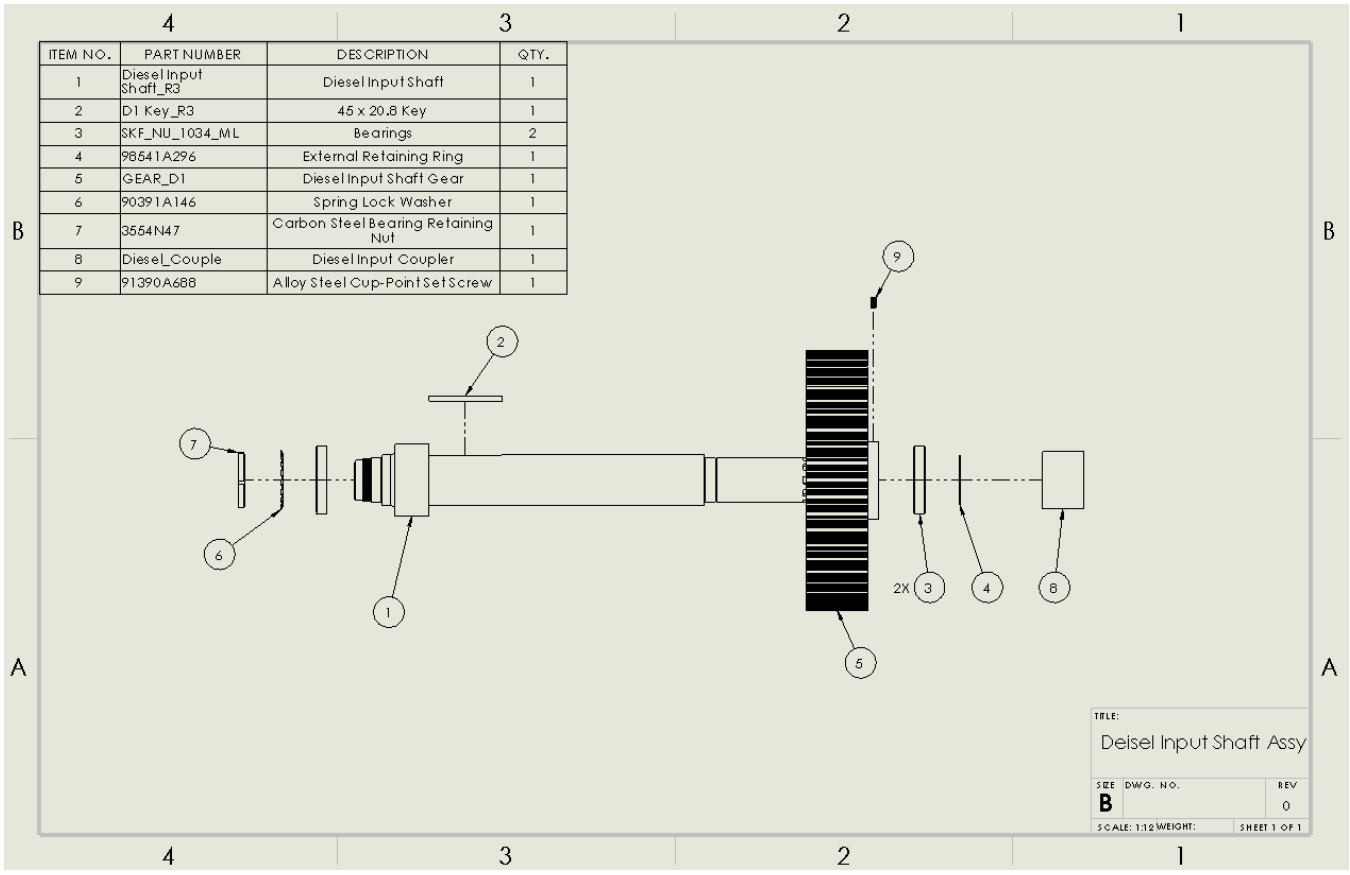

Figure 78: *Diesel input subassembly drawing*

An exploded view is used to visually demonstrate the steps required to assemble the assembly. The parts furthest from the shaft will be mounted last while the parts closest to the shaft will be mounted first. For example, in this case the bearing (or item 3) on the left side will be mounted onto the shaft before the locking washer. The gear shaft assembly steps for each shaft is as follows:

1. Place the key (2) in the keyseat
2. Mount the gear (5) onto the key using keyway in gear
3. Secure set screw (9) to shaft by screwing through gear tapped hole
4. Mount bearings (3) on both sides by press fitting using hot hot mounting [18]
5. Attach retaining ring on free side of shaft (4)
6. Place shaft inside housing (not shown)
7. Attach spring washer (6) then lock nut (7) to fixed side
8. Mount coupler (8) to side with spline

4.6.2 Electric Input Subassembly

The electric input shaft assembly can be observed in **Figure 79** below.

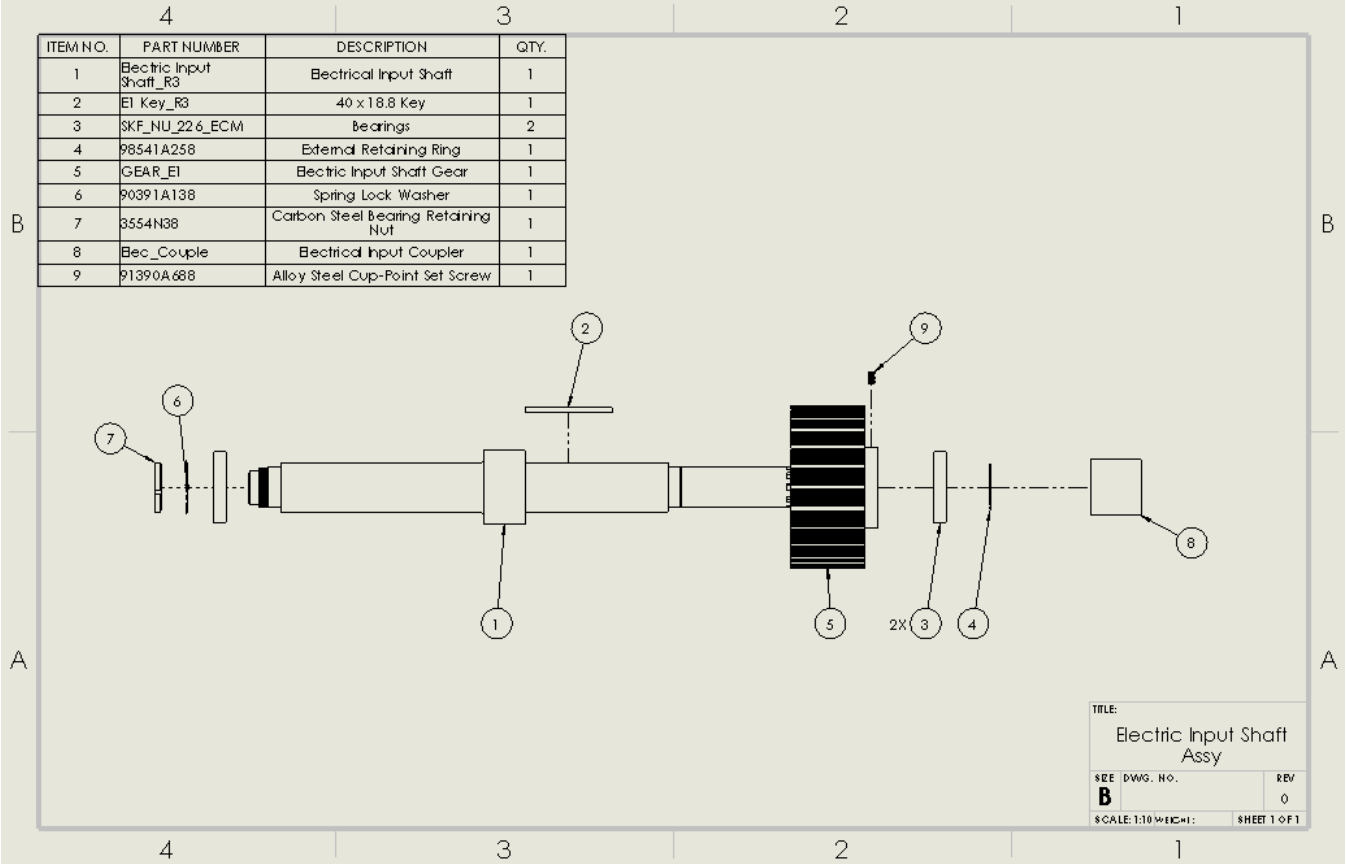

Figure 79: *Electric input subassembly drawing*

The assembly steps are the same as the diesel input subassembly.

4.6.3 Reduction Subassembly

The reduction subassembly is slightly more complicated as it requires three gears instead of one. It also does not have a couple. The exploded view drawing of this subassembly is shown in **Figure 80** below.

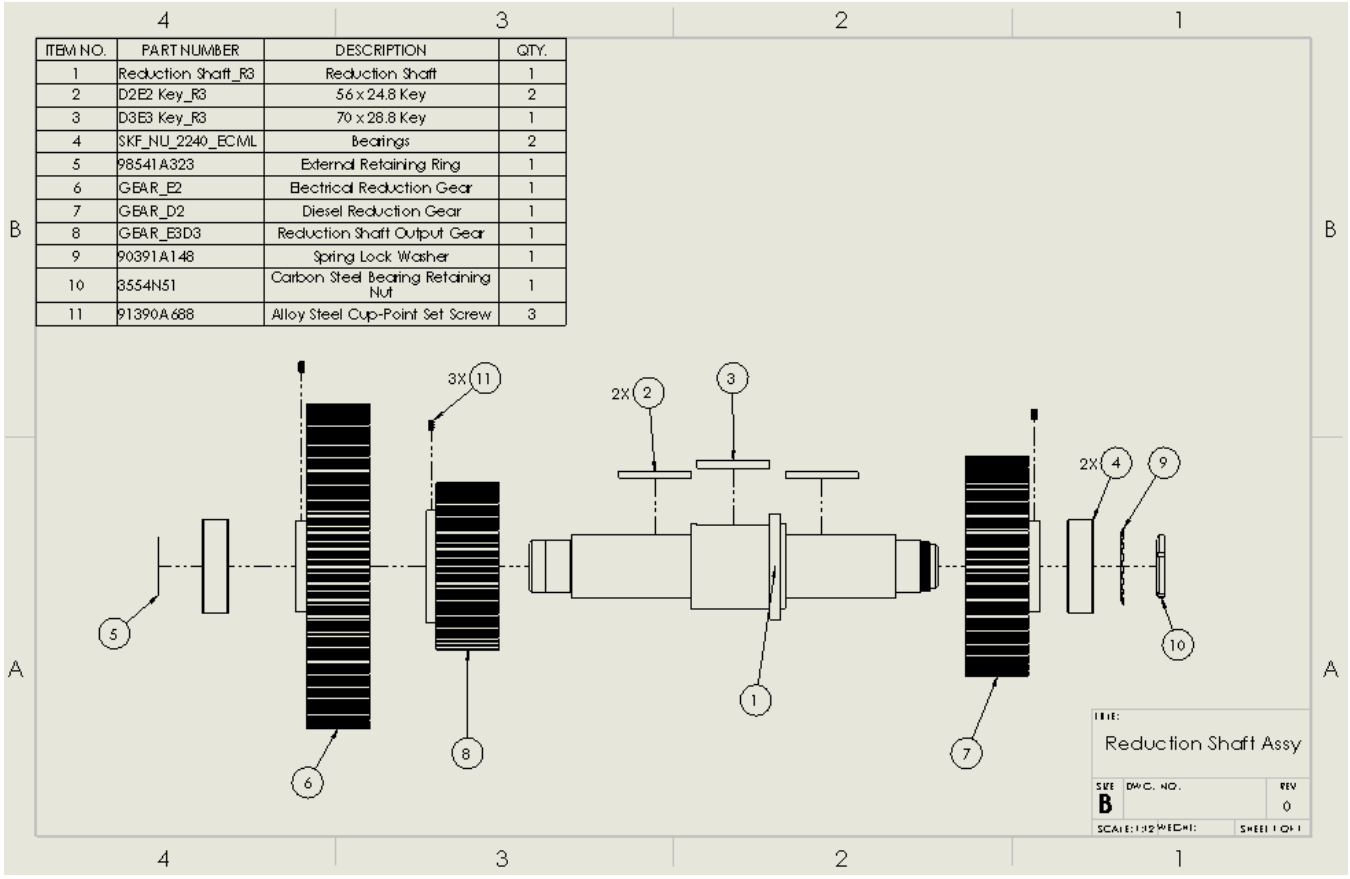

***Figure 80**: Reduction shaft subassembly drawing*

The steps followed for the reduction shaft subassembly are the same as the input shafts but the gears must be assembled onto the shaft from inside out. This means that the middle gear (8) is placed on first, then the outside gears (6,7) can be mounted after. The keys for each gear are placed in the proper keyseat right before the gear is mounted.

4.6.4 Output Subassembly

The output subassembly follows the identical steps as the two input assemblies as it similarly only has one gear. The subassembly drawing for the output can be observed in **Figure 81** below.

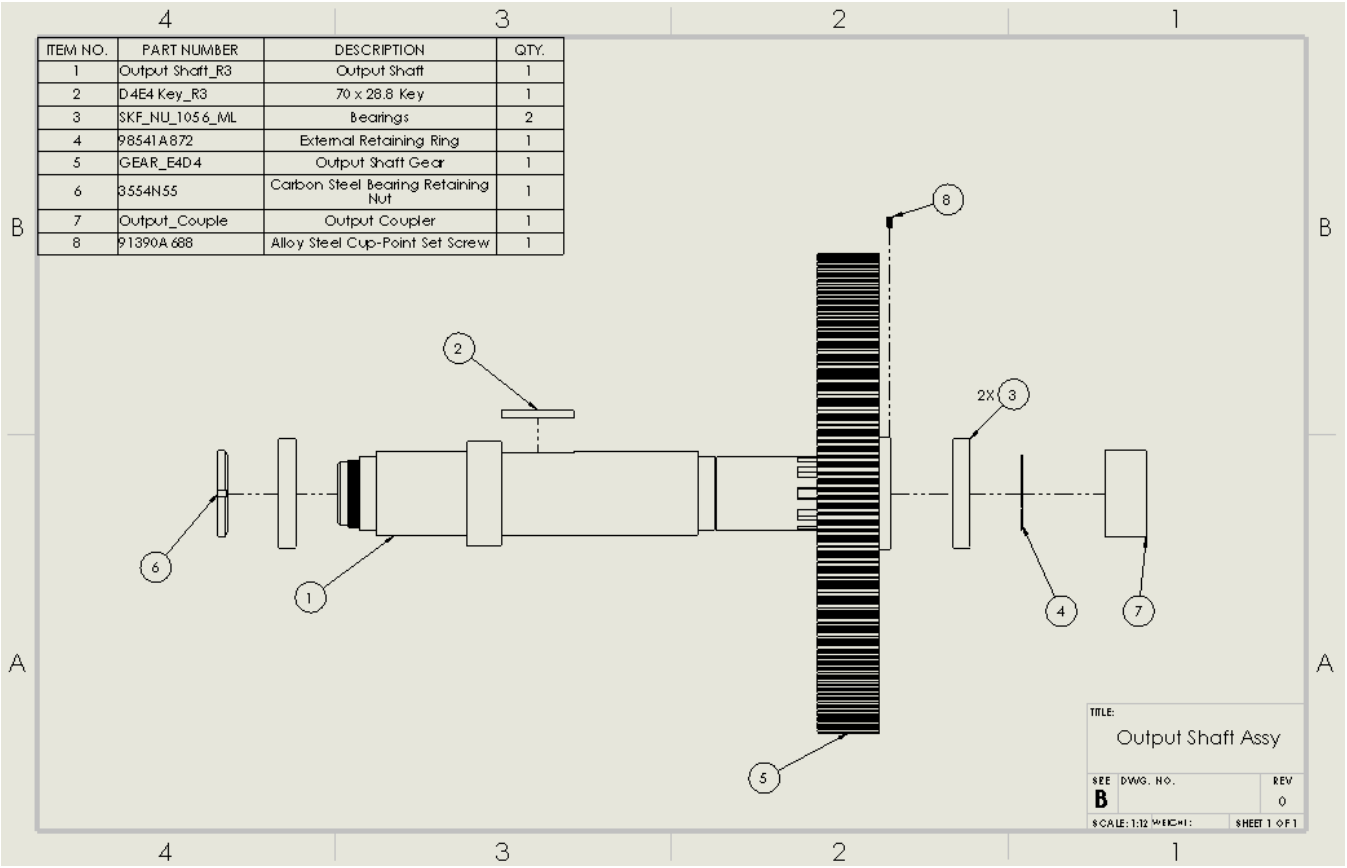

***Figure 81**: Output shaft subassembly drawing*

4.6.5 Full Assembly

Once each shaft subassembly has been assembled as described in the previous section, they are ready to be installed in the gearbox itself. The full assembly procedure is detailed in **Figure 82** below.

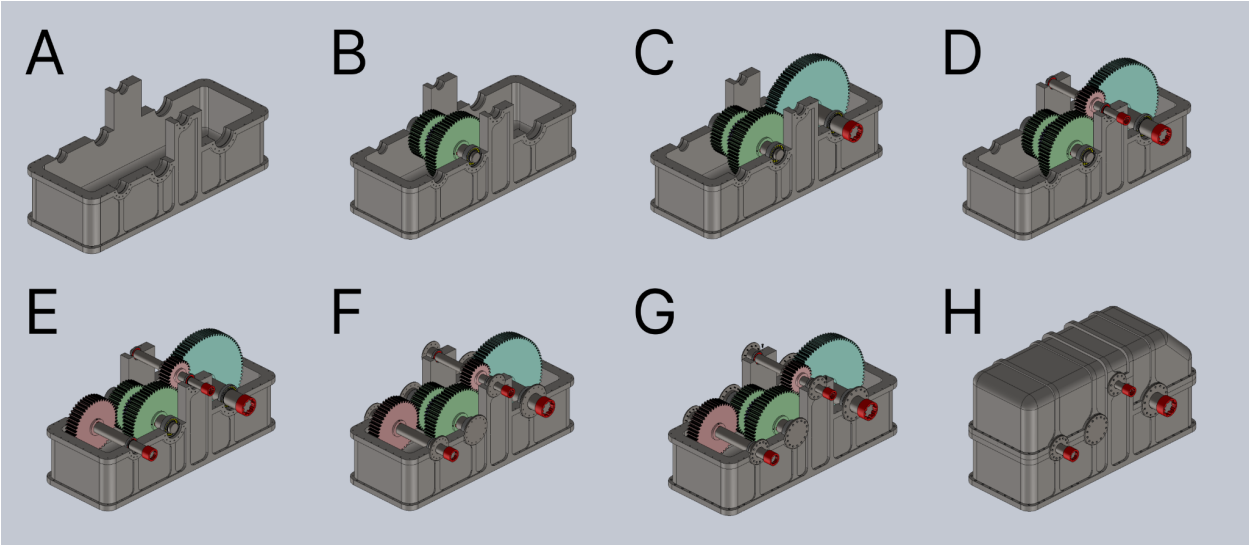

***Figure 82**: Gear Box Housing Assembly Process*

A: Housing tub is secured to the vessel's frame using thirty-eight ¾-26 hex head screws

B: Reduction shaft subassembly added along with two NU 2240 ECML bearings

C: Output shaft subassembly added along with two NU 1056 ML bearings

D: Electric input shaft subassembly added along with two NU 226 ECM bearings

E: Diesel input shaft subassembly added along with two NU 1034 ML bearings

F: Cover plates added with o-rings to seal all four shaft subassemblies

G: Cover plates secured in place using M20 hex head screws

H: Housing lid added to assembly and secured in place using thirty-eight ¾-26 hex head screws

4.6.6 Bill of Materials

Below in **table 71** is included the bill of materials for the full gearbox assembly.

***Table 71**: Full gearbox assembly bill of materials*

Part Number	Component	Quantity
Electrical input shaft_R3	Electric input shaft	1
E1 Key_R3	40 x 18.8 key	1
SKF_NU_226_ECM	Electric input shaft bearing	2
98541A296	External retaining ring	1
GEAR_E1	Electric input shaft gear	1
90391A138	Spring lock washer	1
3554N38	Carbon steel bearing retaining nut	1
Elec_Couple	Electric input coupler	1
91390A688	Alloy steel cup-point set screw	6
Diesel Input Shaft_R3	Diesel input shaft	1
D1 Key_R3	45 x 20.8 key	1
SKF_NU_1034_ML	Bearing	2
98541A296	External retaining ring	1
GEAR_D1	Diesel input shaft gear	1
90391A146	Spring lock washer	1
3554N47	Carbon steel bearing retaining nut	1
Diesel_Couple	Diesel input coupler	1
Reduction shaft_R3	Reduction shaft	1
D2E2 Key_R3	56 x 24.8 key	2
D3E3 Key_R3	70 x 28.8 key	1

SKF NU 2240 ECML	Reduction shaft bearing	2
98541A323	External retaining ring	1
GEAR_E2	Electrical reduction gear	1
GEAR_D2	Diesel reduction gear	1
GEAR_E3D3	Reduction shaft output gear	1
90391A148	Spring lock washer	1
665N51	Carbon steel cup-point set screw	3
Output Shaft_R3	Output shaft	1
D4E4 Key R3	70 x 28.8 key	1
SKF_NU_1056_ML	Bearing	2
98541A872	External retaining ring	1
GEAR_E4D4	Output shaft gear	1
3554N55	Carbon steel bearing retaining nut	1
Output_Couple	Output coupler	1
Housing_Tub	Bottom half of housing	1
Housing_Lid	Top half of housing	1
92240A382	Stainless steel hex head screw	180
Housing_Cover1a	Hollow disk cover for output shaft port	1
Housing_Cover1b	Solid disk cover for output shaft port	1
Housing_Cover2a	Solid disk cover for reduction shaft ports	1
Housing_Cover2b	Solid disk cover for reduction shaft ports	1
Housing_Cover3a	Hollow disk cover for electric input port	1
Housing_Cover3b	Solid disk cover for electric input port	1
Housing_Cover4a	Hollow disk cover for diesel input port	1
Housing_Cover4b	Solid disk cover for diesel input port	1

Buna-N O-Ring, 265mm OD	O-ring to seal output shaft ports	2
Buna-N O-Ring, 365mm OD	O-ring to seal reduction shaft ports	2
Buna-N O-Ring, 265mm OD	O-ring to seal electric input shaft ports	2
Buna-N O-Ring, 235mm OD	O-ring to seal diesel input shaft ports	2

Conclusion

This report presented the design of a gearbox for a hybrid-electric tugboat, developed for Robert Allan Naval Architects & Marine Engineers (RAL). Initial gear reduction and powertrain calculations were made, to ensure specified output speeds and torques, and powers were met. Bearings were selected to facilitate smooth rolling of the shafts and carry the reaction loads.

Fatigue analysis was conducted on the gears, shafts, and bearings, to ensure a lifetime of 20 years. A housing was designed to enclose the gearbox, to contain the lubrication, and prevent contaminant ingress, and an itemized assembly process was written, to ensure smooth assembly and installation of all gearbox components.

References

[1] "Shipbuilding customized marine gearboxes: Novagear AG," *Novagear*, 31-Aug-2018. [Online]. Available: https://www.novagear.ch/en/shipbuilding/. [Accessed: 22-Oct-2022].

[2] "Flender Gearboxes", *Flender*. [Online]. Available: https://www.flender.com/en/media-download/media/PCMD-B10012-00-WS-Marine-2-Gang-Getriebe. [Accessed: 22-Oct-2022]

[3] "Marine Services," *KOTUG Canada*, 06-Apr-2021. [Online]. Available: https://www.kotugcanada.ca/activities/marine-services. [Accessed: 22-Oct-2022].

[4] "About HaiSea Marine," *HaiSea Marine*, 17-May-2022. [Online]. Available: https://haiseamarine.com/. [Accessed: 22-Oct-2022].

[5] "Average design engineer salary in Vancouver, British Columbia," *PayScale*. [Online]. Available: https://www.payscale.com/research/CA/Job=Design_Engineer/Salary/51df3258/Vancouver-BC. [Accessed: 22-Oct-2022].

[6] "How Much Does SOLIDWORKS Cost?," *Solidworks price*, 20-Jun-2022. [Online]. Available: https://www.cati.com/solidworks-price/. [Accessed: 22-Oct-2022].

[7] A. Vincze, "Involute Spur Gear Generator and simulator," *Gear Generator*, 22-Oct-2022. [Online]. Available: https://geargenerator.com/#400,400,400,30,0,0,0,5,1,16,0.16,100,27,-90,0,0,0,0,0,0,0,60,0.6,100,27,-90,0,0,0,0,1,1,40,0.4,100,27,-90,0,0,0,0,2,0,80,0.8,100,27,-90,0,0,0,0,2,0,32,0.32,100,27,-90,0,0,0,0,0,0,3,403. [Accessed: 22-Oct-2022].

[8] "Drivetrain losses (efficiency)," *X-Engineer*. [Online]. Available: https://x-engineer.org/drivetrain-losses-efficiency/. [Accessed: 22-Oct-2022].

[9] "McMaster Carr," *Catalog*. [Online]. Available: https://www.mcmaster.com/. [Accessed: 13-Nov-2022].

[10] Engineering ToolBox, (2005). Torsion of Shafts. [Online] Available at: https://www.engineeringtoolbox.com/torsion-shafts-d_947.html [Accessed: 13-Nov-2022].

[11] R. L. Norton, *Machine design: An integrated approach*. Hoboken, NJ: Pearson, 2020.

[12] *SKF*. [Online]. Available: https://www.skf.com/ca/en. [Accessed: 13-Nov-2022].

[13] "NU 1034 ML," *SKF*. [Online]. Available: https://www.skf.com/ca/en/products/rolling-bearings/roller-bearings/cylindrical-roller-bearings/single-row-cylindrical-roller-bearings/productid-NU%201034%20ML. [Accessed: 15-Dec-2022].

[14] "NU 226 ECM," *SKF*. [Online]. Available: https://www.skf.com/ca/en/products/rolling-bearings/roller-bearings/cylindrical-roller-bearings/single-row-cylindrical-roller-bearings/productid-NU%20226%20ECM. [Accessed: 15-Dec-2022].

[15] "NU 2240 ECML," *SKF*. [Online]. Available: https://www.skf.com/ca/en/products/rolling-bearings/roller-bearings/cylindrical-roller-bearings/single-row-cylindrical-roller-bearings/productid-NU%202240%20ECML. [Accessed: 15-Dec-2022].

[16] "NU 1056 ML," *SKF*. [Online]. Available: https://www.skf.com/ca/en/products/rolling-bearings/roller-bearings/cylindrical-roller-bearings/single-row-cylindrical-roller-bearings/productid-NU%201056%20ML. [Accessed: 15-Dec-2022].

[17] “General information,” *The Transmission Centre*. [Online]. Available: http://thetransmissioncentre.com.au/?page_id=105. [Accessed: 17-Dec-2022].

[18] “SKF Mounting Instructions,” *SKF*. [Online]. Available: https://mount.skf.com/?lang=en. [Accessed: 17-Dec-2022].

[19] E. Edge, “Metric Key Keyway Dimensions,” *Engineers Edge - Engineering, Design and Manufacturing Solutions*. [Online]. Available: https://www.engineersedge.com/hardware/metric_key_keyway_dimensions_13448.htm. [Accessed: 17-Dec-2022].

Appendix A - Bearing Printouts

NU 2240 ECML - Reduction Shaft

SKF

Technical Specification

SKF performance class	SKF Explorer

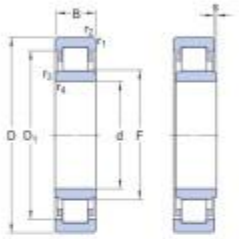

Dimensions

d	200 mm	Bore diameter
D	360 mm	Outside diameter
B	98 mm	Width
D_1	≈ 312.9 mm	Shoulder diameter of outer ring
F	241 mm	Raceway diameter of inner ring
$r_{1,2}$	min. 4 mm	Chamfer dimension
$r_{3,4}$	min. 4 mm	Chamfer dimension
s	max. 5.1 mm	Permissible axial displacement

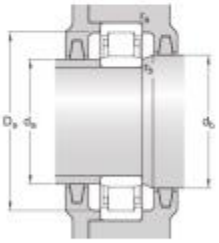

Abutment dimensions

d_a	min. 217 mm	Diameter of spacer sleeve
d_a	max. 236 mm	Diameter of spacer sleeve
d_b	min. 245 mm	Diameter of shaft abutment
D_a	max. 341.6 mm	Diameter of housing abutment
r_a	max. 3 mm	Radius of fillet
r_b	max. 3 mm	Radius of fillet

Calculation data

Basic dynamic load rating	C	1 370 kN
Basic static load rating	C_0	1 800 kN
Fatigue load limit	P_u	180 kN

NU 226 ECM - Electric Input Shaft

SKF

Technical Specification

SKF performance class	SKF Explorer

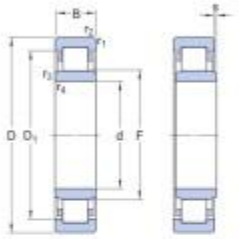

Dimensions

d	130 mm	Bore diameter
D	230 mm	Outside diameter
B	40 mm	Width
D_1	≈ 200.3 mm	Shoulder diameter of outer ring
F	153.5 mm	Raceway diameter of inner ring
$r_{1,2}$	min. 3 mm	Chamfer dimension
$r_{3,4}$	min. 3 mm	Chamfer dimension
s	max. 2.1 mm	Permissible axial displacement

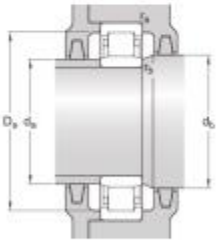

Abutment dimensions

d_a	min. 144 mm	Diameter of spacer sleeve
d_a	max. 150 mm	Diameter of spacer sleeve
d_b	min. 157 mm	Diameter of shaft abutment
D_a	max. 215.4 mm	Diameter of housing abutment
r_a	max. 2.5 mm	Radius of fillet
r_b	max. 2.5 mm	Radius of fillet

Calculation data

Basic dynamic load rating	C	415 kN
Basic static load rating	C_0	455 kN
Fatigue load limit	P_u	51 kN

NU 1056 ML - Output Shaft

SKF

Technical Specification

SKF performance class	SKF Explorer

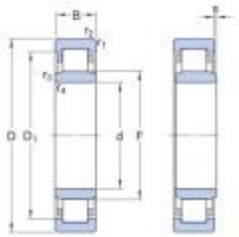

Dimensions

d	280 mm	Bore diameter
D	420 mm	Outside diameter
B	65 mm	Width
D_1	≈ 373.1 mm	Shoulder diameter of outer ring
F	316 mm	Raceway diameter of inner ring
$r_{1,2}$	min. 4 mm	Chamfer dimension
$r_{3,4}$	min. 4 mm	Chamfer dimension
s	max. 8 mm	Permissible axial displacement

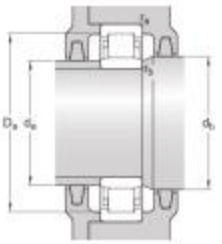

Abutment dimensions

d_a	min. 295 mm	Diameter of spacer sleeve
d_a	max. 312 mm	Diameter of spacer sleeve
d_b	min. 321 mm	Diameter of shaft abutment
D_a	max. 405 mm	Diameter of housing abutment
r_a	max. 3 mm	Radius of fillet
r_b	max. 3 mm	Radius of fillet

Calculation data

Basic dynamic load rating	C	765 kN
Basic static load rating	C_0	1 060 kN
Fatigue load limit	P_u	102 kN

NU 1034 ML - Diesel Input Shaft

SKF

Technical Specification

SKF performance class	SKF Explorer

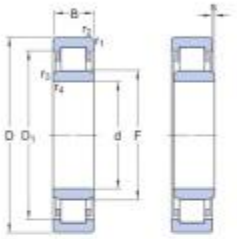

Dimensions

d	170 mm	Bore diameter
D	260 mm	Outside diameter
B	42 mm	Width
D_1	≈ 226.9 mm	Shoulder diameter of outer ring
F	193 mm	Raceway diameter of inner ring
$r_{1,2}$	min. 2.1 mm	Chamfer dimension
$r_{3,4}$	min. 2.1 mm	Chamfer dimension
s	max. 5.8 mm	Permissible axial displacement

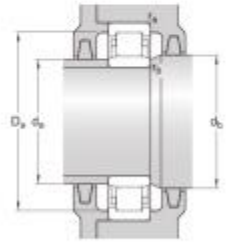

Abutment dimensions

d_a	min. 180 mm	Diameter of spacer sleeve
d_a	max. 189 mm	Diameter of spacer sleeve
d_b	min. 197 mm	Diameter of shaft abutment
D_a	max. 250 mm	Diameter of housing abutment
r_a	max. 2 mm	Radius of fillet
r_b	max. 2 mm	Radius of fillet

Calculation data

Basic dynamic load rating	C	320 kN
Basic static load rating	C_0	400 kN
Fatigue load limit	P_u	41.5 kN

Appendix B - Sample hand calculations

B-1: Spur Gear Fatigue Bending

Spur Gear Fatigue Bending

Material Strength (Bending) Output

$$S_{fb} = \frac{K_L}{K_T K_R} S'_{fb} \quad \text{(AGMA)}$$

Where

$S'_{fb} = 340\,MPa$ (A5 steel)

$K_T = 1$ (operating below 250°F)

$K_R = 1$ (For 99% reliability)

$K_L = (1.6831)N^{-0.0323} = 0.9063$ (For $N = 2.1 \times 10^8$ cycles)

$S_{fb} = 308\,MPa$ ← Fatigue strength of output

Bending Stress

$$\sigma_b = \frac{W_t}{m\,F\,J} \cdot \frac{K_a K_m}{K_v} \cdot K_s K_B K_I$$

0-

where

$m = 20\,mm$ (module)

$J = 0.4193$ (Bending Strength Geometry factor)

$F = 240mm$ (face-width)

and

$K_a = 1.66$ (Driven by $\frac{1}{3}$ electric $\frac{2}{3}$ Diesel, moderate shock)

$K_s = 1$

$K_B = 1$

$K_I = 1$

$K_m = 1.77$

$K_v = 0.8470$

Tangential load

$$W_t = \frac{T}{r} = 38618.4\ N$$

Where

T = torque $= 95493\ N \cdot m$

r = gear radius $= 0.9m$

$\sigma_b = 183.6\,MPa$ ← Bending Stress of E.

Safety Factor

$$SF = \frac{S_{fb}}{\sigma_b} = 1.67$$ ← safety factor, bending output gear

B-2: Spur gear surface fatigue

Spur Gear Surface Fatigue

Material Strength (surface fatige) E4D4 meshing E3D3

$$S_{fc} = \frac{C_L C_H}{C_T C_R} S'_{fc}$$

where

$S'_{fc} = 1150\ MPa$ (AS steel)

$C_R = 1$ (99%)

$C_T = 1$ (<250°F)

$C_H = 1$

$C_L = 0.8432$

$S_{fc} = 4.097\ MPa$ ← Surface fatigue strength, output gear.

Surface Fatigue Stress

$$\sigma_c = C_p \sqrt{\frac{W_t}{F I d} \cdot \frac{C_a C_m}{C_v} \cdot C_s C_f}$$

where

$$I = \frac{\cos\phi}{\left(\frac{1}{S_p} \pm \frac{1}{S_g}\right) d_p} = 0.136$$

$F = 240mm$ (face width)

$d = 1.8m$ (Diameter)

$W_t = 106103.3\ N$ (Tangential contact force)

and

$C_a = 1.66$

$C_s = 1$

$C_m = 1.777$

$C_v = 0.847$

$C_p = 191\ MPa^{\frac{1}{2}}$

$C_f = 1$

$\sigma_c = 479.04\ MPa$ ← Surface fatigue stress, output

Safety Factor, Surface fatigue

$$SF = \left(\frac{S_{fc}}{\sigma_c}\right)^2 = 4.097$$ ← Safety factor, surface fatigue output

B-3: Shaft reaction loading, single gear shaft

Shaft reaction loading Single Gear Shaft

Where

W_t = tangential force
W_r = radial force
r_{ij} = length from bearing at 1 to the abutment of the gear of intrest.
r_{1G} = length from bearing at 1 to the center of the gear of interest
R_i = reaction force

Taking Sum of Moments'

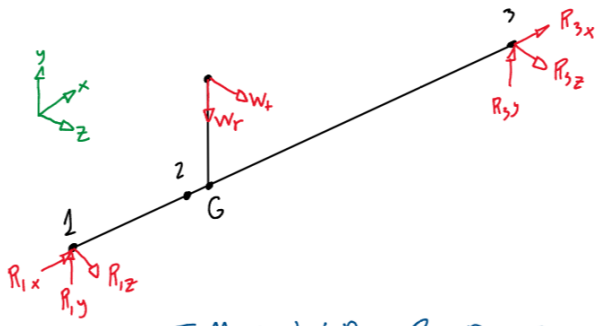

$$r_{1G} = r_{12} + \frac{w}{2}$$

$$\Sigma M_{1z}: -W_r r_{1G} + R_{3y} r_{13} = 0 \qquad \Sigma F_y: R_{1y} - W_r + R_{3y} = 0$$

$$R_{3y} = \frac{W_r r_{1G}}{r_{13}} \qquad R_{1y} = W_r - R_{3y}$$

$$\Sigma M_{1y}: -W_t r_{1G} - R_{3z} r_{13} = 0 \qquad \Sigma F_z: R_{1z} + W_t + R_{3z} = 0$$

$$R_{3z} = \frac{-W_t r_{1G}}{r_{13}} \qquad R_{1z} = -W_t - R_{3z}$$

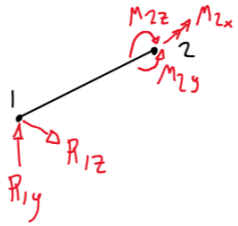

$$M_{2z} = R_{1y} r_{12}$$

$$M_{2y} = R_{1z} r_{12}$$

Net moment 2: $\sqrt{(R_{1y} r_{12})^2 + (R_{1z} r_{12})^2}$

B-4: Shaft reaction loading, Reaction shaft

Shaft reaction Loading Reduction Shaft

Where
- W_t = tangential force
- W_r = radial force
- r_{ij} = length from bearing at 1 to the abutment of the gear of intrest.
- r_{ig} = length from bearing at 1 to the center of the gear of interest
- R_i = reaction force

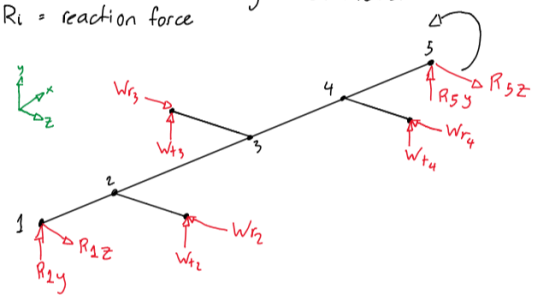

$$\Sigma M_{1z}: \; W_{t2}r_{12} + W_{t3}r_{13} + W_{t4}r_{14} + R_{5y}r_{15} = 0$$

$$R_{5y} = \frac{-(W_{t2}r_{12} + W_{t3}r_{13} + W_{t4}r_{14})}{r_{15}}$$

$$\Sigma F_y: \; R_{1y} + W_{t2} + W_{t3} + W_{t4} + R_{5y} = 0$$

$$R_{1y} = -(W_{t2} + W_{t3} + W_{t4} + R_{5y})$$

$$\Sigma F_z: \; R_{1z} - W_{r2} + W_{r3} - W_{r4} + R_{5z} = 0$$

$$R_{1z} = W_{r2} - W_{r3} + W_{r4} - R_{5z}$$

$$\Sigma M_{1y}: \; W_{r2}r_{12} - W_{r3}r_{13} + W_{r4}r_{14} - R_{5z}r_{15} = 0$$

$$R_{5z} = \frac{W_{r2}r_{12} - W_{r3}r_{13} + W_{r4}r_{14}}{r_{15}}$$

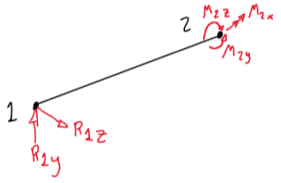

$$M_{zz} = R_{1y}r_{12}$$

$$M_{zy} = R_{1z}r_{12}$$

2: Net bending Moment: $\left((R_{1y}r_{12})^2 + (R_{1z}r_{12})^2\right)^{1/2}$

4: Net bending Moment: $\left(\left(R_{5y}(r_{15}-r_{14})\right)^2 + R_{5z}(r_{15}-r_{14})\right)^{2}\Big)^{1/2}$

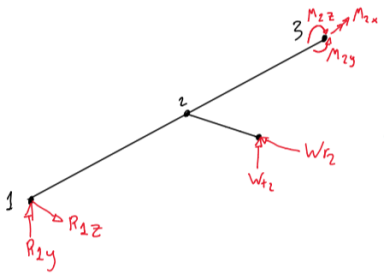

$$M_{zz} = R_{1y}r_{13} + W_{t2}(r_{13} - r_{12})$$

$$M_{zy} = R_{1z}r_{13} - W_{r2}(r_{13} - r_{12})$$

3: Net bending Moment: $\left[\left(R_{1y}r_{13} + W_{t2}(r_{13}-r_{12})\right)^2 + \left(R_{1z}r_{13} - W_{r2}(r_{13}-r_{12})\right)^2\right]^{1/2}$

B-5: Stress Concentrations, Shaft shoulders

Stress Concentrations, Shaft shoulders

Most complex case: Reduction

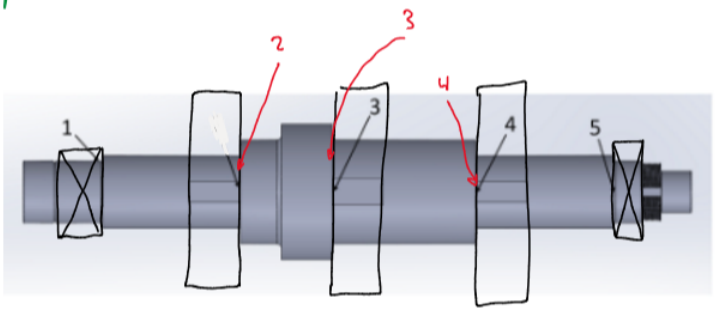

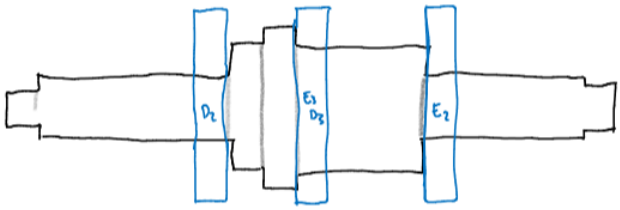

Point (2)

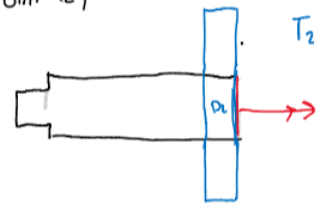

Point (3)

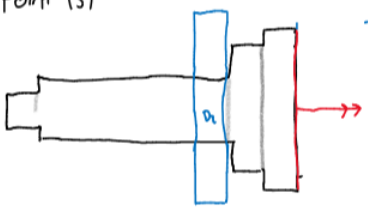

Point (4)

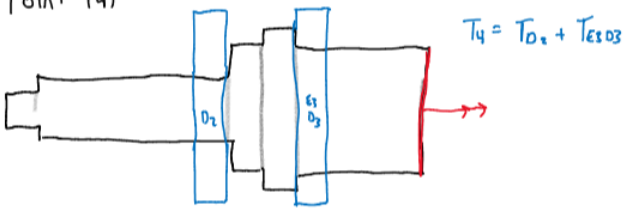

Taking torsion values from spreadsheet, T_1, T_2, T_3, T_4 can be determined.

Stress Concentration Factors

$$K_t^{(bending)} = A\left(\frac{r}{d}\right)^b \qquad \text{(Norton, C-2)}$$

$$K_t^{(torsion)} = A\left(\frac{r}{d}\right)^b \qquad \text{(Norton, C-3)}$$

Solved in spreadsheet for each stress concentration location.

Fatigue Factors

$$K_f^{(bending)} = 1 + q(K_t^{(bending)} - 1)$$
$$K_f^{(torsion)} = 1 + q(K_t^{(torsion)} - 1)$$

where
q = notch sensitivity (Norton, 6-36)

Von Mises Stress (solving point 2)

$$\sigma' = \sqrt{(\sigma_b K_f^b)^2 + 3(\tau_{xy} K_f^t)^2}$$

where
σ' = von mises stress
$K_t^b = 1.614$ (see spreadsheet)
$K_t^t = 1.411$

Bending

$$\sigma_b = \frac{-Mg}{I_z}$$

where
$M = 7145.3\ Nm$ (Bending moment)
$g = 0.0985\ m$ (shaft radius)
$I_z = 0.0000739\ m^4$ (2nd moment of area)

$\sigma_b = 9.52\ MPa$

Torsion

$$\tau = \frac{Tg}{J}$$

where
$T = 23.87\ KPa$ (Torsion)
$g = 0.0985\ m$ (radius)
$J = 0.000148\ m^4$ (2nd Polar moment of area)

$\tau = 15.90\ MPa$

$\sigma' = 41.80\ MPa$ ← Von Mises stress at point (2) on reduction shaft

Safety Factor

$$SF = \frac{Se}{\sigma'}$$

where
$Se = 99.9\ MPa$ (see spreadsheet)

$SF = 2.39$ ← fatigue safety factor, reduction shaft, point (2)

B-6 Total Cycles of electric input shaft

Total Cycles

Electric Input Shaft

Max speed = 3000 rpm → At full power + high speed transit
Min speed = 1875 rpm ↔ At low speed transit

Max speed at 5% + 23% of 20 years operation

$(0.05 + 0.23)(10512000 \text{ min}) = 2943360 \text{ min}$

Min speed at 12% of 20 years operation

$(0.12)(10512000) = 1261440 \text{ min}$

Total Cycles

$(2943360 \text{ min})(3000 \text{ rpm}) + (1261440 \text{ min})(1875 \text{ rpm})$

$= 1.12 \times 10^{10}$ cycles for E1 gear

Appendix C - SKF Seat Tolerance Chart

table 2 - Tolerances for solid steel shafts - seats for radial roller bearings[1)]

Conditions	Shaft diameter	Dimensional tolerance[2)]
	mm	–
Rotating inner ring load or direction of load indeterminate		
Light loads (P = 0,05 C)	= 25	j6
	> 25 to 60	k6
	> 60 to 140	m6
Normal to heavy loads (0,05 C < P = 0,1 C)	= 30	k6
	> 30 to 50	m5
	> 50 to 65	n5
	> 65 to 100	n6
	> 100 to 280	p6
	> 280 to 500	r6
	> 500	r7
Heavy to very heavy loads and high peak loads under difficult operating conditions (P > 0,1 C)	> 50 to 65	n5
	> 65 to 85	n6
	> 85 to 140	p6
	> 140 to 300	r6
	> 300 to 500	r6 + IT6[4)]
	> 500	r7 + IT7[4)]